LUND UNIVERSITY

Development and Application of Pure Rotational CARS for Reactive Flows

Bohlin, Alexis

2012

[Link to publication](#)

Citation for published version (APA):
Bohlin, A. (2012). *Development and Application of Pure Rotational CARS for Reactive Flows*. [Doctoral Thesis (compilation), Combustion Physics].

Total number of authors:
1

Development and application of pure rotational CARS for reactive flows

Doctoral Thesis

Alexis Bohlin

Division of Combustion Physics
Department of Physics
Faculty of Engineering LTH

LUND UNIVERSITY

In memory of my father Thomas Alexis Åkerlund
To Charlotta and my daughters Idun and Saga

ABSTRACT

The thesis deals with the further development of pure rotational coherent anti-Stokes Raman spectroscopy (RCARS) for improving the capabilities of gas phase thermometry. The main effort has been to make the technique more robust when employed under a wide range of temperatures and operational conditions.

A primary aim has been to investigate the impact of collisional broadening on N_2 RCARS thermometry, especially in an environment in which N_2 is perturbed by H_2. Since an interaction of this sort is species-specific and temperature-dependent, it plays a very critical role in RCARS thermometry. It was found that in a sequence of implementation, validation and application, thermometric accuracy could be improved by the implementation of N_2-H_2 line-broadening coefficients. Investigation of these topics involved exploring a novel technique of time-resolved picosecond RCARS for direct measurements of S-branch N_2-N_2/N_2-H_2 Raman linewidths.

The N_2 and O_2 Herman-Wallis factors, used to quantify vibration-rotation interaction and breakdown of the rigid rotor model were also investigated. This correction affects the line-intensities, and also has an impact on RCARS thermometry. Conclusions regarding the sensitivity related to this factor could be achieved by employing different expressions available in the specialized literature.

A theoretical code for N_2O concerned with thermometric accuracy in a set of temperature-calibrated cell experiments was developed and was validated. This work expands the list of RCARS molecules previously developed, and points to interesting possibilities such as that of improving the thermometric precision.

The technique was also applied to flame diagnostics. Temperatures were mapped along the centerline of a one-dimensional flame provided on a McKenna burner, this serving as important input data for other related optical techniques. The homogeneity of this flame was investigated for two different operational shielding co-flows, those of N_2 and of air. Measurements were also performed in a low-swirl turbulent premixed flame, for validating existing models of large eddy simulations. Probability density functions for a large range of temperatures (300 K to 1700 K) and relative O_2 concentrations were provided. The simultaneous measurements of these quantities provided a better understanding than possessed earlier of air entrainment from the surroundings.

POPULÄRVETENSKAPLIG SAMMANFATTNING

Eftersom mer än 80% av världens samlade energianvändning är beroende av förbränning i någon form är vidare kunskap om förbränningsprocessen viktig. Fortsatt effektivisering av förbränningsprocessen är idag högaktuell för uppbyggnad av framtidens mer miljövänliga energisystem och för utvecklingen utnyttjas omfattande diagnostikarbeten. Inom området anses diagnostik med hjälp av laser som det mest lovande. Med detta verktyg kan mätningar göras *in situ* (på plats) samt beröringsfritt med extraherad data av både hög tids- och rumsupplösning. Den här avhandlingen har bedrivits inom utveckling och tillämpning av en sådan mätteknik (CARS), där särskilt fokus ägnats åt förmågan att mäta precisa temperaturer. Temperatur är central för karakteriseringen av ett förbränningsförlopp och indikerar bland annat hur mycket energi som frigjorts.

CARS är en förkortning för coherent anti-Stokes Raman spectroscopy och är en avancerad lasermätmetod för temperaturer och koncentrationer av system i gasfas. Genom att detektera de hos systemet innefattande molekylernas rotationer (alternativt vibrationer) kan temperaturen erhållas. Hur molekyler vibrerar och roterar är nämligen starkt kopplat till temperaturen. En förenklad beskrivning är att vid höga temperaturer vibrerar och roterar molekyler snabbare än vid låga temperaturer. Tekniken fungerar på så sätt att tre laserstrålar fokuseras samman i en mätpunkt varvid en fjärde genereras om energiskillnaden mellan två av de infallande laserstrålarna sammanfaller med molekylernas interna vibrations- och rotationsfrekvenser. Den fjärde, den så kallade CARS-signalen, leds till en detektor och tas upp i form av ett spektrum. Formen av spektrumet bestäms till största del av statistiskt fördelade rotationsfrekvenser som beror på den makroskopiska temperaturen i gasen. Det experimentella spektrumet jämförs sedan numeriskt med ett bibliotek av teoretiskt beräknade spektrum vid olika temperaturer och den utvärderade temperaturen ges av det teoretiska spektrum som visar bäst överensstämmelse.

Tekniken har använts för att mäta i kemiskt reaktiva flöden. Applicerad inom ett typfall av turbulent förbränning erhölls temperaturer samt relativa N_2/O_2-koncentrationer för att validera numeriska simuleringsmodeller. Resultaten möjliggör en bättre förståelse av flammors utsläckning samt hur inblandning av luft sker från omgivningen. En temperaturprofil har också uppmätts i en bränslerik förblandad etylen/luft-flamma. Den speciella flamman används bland annat för att studera olika stadier hos den komplexa förbränningsprocessen, men speciellt också för bildandet av sot. Vid applicering i produktgaserna uppvisades en systematisk förbättrad noggrannhet för tekniken, uppnådd via implementering av ny kunskap om hur rotationslinjerna i ett kvävgasspektrum

störs av molekylkollisioner från vätgas. Samma förbättring dokumenterades vid temperaturmätningar på bränslesidan av en laminär vätgas-diffusionsflamma. Detta blev möjligt med detektion av första rotations-Raman-linjen från vätgas, för att med denna information om koncentration kunna vikta dess ämnesspecifika störning på kvävgasspektrumet. Temperaturinformation från bränslesidan av laminära diffusionsflammor är viktig för att följa hur bränslet uppvärms innan antändning.

För att uppnå hög noggrannhet har krävts detaljerade studier kring några särskilt kritiska parametrar, vilket är ett viktigt led i teknikutvecklingen.

En sådan parameter är Ramanlinjebredder, som modellerar hur mätprocessen störs av molekylkollisioner. Samarbete har bedrivits med Pierre Joubert och Jeanine Bonamy (Université Franche-Comté, Besançon, Frankrike) kring hur rotationslinjerna i ett kvävgasspektrum påverkas av molekylkollisioner från vätgas. I serien från implementering, via validering till applicering kunde en väsentlig systematiskt förbättring bekräftas med hänsyn taget till detta. Vidare utröntes förmågan att direkt mäta linjebreddskoefficienter med hjälp av ljuspulser som är nedkortade från nanosekunds- till pikosekundsregimen. Det gjordes i samarbete med Christopher J. Kliewer och Thomas B. Settersten vid Sandia National Laboratories i Livermore, USA. Med så korta ljuspulser kan de tre laserstrålarna separeras att isolerat växelverka med molekylerna skilda i tiden. Den experimentella principen baseras på att som funktion av olika tidsförskjutningar mäta en avklingning hos signalen som beror av molekylernas kollisioner. De enskilda rotationslinjernas spektralbredd bestäms sedan genom en transformbegränsad relation till signalens livstid.

Undersökningar har också bedrivits kring spektral känslighet från olika Herman-Wallis faktorer samt deras påverkan på termometrin, utvecklat i ett samarbete med Michele Marrocco (ENEA, Rom, Italien). Dessa faktorer beskriver hur styrkan på spektrallinjerna ändras vid centrifugal deformation av molekylstrukturen. Detta fenomen bör tas till hänsyn inom förbränningsstudier vid höga temperaturer som innebär snabba molekylrotationer.

Vidare finns alltid en inneboende strävan att utveckla tekniken. Som ett led i detta ingår att utvidga listan för implementerade molekyler. Inom ramen för avhandlingsarbetet valdes N_2O, en treatomig molekyl med linjär asymmetrisk struktur som bland annat är central i atmosfärsforskningen. En teoretisk kod utvecklades och testades genom spektralanpassningar i en serie valideringsmätningar vid olika temperaturer. God överensstämmelse erhölls mellan experimentella och teoretiskt beräknade spektra, och även en hög temperaturnoggrannhet.

LIST OF PUBLICATIONS

The thesis is based on the following papers, which will be referenced by Roman numerals in the text. The papers are appended to the thesis in the order listed. The order in which they are presented is oriented to the overall organization of the work and of the topics taken up rather than to their dates of publication.

I.   A. Bohlin, F. Vestin, P. Joubert, J. Bonamy, and P.-E. Bengtsson
Improvement of rotational CARS thermometry in fuel-rich hydrocarbon flames by inclusion of N_2-H_2 Raman linewidths
J. Raman Spectroscopy 40, 788-794 (2009)

II.   A. Bohlin, F. Vestin, P. Joubert, J. Bonamy, and P.-E. Bengtsson
Rotational CARS N_2 thermometry: Validation experiments for the influence of nitrogen spectral line broadening by hydrogen
J. Raman Spectroscopy 41, 875-881 (2010)

III.   A. Bohlin and P.-E. Bengtsson
Rotational CARS thermometry in diffusion flames: On the influence of nitrogen spectral line-broadening by CH_4 and H_2
Proc. Combust. Inst., 33, 823-830 (2011)

IV.   C. J. Kliewer, A. Bohlin, E. Nordström, B. D. Patterson, P.-E. Bengtsson, and T. B. Settersten
Picosecond pure rotational coherent anti-Stokes Raman spectroscopy for time-domain measurements of S-branch N_2-N_2 Raman linewidths
Accepted to Appl. Phys. B, DOI: 10.1007/s00340-012-5037-2

V.   A. Bohlin, E. Nordström, M. Dhyne, B. D. Patterson, P. Joubert, P.-E. Bengtsson, and C. J. Kliewer
Direct measurement of S-branch N_2-H_2 Raman linewidths using time-resolved pure rotational coherent anti-Stokes Raman spectroscopy
Submitted to J. Chemical Physics

VI.   A. Bohlin, P.-E. Bengtsson, and M. Marrocco
On the sensitivity of rotational CARS N_2 thermometry to the Herman-Wallis factor
J. Raman Spectroscopy 42, 1843-1847 (2011)

VII.   A. Bohlin, E. Nordström, P.-E. Bengtsson, and M. Marrocco
On the sensitivity of rotational O_2 CARS thermometry to the Herman-Wallis factor
J. Raman Spectroscopy (2011), DOI:10.1002/jrs.3147

VIII. A. Bohlin, A. Kindeya, E. Nordström, and P.-E. Bengtsson
Validation of a rotational coherent anti-Stokes Raman scattering model for N_2O at temperatures from 295 K to 796 K
J. Raman Spectroscopy (2011), DOI:10.1002/jrs.3148

IX.   A. Bohlin and P.-E. Bengtsson
Effective Suppression of Stray Light in Rotational Coherent Anti-Stokes Raman Spectroscopy Using an Angle-Tuned Short-Wave-Pass Filter
Appl. Spectrosc. 64, 964-966 (2010)

X.   A. Bohlin, E. Nordström, H. Carlsson, X.-S. Bai, and P.-E. Bengtsson
Pure rotational CARS measurements of temperature and O_2-concentration in a low swirl turbulent premixed flame
Accepted for oral presentation at the 34th International Symposium on Combustion, Warsaw, Poland

RELATED WORK

A.   H. Bladh, J. Johnsson, N.-E. Olofsson, A. Bohlin, and P.-E. Bengtsson
Optical soot characterization using two-color laser-induced incandescence (2C-LII) in the soot growth region of a premixed flat flame
Proc. Combust. Inst., 33, 641-648 (2011)

B.   N.-E. Olofsson, H. Bladh, A. Bohlin, J. Johnsson, and P.-E. Bengtsson
Are sooting premixed porous-plug burner flames one-dimensional? A laser-based experimental investigation
Submitted to Combustion Science and Technology

C.   Y. Gao, A. Bohlin, P.-E. Bengtsson, T. Seeger, and C. J. Kliewer
In-situ determination of broadening coefficients for rotational CARS thermometry in flames
Accepted for oral presentation at the 34th International Symposium on Combustion, Warsaw, Poland

SUMMARY OF PAPERS

I. This paper investigates the impact on N_2 RCARS thermometry in fuel-rich hydrocarbon flames of including N_2-H_2 Raman linewidths. Spectral libraries were generated incorporating newly derived line-broadening coefficients to re-fit a previous dataset. The experimental data were recorded in the product gases of premixed ethylene/air flames. Previously, a model employing line-broadening coefficients from N_2-N_2, N_2-H_2O, N_2-CO_2, and N_2-CO had been employed. Implementing the N_2-H_2 Raman linewidths enabled all five major species colliders to be considered.
    Per-Erik and Fredrik planned the paper. Pierre calculated the line-broadening coefficients and I conducted the analysis. Per-Erik, Pierre and I prepared the manuscript. I presented the work in a talk held at the European Conference on Non-linear Optical Spectroscopy (ECONOS) in Rome, Italy in 2009.

II. In this work, validation experiments concerning the effects of N_2 spectral line-broadening by H_2 were performed in binary mixtures of N_2 and H_2 under temperature-calibrated cell conditions. The work was a follow-up to Paper I, aimed at confirming a major underestimation in thermometry that can occur if N_2-H_2 Raman linewidths in environments in which the collisions are dominated by H_2 are neglected. N_2 CARS temperatures were extracted employing two different linewidth models, the one with are of purely self-broadened N_2 coefficients and the other with each of the species-specific coefficients weighted in accordance with their mole fraction.
    A further investigation involved comparing estimated temperatures based on S-branch linewidths, resulting in the case from pure rotational calculations and in the other case derived by the processing of Q-branch coefficients.
    Per-Erik and I performed the experiments and prepared the manuscript. Pierre calculated the line-broadening coefficients and I conducted the analysis. I presented the work in a talk held at the European Conference on Non-linear Optical Spectroscopy (ECONOS) in Bremen, Germany in 2010.

III. In this study, N_2 RCARS temperatures were measured on the fuel-side of a H_2 diffusion flame. N_2 was probed simultaneously with detection of the H_2 S_0-transition in order to weight the species-specific Raman linewidths by information concerning the relative concentrations. Calibration

measurements involving use of N_2 in binary mixtures with H_2 supported the results of flame diagnostics in extracting the relative concentrations.

In addition, the effects of collisions with CH_4 were investigated by means of experiments carried out in binary mixtures of N_2 and CH_4. Subsequent temperature analysis employing purely self-perturbed N_2 coefficients was performed to investigate the extent to which temperature estimates were reproducible independent of CH_4 concentration.

Per-Erik and I performed the experiments and prepared the manuscript, I conducted the analysis. I presented the work in a talk held at the International Symposium on Combustion in Beijing, China in 2010.

IV.   The paper investigates recent progress in measuring S-branch N_2-N_2 Raman linewidths by use of time-resolved picosecond RCARS. Coherence decays were detected directly in the time-domain by following the *J*-dependent CARS signal decay as a function of probe delay. The rotational Raman N_2-N_2 linewidths were derived from these time-dependent decays and were evaluated in terms of thermometric accuracy. Comparisons were made of energy-corrected sudden and of modified exponential gap dynamical scaling laws, the results being used to quantify the sensitivity of RCARS thermometry carried out detected in the frequency domain.

The collaborative project carried out employed two different experimental setups. The linewidth measurements were performed at the Combustion Research Facility of Sandia National Laboratory in Livermore (USA) and the thermometric validation was carried out employing a nanosecond setup in Lund.

Chris planned the paper. All of the authors participated in the time-domain experiments. Chris processed the linewidth data. I conducted the validation experiments and the thermometric evaluations in Lund. Chris prepared most of the manuscript and I contributed to the text. The work was presented by Chris in a talk held at the European Conference on Non-linear Optical Spectroscopy (ECONOS) in Enschede, The Netherlands in 2011.

V.   The material for this paper was collected in connection with Paper IV. The same route as before was followed in deriving the S-branch Raman linewidths, but the focus of the investigation was changed, its involving a system in which N_2 was perturbed by a foreign collider, H_2. The results of the work are discussed within the framework of Papers I, II, and III. The N_2-H_2 time-domain coefficients obtained were compared with semiclassical line-broadening calculations of the N_2-H_2 system using an *ab inito* potential energy surface. Both sets of data were quantified for

RCARS thermometry, being employed in spectral fits of N_2 spectra recorded in binary mixtures with H_2 at calibrated temperatures.

Chris, Per-Erik and I planned the paper and together with Emil and Brian we performed the time-domain experiments. Chris processed the linewidth data. Pierre and Miguel developed the semiclassical calculations and wrote the parts of the text concerning these. Emil and I performed the validation experiments in Lund and I conducted the thermometric analysis. I prepared most of the manuscript Chris also contributing to it.

VI. This paper investigates the sensitivity of N_2 CARS thermometry to the Herman-Wallis factor. Different expressions reported in the specialized literature were compiled and were tested in terms of spectral sensitivity. The general impact these had on the thermometry was investigated by use of spectral fits in comparing a given reference with the others.

Michele planned the paper and compiled the expressions, I conducted the analysis. Michele, Per-Erik and I developed the manuscript.

VII. The paper is a follow-up to Paper VI, but instead concerned O_2. The same method was employed in comparing one reference expression with the others. In addition, the impact on O_2 and N_2 RCARS thermometry if omitting this parameter in the calculations was investigated (rigid rotor approximation).

Michele compiled the expressions and I conducted the analysis. Michele and I prepared most of the manuscript, with contributions from Emil and Per-Erik.

VIII. In this paper a theoretical RCARS code for N_2O was developed and was validated by use of temperature-calibrated cell measurements. Spectral fits of the recordings obtained to the theoretically generated spectra were used to test the accuracy of the model. Spectroscopic entities were collected from the reference literature and were tuned so as to achieve the best fit possible.

Per-Erik and I planned the paper, and I performed the implementation of the code as well as the validation experiments. Alem contributed to the experiments in the initial stages. I prepared most of the manuscript, Emil and Per-Erik also contributing to it. I presented the work in a talk held at the European Conference on Non-linear Optical Spectroscopy (ECONOS) in Enschede, The Netherlands in 2011.

IX. This short communication reports on a study of the effective suppression of stray light in RCARS by use of an angle-tuned short-wave-pass filter,

which improves the technique when employed in a situation in which optical windows are present.

Per-Erik and I performed the experiments, I conducted the data analysis. Per-Erik prepared most of the manuscript.

X. In this paper, RCARS temperatures and relative O_2 concentrations were measured in a low-swirl turbulent flame. The experimental results obtained were compared with the results of numerical large eddy simulations. In an environment of this type there are various diagnostics challenges to be solved, such as spatial averaging effects, the wide dynamic range of the signals and broadening of the N_2 spectral lines through collisions with H_2O.

Per-Erik, Emil and I performed the measurements. I conducted most of the data analysis, Emil also contributing to it. Henning and Xue-Song performed the numerical simulations. Per-Erik compiled the paper, all the authors contributing to it.

A-B. The RCARS diagnostics included in works A and B (Related work, see above) concerned temperatures extracted along the centerline and radially at a fixed height in a standard McKenna burner flame operated with use of two different shielding co-flows. The results can provide help in the choice of suitable operating conditions.

Per-Erik and I performed the experiments and I conducted the data analysis. I presented the work in a talk held at the Joint Combustion meeting between the French and Scandinavian-Nordic Sections of the Combustion Institute in Snekkersten, Denmark in 2009.

TABLE OF CONTENTS

INTRODUCTION

Combustion processes have served and will continue serving as a fundamental source of energy in the foreseeable future. Today it is estimated that more than 80 % of the total world energy consumption is dependent upon the combustion of fuel of some form (source: *World energy statistics,* International Energy Agency). Constant improvement in the efficiency of the combustion process is thus of central importance in developing future energy systems that are more environmentally friendly than those currently employed. Improved knowledge of the combustion process itself can help provide combustion devices that are better designed from the standpoint of their application, and possibilities to achieve a reduction in the emission of various pollutants.

To achieve this, extensive diagnostic work needs to be performed so as to be able to validate the predictions of numerical simulations carried out within the existing framework of combustion modeling. Optical measurement techniques have played a key role in the progress achieved in this area so far, due to its capability of extracting data *in situ* in a non-intrusive way, and in providing assessments with a high spatial as well as temporal resolution.

The present thesis deals with one such method, a laser spectroscopy tool termed coherent anti-Stokes Raman spectroscopy (CARS), there being two main versions of it: vibrational and rotational CARS. The technique has been developed since the early 70s to now have become a kind of gold standard for point-wise gas-phase thermometry, through the accuracy and precision of the measurements it provides. Temperature is central in the characterization of a combustion process, partly since information regarding it makes it possible to assess rather accurately how much energy is released in a specific application. The CARS technique can also provide quantitative data concerning the relative species concentrations in the case of molecules that are Raman active and are present in appreciable concentrations. Relative concentration measurements can also provide knowledge of local equivalence ratios as these develop in the course of the combustion process.

The work reported here has concerned the further improvement of rotational CARS under a wide variety of temperatures and of operational conditions. To assess the accuracy of the results satisfactorily, thorough account need to be taken of the technique-specific parameters that are relevant. Development in experiments, related to the experimental apparatus and new approaches, help to achieve improved capacity of the technique.

The outline of the thesis is as follows. The next chapter, *Background Physics*, deals with the objects that temperature probing concerns, namely the

molecules that are involved. Chapter 3, *Rotational anti-Stokes Raman Spectroscopy*, takes up the basic principles of this optical measurement technique, as well as possible improvements of it that can be achieved. Chapter 4, *Developments and application*, considers a number of separate topics concerned with these matters, and discusses a variety of matters of interest not brought up in the papers. Chapter 5, finally, summarizes the results and explores the possible outlook for investigations in this area in the future.

BACKGROUND PHYSICS

To understand adequately the underlying process that CARS involves and how quantities can be extracted from quantum molecular systems, a physical explanation of it is needed to be given. This chapter provides an overview of the physics related to it including matter of molecular structure, internal energy and population probability distributions involving different energy states. At the end of the chapter a brief summary of how light is scattered by matter is provided.

2.1 THE DIATOMIC ROTATOR

Two simplified drawings presented in Figure 2.1 can help one to understand in intuitive terms the vibrating and rotating motion of a diatomic molecule. For both types of motion, the atoms in the molecules are modeled here as point masses connected by a bond represented by a spring and by a stiff rod in the vibrational and the rotational case, respectively. Regarding the atoms as point masses can be seen as a valid approximation, since the weight of the atom is dominated by the ~femtometer (10^{-15} m) sized nucleus. This makes it possible to derive the internal energy of the system by use of classical mechanical concepts. To obtain a more complete model of what occurs, the energy involved needs to be quantized by the use of the more advanced tools of quantum mechanics. Not all of these steps are shown here in detail but thorough descriptions of them are found in many textbooks, see Herzber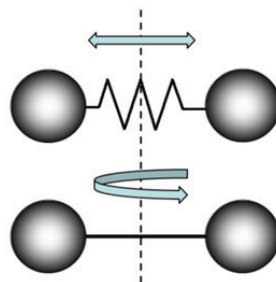g [1] and Banwell and McCash [2]. The total internal energy of the diatomic molecule can be decoupled in parts of the potential and the kinetic energy contributions involved. The potential energy is related to the bounded states found in the electronic configurations, whereas the kinetic energy components are based on translational, vibrational and rotational motions. The translational energy, manifested by the speed, is related to the temperature. High levels of translational energy lead to frequent collisions between molecules, these collisions having an impact on the broadening of the spectral lines. Nevertheless, the translational energy involved will not be discussed further here, since the main kinetic energy components of interest for the CARS process are the rotational and the vibrational motions involved. A molecule shows about 1000 vibrations in the course of a single rotation. For this

Figure 2.1. *The harmonic oscillator (above) and the rigid rotator (below).*

reason, the various motions can be considered, in a first approximation, to proceed independently of one other. This is called the Born-Oppenheimer approximation, in terms of which the total energy, with exclusion of the electronic energies, is calculated as the sum of the energies involved in both these motions.

Vibrational motion

As a first approximation, one can say that vibrational motion proceeds as a simple harmonic oscillator, i.e. with a sinusoidal oscillation centered at around the point of the equilibrium internuclear distance. Here the basic idea is that when two masses are separated from their equilibrium position they experience a force that is proportional to the distance separating them. The strength of this force is determined by the strength of the bond between the atoms. The force is electromagnetic and can be explained by the attraction (or repulsion) of opposite (or same) charges. When the two atoms become compressed, the positively charged nuclei act to repulse on each other. On the other hand, when the atoms are at a greater distance from each other the positively charged nucleus and the negatively charged electron cloud act attractively. This behavior is displayed in Figure 2.2, in which the dashed line shows the harmonic oscillator potential. The energy solutions (E_v) of this potential are given by the eigenvalues of a given set of eigenfunctions of the Hamiltonian (H);

$$H = -\frac{\hbar^2}{2\mu} \cdot \frac{\partial^2}{\partial r^2} + \frac{1}{2}kr^2, \; r = r_{eq} - r', \; E_v = \hbar\omega_{vib}\left(v + \frac{1}{2}\right) \text{[Joule]},$$

$$(v = 0, 1, 2, \dots), \; \omega_{vib} = \frac{1}{2\pi}\sqrt{\frac{k}{\mu}} \text{ [Hz]}, \; \frac{1}{\mu} = \frac{1}{m_A} + \frac{1}{m_B} \tag{2.1}$$

Here, μ is the reduced mass of the system, k is the oscillator strength, ω_{vib} is the vibrational frequency and v is the vibrational quantum number. The modeled harmonic oscillator is only valid at the bottom of the potential close to the equilibrium internuclear distance. At larger distances the attractive force between the atoms is no longer sufficiently strong to hold the atoms together, breaking the bond between the atoms. A better description for simulating this behaviour is given by the empirical Morse potential;

$$V = D_{eq}[1 - exp(a \cdot r)]^2, r = r_{eq} - r' \tag{2.2}$$

Here the constant a is species-specific and D_{eq} is the associated dissociation energy. In contrast to the harmonic oscillator potential, no analytical solutions to this potential exist, the solutions having to be obtained by use of numerical

methods. The energy solutions of the anharmonic potential contain higher order terms according to

$$E_v = \hbar\omega_{vib}\left(v + \frac{1}{2}\right) - \hbar\omega_{vib}x_e\left(v + \frac{1}{2}\right)^2 + \cdots \text{ [Joule]} \qquad (2.3)$$

where x_e is the anharmonicity constant. The reason for showing these equations explicitly is to underline the fact that the energies of a vibrational band are not equidistant, as they are for analytical solutions of the harmonic oscillator. The broadening of the potential is different, this effecting the position of the higher energies. At such energies, the molecule vibrates more strongly and, as can be seen in Figure 2.2, the average distance between the atoms increases. This has an impact on the rotational motion of the molecule, a matter that will be discussed further when the concept of rotational motion has been introduced.

Rotational motion

The rotational motion shown in Figure 2.1 can be modeled as a rigid rotator. For a linear rotor the Hamilton operator and its corresponding eigenenergies can be expressed as

$$H = \frac{J^2}{2I}, \; E_J = \frac{\hbar^2}{2I}J(J + 1) \text{ [Joule]},$$
$$(J = 0, 1, 2, \dots) \qquad (2.4)$$

where J is the rotational quantum number. This expression can be rearranged through a division by the Planck constant h and the velocity of light c (cm s^{-1}) in order to express the energies in terms of wavenumbers, as is commonly done in spectroscopy.

$$\varepsilon_J = \frac{E_J}{hc} = BJ(J + 1) \text{ [cm}^{-1}\text{]}, \; B = \frac{h}{8\pi^2 Ic}, \; (J = 0, 1, 2, \dots) \qquad (2.5)$$
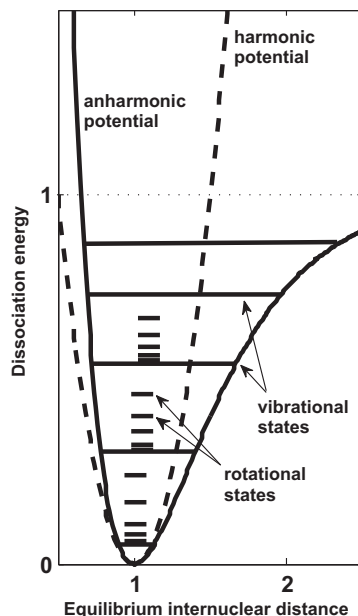

Figure 2.2. *The realistic anharmonic potential (solid line) and the harmonic oscillator potential (dashed line). The vertical axis is scaled with the dissociation energy and the horizontal axis with the equilibrium distance between the atoms of the molecule. The rotational bands of each vibrational level is indicated.*

The constant B is termed the rotational constant. It is inversely proportional to the moment of inertia I, which depends on the mass of the molecule. A first order correction term can be introduced to improve the description of a rigid rotor

$$\varepsilon_J = BJ(J+1) - DJ^2(J+1)^2 + \cdots \; [\text{cm}^{-1}], \; D = \frac{4B^3}{\omega_{vib}} \qquad (2.6)$$

where D is termed the centrifugal constant. Both the molecular constants, B and D, for various species relevant for CARS are shown in Table 2.1. The correction implies that an authentic molecule is non-rigid and experiences shape distortion when rotating fast. To correct for the anharmonicity in the force field, further correction terms are required. A more complete expression for calculating the rotational energy can be found in [1]. It is important, however, in calculating the positions of the CARS spectral lines, to introduce correction terms for the constants B and D. Such correction is called the breakdown of the Born-Oppenheimer approximation. It aims at simulating what was mentioned earlier, namely that strong vibrations have an indirect impact on the rotational motion of the molecule. Since the stronger vibrations increase the average distance between the atoms, the moment of inertia around the rotational symmetry axis likewise increases. The rotational energies then decrease, due to their inverse dependence upon the moment of inertia, see Eqn. (2.5). Since there is a rotational band for each vibrational energy level, this effect can be modeled by changes in the constants B and D in the form of

Table 2.1. *Rotational constant B and centrifugal constant D for various species (cm^{-1}).*

Species	B	D x10^{-6}
N_2	1.998	5.760
O_2	1.445	4.839
H_2	60.853	4.710
CO	1.931	6.121
CO_2	0.390	0.133
N_2O	0.419	0.176

$$B_v = B - \alpha\left(v+\tfrac{1}{2}\right) + \gamma\left(v+\tfrac{1}{2}\right)^2 + \cdots, \; D_v = D + \beta\left(v+\tfrac{1}{2}\right) + \cdots \quad (2.7)$$

where B and D are the equilibrium values. The constants α, γ, β are termed rotational-vibrational interaction constants.

2.2 POPULATION DISTRIBUTION

The wave-particle dualism is a basic concept within quantum mechanics. Here wavefunctions are utilized in order to describe the state of a quantum

mechanical particle. The use of general wave properties, such as those of interference and superposition, can be seen as instructive in this state representation, yet its interpretation can be rather difficult. The probability distribution of a quantum mechanical particle can be described here as the squared modulus of its wavefunction. If the wavefunction consists in a weighted combination (i.e. a superposition) of a linearly independent base (ϕ_i), the integral sum of the probability distribution is the sum of the squared modulus of all the weights involved. If the wavefunction is normalized, this means that this sum is equal to one and being termed the enclosure relation. The formalism for this can be written as

$$\psi = a\phi_1 + b\phi_2, \ \Sigma|\psi|^2 = |a|^2 + |b|^2 = 1 \tag{2.8}$$

This states that each of the two coefficients (a, b) is related to the statistical weight of the corresponding state. The statistical weight of each the two states provides information concerning its relative fractional population, this explaining why the sum of the two is equal to one. One aim of the discussion here is to show, in compact terms, how a quantum mechanical formalism can be used to express probabilities. In simplified terms, the linearly independent base can be thought of as representing vibrational and rotational states that are spread over a number of isolated discrete energy levels. If the system is in thermal equilibrium, each the states have a certain population probability. This probability is calculated by means of the normalized Boltzmann factor P for each of the states s. This is one of the most powerful results of statistical physics;

$$P(s) = \frac{1}{Z}exp(-E(s)/kT), Z = \sum_s exp(-E(s)/kT) \tag{2.9}$$

Here the partition function Z normalizes the expression, which means that the sum of all Ps is equal to one. Note, that for systems described by the Boltzmann distribution, only the squared modulus of the expansion coefficients in Eqn. (2.8) is known.

To be more specific regarding how these probabilities depends upon temperature, the fractional populations of N_2 rotational and vibrational states are shown in Figure 2.3 (a) at different temperatures. It can be seen how the distribution becomes more spread if the temperature increases and the centre of the distribution becoming positioned at higher rotational levels. Described in the simplest terms, this means that the higher the temperature, the faster the rotations of the molecules become. Note that for the calculations here a ($2J$-1) spin projection degeneracy needs to be included for each of the levels involved as well as a statistical weight factor (6 for even and 3 for odd N_2 rotational quantum numbers). The latter principle depends upon the coupling to the spin of

the nucleus, although this has been omitted in the calculations so as to better clarify the temperature dependence involved.

The fraction of the population located at different vibrational levels can be calculated in a similar way. For the different vibrational levels there is no degeneracy, the statistical weight factor being equal to one. In Figure 2.3 (b), one can note that the N_2 fractional population is distributed over the first three vibrational states within a temperature range of 300-2000 K. At lower temperatures, N_2 vibrates mainly with the ground level frequency, whereas at about 1000 K the first excited state starts to become thermally populated. At a detailed level, this behaviour is species-specific and it depends on the molecular energy spacing. This will be discussed further in section 3.2.3, in which a triatomic molecule, N_2O, is introduced. To conclude, one can note that it is the ability of detecting how the rotational and vibrational populations are distributed thermally which makes CARS excellent for gas-phase thermometry.

Figure 2.3. (a) *The relative populations of N_2 rotational states, displayed at three temperatures: 300 K (closed circles), 1000K (open circles), and 1700 K (crosses).* **(b)** *The fractional population distribution of the first three vibrational states in N_2 at temperatures ranging from 300 K to 2000 K.*

2.3 SCATTERING OF LIGHT

One way in which incident photons can interact with molecules is termed scattering. This process can be thought of in classical terms as a collision between the two, and with an energy exchange shown in Figure 2.4. The combined system of a molecule and a photon can be viewed as a virtual level of the molecule that relaxes to the real level through instantaneous emission of a photon. The energy of the molecule can be left then either as changed or as unchanged, processes of this sort being termed inelastic (Raman) and elastic (Rayleigh) scattering, respectively. In the case of inelastic Raman scattering there are two possibilities, namely that the energy has been absorbed (Stokes) by the molecule or has been lost by it (anti-Stokes). The energy difference is due to changes in motion of the molecule (either rotational or ro-vibrational in character), a change in this sort being termed a Raman shift. Many diatomic and triatomic molecules are not accessible spectroscopically through electronic transitions in the visible spectral range, where efficient photodetectors are
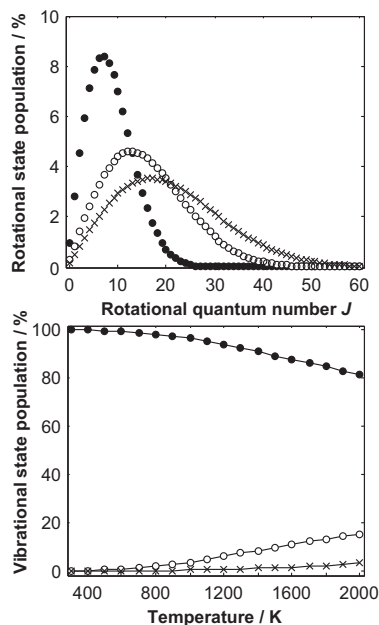
available. However, these molecules can still be probed in this optical region through use of Raman spectroscopic methods, since with use of these methods the Raman frequencies can be coupled to a probe laser selected or positioned in the visible spectral range. Whereas spontaneous Raman scattering is a relatively weak process, the coherent approach termed coherent anti-Stokes Raman scattering (CARS) provides strong laser-like signals. The photon coupling diagram of the CARS process resembles very much those referred to above but with an additional characteristic, namely that of coherent excitation, which will be discussed in the next chapter.
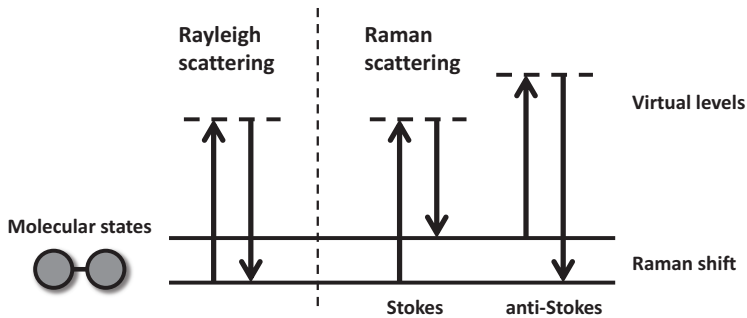
Figure 2.4. *Different possibilities of light being scattered by the molecule. In the Rayleigh process (at the left) the light is scattered elastically, whereas in the Raman process (at the right) the light is scattered inelastically changing the state of the molecule.*

COHERENT ANTI-STOKES RAMAN SPECTROSCOPY

The thesis deals with the use of rotational coherent anti-Stokes Raman spectroscopy (CARS) for combustion diagnostics. A first section of this chapter deals with theoretical considerations in connection with CARS, the aim being to introduce the reader to the basics of CARS, in terms both of the spectroscopic measurements involved and of how it relates to molecular physics. The brief discussion of the technique here provides a background to consideration of the various projects carried out. In most of the projects reported on, the work in question was divided in two separate parts: the data acquisition using an experimental CARS setup, and data analysis with use of a numerical code. The later sections are dealing with these two parts separately: the one concerning development of the code, and the other the experimental setup and its development.

3.1 CARS THEORETICAL CONSIDERATIONS

The pioneering work in developing CARS for combustion diagnostics was carried out during the 1970s by Taran and co-workers [3]. Since then, the technique has been developed to the point of its being accepted as a gold standard of sorts as a procedure for gas-phase temperature measurements. Substantial reviews of CARS generally and of its progress can be found in [4, 5] and the references therein.

Primarily, CARS has been applied to N_2, because of its inert properties and its presence at high concentrations in most combustion applications. It has also been widely used to measure concentrations of major species other than N_2, for those detectable and present at concentrations higher that ~0.1-1%. The two most familiar approaches of the technique are vibrational and rotational CARS, which, though sharing many features that are similar are complementary in character (see discussion in Paper X). In terms of thermometric accuracy, vibrational CARS can be seen as suitable in a high temperature regime (from 1200 K and above) and rotational CARS as best applicable at temperature up to ~1800 K. Precise statements regarding these temperature regions and their limits can be debated, however, due to improvements in both techniques over time. Generally speaking, the advantages in choosing the one rather than the other technique depend primarily on the measurement conditions involved. Two particularly beneficial properties for the rotational CARS approach, however, are its relatively simple multi-species detection abilities and its capability of providing measurements under elevated pressure conditions.

In the rotational CARS (RCARS) approach, transitions between different rotational levels are probed within a given vibrational state. Since the spectral information regarding diatomic molecules is well understood, theoretical models pertaining to them are relatively straightforward to implement, such models having been developed for several molecules of combustion interest, in particular N_2 [6], O_2 [7], and CO [8]. Successful attempts have also been made to develop such models for symmetric tri- and four-atomic molecules, specifically for CO_2 [9, 10] and C_2H_2 [11, 12].

The coherent anti-Stokes Raman scattering signal is generated by means of a four-wave-mixing nonlinear optical process. Photons from three incident laser beams interact with the energy levels of the probed molecules to produce a fourth coherent light beam. This is illustrated in Figure 3.1(a), in a schematic energy-level diagram of the RCARS process. The probed molecule is coherently excited to levels that match the frequency difference of the two photons, termed pump and Stokes. In RCARS making use of a dual-broadband approach [13, 14], the pump and the Stokes photons are provided by a single broadband dye laser source. They induce transitions within the entire rotational manifold. A third photon, termed the probe, which originates from a narrowband laser source, is scattered from the induced states, producing an anti-Stokes shifted photon that completes the four-wave mixing process.

Figure 3.1. *Schematic representation of the dual-broadband RCARS process. (a) Energy principle of the photon coupling. (b) The spectral profiles of the incident laser beams involved.*

Figure 3.1(b), which provides a different representation of the RCARS process, shows the wavelength dependence of the spectral emission profiles of the three laser beams. Two photons of differing wavelength from each of the pump and the Stokes emission profiles, respectively, match a specific Raman shift (ΔE_{Raman}) of the probed molecule. The RCARS signal that is emitted, which includes all the induced Raman shifts, is thus spectrally shifted "towards the blue" relative to the green probe beam. Since these Raman shifts are dependent upon the specific energy levels of the probed molecule, the spectral information serves as a fingerprint of the molecule.

For the pure rotational Raman scattering process of a diatomic molecule, only certain specific transitions are allowed. The selection rules are
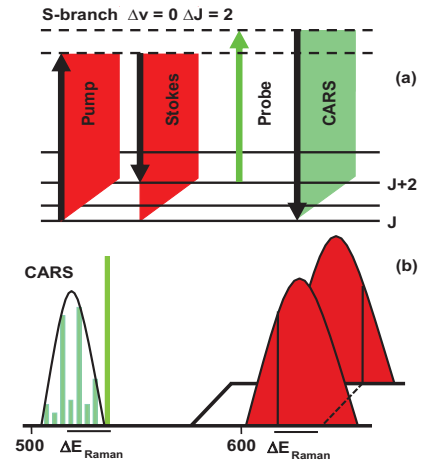
$$\Delta v = 0, \Delta J = \pm 2 \tag{3.1}$$

Here $\Delta J = -2$, and $\Delta J = 2$ denote the O-branch (Stokes) and the S-branch (anti-Stokes), respectively. The corresponding energy for the S-branch transitions can be calculated in the simplest form by use of Eqn. (2.5):

$$\Delta\varepsilon_{J,J+2} = 4B\left(J + \frac{3}{2}\right) \qquad (3.2)$$

In Figure 3.2, theoretical N_2 CARS spectra are shown for temperatures of 300 K, 1000 K, and 1700 K. The spectral structure of equidistant lines separated according to Eqn. (3.2) by ~$4B$ (= 8 cm^{-1}) in the case of S-branch transitions can be seen there. The Raman shift increases approximately linearly with increasing J-level. Note the intensity alternation between neighbouring lines of even and odd parity, which is due to the nuclear spin degeneracy. The spectral envelope shows a strong sensitivity to temperature. At increasing temperatures the distribution become broader and is located at higher Raman shift. This is related to the population statistics of the rotational quantum states, as discussed in section 2.2. To describe the characteristics of the RCARS spectral envelope in its entirely, an equation for the CARS signal strength needs to be introduced.
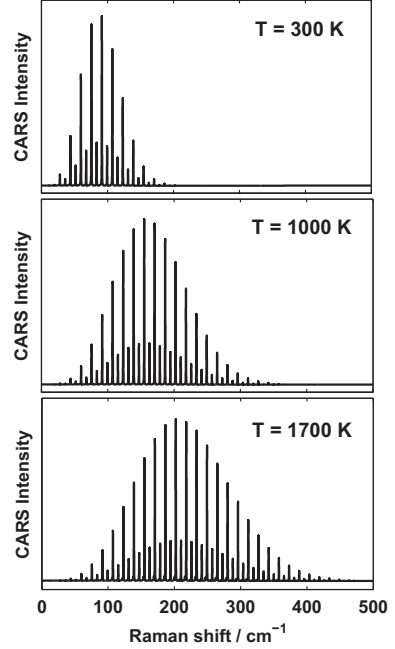

Figure 3.2. *Theoretical rotational CARS spectra from N_2 calculated for temperatures of 300 K, 1000 K, and 1700 K, respectively.*

CARS signal strength

As indicated in the preceding section, CARS is generated by a nonlinear optical process. The electric field from the incident laser beams polarizes a dielectric medium through a displacement of the electron cloud relative to the atomic nuclei. The relationships involved are described by the power expansion

$$\vec{P} = \varepsilon_0\left(\chi\vec{E} + \chi^{(2)}\vec{E}^2 + \chi^{(3)}\vec{E}^3 + \cdots\right) \qquad (3.3)$$

where $\vec{P}$ is the induced polarization, $\vec{E}$ is the electric field applied, ε_0 is the permittivity of free space and $\chi^{(n)}$ is the nth order electric susceptibility tensor. The higher order terms involved are much weaker than the linear term, but they become significant when an electric field of considerable strength is applied. In

gaseous media having isotropic properties, all even-order terms vanish due to inversion symmetry properties. The equation for the CARS signal strength is derived by means of the electromagnetic wave equation obtained by manipulating Maxwell's equations. In solving the electromagnetic wave equation, the linear term in Eqn. (3.3) is added as a component to the electric field, whereas the non-linear polarization acts as a source term. The details of deriving of the CARS signal equation are not shown here, but can be found in the comprehensive work of Boyd [15]. It leads to a final expression of

$$I_{CARS}(z) = \frac{16\pi^4 \omega_{CARS}^2}{n^4 c^4} I_{pump} I_{Stokes} I_{probe} \left| \chi^{(3)} \right|^2 z^2 \text{sinc}^2 \left(\frac{\Delta kz}{2} \right) \qquad (3.4)$$

where ω_{CARS} is the frequency of the CARS signal, I_{pump}, I_{Stokes}, and I_{probe} are the intensities of the generating laser beams, $\chi^{(3)}$ is the third-order susceptibility, z is the distance of interaction (the probe volume length), and the sinc² term is a phase matching condition. It follows that the strength of the CARS signal is linearly dependent upon the intensity of each of the generating beams, meaning that the use of high-power lasers is favourable for generating a strong signal, an interaction length of considerable size being advantageous too. The dependencies upon the strength of the signal that are most critical are those of the phase matching condition and the third-order susceptibility, which are discussed next.

The phase matching condition is dependent upon a mismatch (Δk) in wave vectors between the incident laser beams and the generated CARS beam;

$$\Delta k = \left(k_{pump} - k_{Stokes} + k_{probe} \right) - k_{CARS} \qquad (3.5)$$

The energy conversion is enhanced by minimizing the mismatch in wavevectors, this being termed perfect phase matching ($\Delta k = 0$). The length of a wavevector [15],

$$|k| = 2\pi \cdot n(\omega) / \lambda \qquad (3.6)$$

depends upon the wavelength λ and the index of refraction $n(\omega)$. The last entity is frequency dependent, but is approximately the same (= 1) for all the frequencies found in a gaseous media. There are different spatial geometric approaches that can be used to achieve this condition [4], the one employed here being termed a planar BOXCARS scheme (see the sketch of the experimental setup in Figure 3.8).

The spectral information in Eqn. (3.4) can be described in terms of the third-order susceptibility

$$\chi^{(3)} = \chi_{NR} + \sum_n \sum_J \frac{a_{J,J+2}}{\omega_{J,J+2} - \omega_{pump} + \omega_{Stokes} - ip\Gamma_{J,J+2}/2} \qquad (3.7)$$

The susceptibility here can be divided into a resonant and a non-resonant (NR) part. The non-resonant susceptibility originates from instantaneous responses in the molecular electronic configurations due to the incident electric fields. The resonant susceptibility can be described in terms of a summation over all Raman active species (n) in the gaseous medium produced by S-branch transitions from the initial J to the final rotational state $J+2$. Each of the resonant terms in Eqn. (3.7) has a Raman linewidth $\Gamma_{J,J+2}$ (FWHM), expressed in terms of reciprocal centimetres per unit of pressure (p). The amplitude factor, $a_{J,J+2}$, can be expressed as

$$a_{J,J+2} = \frac{4}{45} \frac{N}{\hbar} b_{J,J+2} F^S(J) \gamma^2 \Delta\rho_{J,J+2} \qquad (3.8)$$

where N is the number density of the probed species, $b_{J,J+2}$ is the Placzek-Teller coefficient, F^S is the Herman-Wallis (HW) factor, γ is the polarizability anisotropy, and $\Delta\rho_{J,J+2}$ is the normalized population difference in the rotational states involved in the transition. The population difference factor can be expressed as

$$\Delta\rho_{J,J+2} = \frac{g_J(2J+1)}{Q_J} \left[e^{-E_J/k_B T} - e^{-E_{J+2}/k_B T} \right] \qquad (3.9)$$

where g_J is a statistical weight factor, Q_J is the internal partition function, T is the temperature, and k_B is the Boltzmann constant.

Since the signal strength is proportional to the squared modulus of the third-order susceptibility, it follows that the parameters involved affect the signal in a dependence raised to the second power. The fact that the signal strength scales quadratically on the number density can be used in assessing the relative concentrations of signals having contributions from more than one resonant species. A general feature here is also that of the strength of the signal decreasing with an increase in temperature, this being understood in Eqn. (3.8) in terms of the number density being inversely proportional to the temperature, as described by the ideal gas law. A RCARS spectrum consists of a large number of spectral lines, however, and both its shape and its position are highly temperature dependent. The key attribute of thermometric sensitivity of the technique is thus based on the temperature-dependent amplitude of the J-specific spectral lines originating mainly from the population difference factor of Eqn. (3.9). Note that the relative strength of the spectral lines also depends upon the rotational linewidth and the Herman Wallis factor, as discussed further in the sections that follow.

3.2   CODE DEVELOPMENT

In this section, the history of the rotational CARS code is outlined and implementations of the code in further development of it are discussed. Two main parameters of special interest from a theoretical standpoint were investigated, namely Raman linewidths and the Herman-Wallis factor. A code was also developed for simulating N_2O CARS spectra in the temperature region of 300-800K.

Lund rotational CARS code

The original Lund rotational CARS code was a modification of a vibrational CARS code developed by Hall [16] and implemented by Stefan Kröll, making use of the calculations reported in Ref.[17]. David Nilsson developed the code further in his masters thesis in 1987 [18]. Lars Martinsson made a complete revision of the code then in his doctoral thesis [19] and developed a framework for the simultaneous evaluation of temperature and of relative concentrations of N_2 and O_2 [7]. Since then, several persons have contributed to the construction of a complete tool-box for different RCARS applications. In addition, Joakim Bood [20], Christian Brackmann [21], Mikael Afzelius [22] and Fredrik Vestin [23] have made progress on-line in work on their respective theses, in efforts to make the code more robust. During the years of this progress, Per-Erik Bengtsson has played a role as the principal investigator and has made important inputs to development of the code.

Certain projects that have been carried out should be mentioned specifically, their having served as a basis for some of those carried out within the framework of the present thesis. Mikael Afzelius investigated the interbranch interference effect of CSRS on the CARS side of the spectrum [24, 25], the study of which also carried out in the present Paper VIII. Fredrik Vestin coded the generic structure of a triatomic molecule [10], knowledge and a routine that was employed in Paper VIII. He also developed a species-specific weighting routine [26] that facilitated the simultaneous measurement of temperature and of relative N_2/O_2 concentrations, a code that was employed in the work resulted in Paper X.

3.2.1   Linewidths

Most of the Papers in the thesis are concerned directly with Raman linewidths, or, at least, partly discuss the subject in connection with the accuracy of the measured temperatures. Line-broadening mechanism is central in the analysis of CARS data since it affects the shape of the spectral lines, and needs to be properly implemented in the calculation of theoretical spectra.

There are essentially three basic mechanisms, Doppler broadening, Dicke narrowing and pressure broadening, that are associated with different pressure conditions and depend on the type of CARS spectra (S-branch, Q-branch) being considered [27]. Doppler broadening arises from random molecular velocities distributed in different directions with respect to the spectroscopic reference frame. A finite mean velocity results in spectral shifts of the transition frequency in agreement with the principles of the Doppler effect. The molecular dynamics here is independent of the collisions and depends instead on the translational motion. Dicke narrowing is related to collisions, elastically, since the principle originates from changes in velocity caused by collisions. The collisions affect the velocity and favors transfer from high to low velocities, which narrow the Doppler contribution. For relatively heavy molecules, such as N_2, this effect is negligible and is not considered here. The experimental projects reported on here were performed at atmospheric pressure where the dominant mechanism originates from pressure broadening (molecular collisions). Doppler-broadening contributions to the RCARS signals generated in the forward direction, with small intersection angles of the incident beams, is generally neglected. The Doppler contribution is directly proportional to the optical transition frequency [28], which is relatively small for a fairly heavy molecule with rotational shifts in the region of 0-300 cm^{-1}. As an example for N_2, at a temperature of about 1700 K and a Raman shift of 202.17 cm^{-1} ($J'' = 24$), it is estimated that the Doppler width of ~ 0.0012 cm^{-1} (FWHM) is less than 4% of the collisional width of ~ 0.03 cm^{-1} (FWHM).

An isolated line model is generally valid for N_2 S-branch transitions at intermediate pressure levels. Through this assumption, the third-order susceptibility is computed as a sum of Lorentzian lineshape functions, where each individual transition is treated separately. The Lorentzian lineshape originates from a Fourier transform pair relation between the time and the frequency domain. The radiation from a spectral transition is damped by the collision rate and can classically be represented by an exponentially decaying sine wave [27]. The inelastic collisions restrict the lifetime of any molecular state, making the associated spectral

Figure 3.3. *Fourier transform of a damped oscillation. While the decay determines the linewidth, the oscillating frequency determines the position.*

line wider spectrally in the frequency domain, as shown in Figure 3.3. In accordance with the Heisenberg principle, the collisional width is inversely
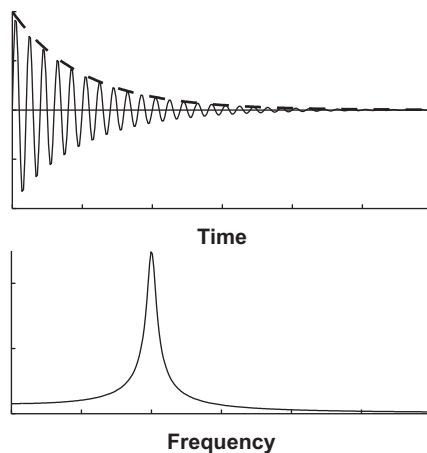
proportional to the lifetime of the state in question. For collisions that result in an energy transfer, the lifetime can be approximated with the time of free flight τ_0 of the radiator. For typical molecules (N_2 and O_2) under standard temperature and pressure conditions, τ_0 is close to 10^{-10} s, the corresponding collisional broadening coefficient being ~0.1 cm^{-1}/atm (FWHM) [28]. Increasing the pressure leads to an increase in the collision rate and a linearly decrease in the lifetime (and analogously to a linear increase in the corresponding spectral width).

Potentially, an effect which considerably complicate the isolated line picture is the motional narrowing, which is due to a coupling of rotational levels that undergo frequent inelastic collisions, as described by Hall *et al*. [29]. However, the energy spacing of N_2 S-branch transitions is sufficient to suppress a probability of motional narrowing effects below 20 MPa [25, 30], and is therefore not considered here.

There are inelastic contributions as well to the width of the rotational spectral lines, contributions that originate from reorientational phase shifts that are due to collision-induced changes in the direction of the molecular axis. The reorientation, however affects mainly the lower *J* states, the angular momentum and gyroscopic stability of the molecule there being low.

Linewidth model for flame thermometry

Evaluations of CARS measurements during the 1980s generally concerned only self-broadened nitrogen Raman linewidths when probing nitrogen in air-fed flames, although often other species, such as carbon dioxide, water, oxygen, hydrogen and carbon monoxide were likewise present, at concentrations as high as some 20-30 %. At the beginning of the 90s the importance of broadening coefficients from molecules other than nitrogen itself was addressed. Since water and carbon dioxide are the most obvious products, line-broadening from these species, i.e. from N_2-H_2O [31] and N_2-CO_2 [32], was included in the theoretical calculations of CARS spectra. In addition, N_2-O_2 Raman linewidths were investigated by Millot *et al*. in 1992 [33] and a N_2-CO line-broadening mechanism was developed in 2004 [34]. Furthermore, an extended set of N_2-H_2 line-broadening coefficients was published in 2008 [35].

Historically, most such work has concerned isotropic N_2 Q-branch coefficients. A common procedure for deriving pure rotational broadening coefficients from these has been through the use of the following random-phase approximation (RPA) [36]:

$$\Gamma_{J,J+2}^{\text{RPA}} = \Gamma_{J,J+2}^{\text{rot.inelastic}} = \frac{1}{2}\left(\Gamma_{J,J} + \Gamma_{J+2,J+2}\right) \qquad (3.10)$$

Using this procedure, the anisotropic broadening caused by the reorientational phase shifts is neglected, its being assumed that it is mostly the inelastic collisions that produce the broadening. In the next step, a total linewidth model for N_2 is employed, one that takes account of the species-specific contributions to the broadening:

$$\Gamma_{J,J+2}^{N_2} = \sum_k X_k \cdot \Gamma_{J,J+2}(N_2 - M_k) \tag{3.11}$$

where $\Gamma_{J,J+2}$ (N_2-M_k) denotes the line-broadening coefficents pertaining to all the major perturber species M_k present in the mixture, weighted by the species mole fraction X_k.

Impact on RCARS thermometry

The molecular dynamics of collisions is species-specific, and is strongly dependent upon the temperature and the specific transition of the perturbed molecule (*J*-dependence). It is known in connection with this that the accuracy of rotational CARS thermometry involving contour spectral fitting is highly dependent upon an adequate Raman linewidth model being employed. All collisional partners need to be incorporated through species-specific line broadening coefficients, the *J*-dependence and temperature dependence of the line-broadening coefficients for each of the species involved also needing to be correctly described. The linewidth model is the most critical parameter next after the Boltzmann population difference factor affecting the contour of the spectral envelope and thus the thermometry performance of the RCARS technique.

In Papers I-V, the impact on N_2 RCARS thermometry was detailed when neglecting the N_2-H_2 Raman linewidths. In paper III, the effect on N_2 spectral line-broadening from CH_4 was investigated and resulted in small impact on the estimated temperatures below 500 K. In Paper X, a temperature correction was calculated for taking the absence of N_2-H_2O collisions in the simulation of spectra into account. It was explained too why the impact of collisions with CO_2 on temperature estimates can be expected to be small. Most of the arguments presented have concerned the *J*-dependence of these coefficients and how these coefficients can differ from those of pure N_2 self-broadened linewidths.

Dependence on temperature and rotational level

Basically, the goal of dynamic modeling of Raman linewidths is to evaluate the collisional cross sections involved. Three main approaches to carrying this out have been developed: a classical approach [37], a semiclassical approach [38] and by means of pure quantum calculations [39]. In paper V, the S-branch

coefficients, where N_2 is perturbed by H_2, was calculated in terms of a semiclassical Robert-Bonamy (RB) model using an *ab initio* potential energy surface (PES) [40]. Many sources of linewidth data, however, involve use of simpler models based on so-called dynamical scaling laws. There, high-resolution Raman linewidths are determined experimentally by use of inverse Raman and stimulated Raman spectroscopy, various scaling laws being fitted to the experimental data sets [41]. The two scaling laws most commonly employed are the energy-corrected sudden exponential law (ECS) [36] and the modified exponential-gap law (MEG) [42, 43]. The ECS model can be described using three dependencies, exponential (ECS-E), polynomial (ECS-P), and exponential-polynomial (ECS-EP) dependency. For the N_2-N_2 and N_2-H_2 coefficients employed in Paper II, use was made of ECS-EP dependency.

A common feature of the ECS and MEG models is that the rotational energy transfer that results from collision is determined by state-to-state rate constants. Accordingly, the linewidth Γ_j of a given rotational state J_j is calculated as the sum of all state-to-state rate constants, from J_j to J_i where $i \neq j$. An important property of these population transfer rates is the principle of detailed balance, which ensures thermal equilibrium. In some proposals in this area there is also a restriction of parity (ΔJ = even) for the change of state. The major distinction between the models is that of the specific conservation law involved. Whereas the MEG scaling law considers energy conservation in connection with inelastic collisions, the ECS scaling law considers the conservation angular momentum [41].

Phenomenologically, these models can be used to understand the dependence of Raman linewidths on temperature and rotational level. In a simplified description, the rotational energy transfer between an initial and the final state is suppressed by a discrepancy in energy or angular momenta between the states. In Figure 3.4 the rotational energy states of a radiator (N_2) and a perturber (N_2 and H_2) are shown together with the thermal population distribution found at a specific temperature.
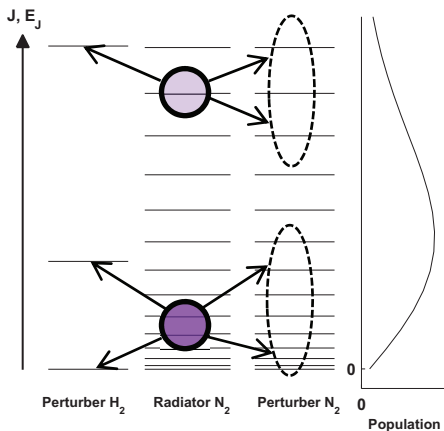

Figure 3.4. *Illustration of a collisionally induced rotational energy transfer process between a radiator (N_2) and a perturber (N_2 and H_2). The process is enhanced with more neighbouring states of the perturber.*

Whereas the rotational energy of the radiator (N_2) can be transferred more easily to neighboring states of the perturber (N_2), the transfer of rotational energy from the lower J states of the radiator is more probable than it is from the higher J states. This is the reason for the decrease in N_2-N_2 Raman linewidths being a function of the rotational state involved (J-dependence). In contrast, for collisions with a foreign molecule H_2, there is a discrepancy in neighboring states between the perturber and the radiator N_2 for each of the J states. This makes the J-dependence of the N_2-H_2 Raman linewidths becoming less pronounced, see Figure 4.5 in section 4.1. The smooth variation of the N_2-H_2 coefficients is an effect of a considerable large spacing between the rotational energy levels of H_2, why the N_2 molecule regardless of J state have difficulties in transferring rotational energy to H_2. When N_2 collides (inelastically) with H_2, the H_2 molecule changes its velocity rather than its rotation. The considerable level in absolute broadening of the N_2-H_2 collision is an effect of the relatively larger speed from a lightweight molecule, such as H_2, reaching closer to the repulsive wall of the N_2 interaction potential.

The linewidths are significantly reduced with an appreciable increase in temperature. The temperature dependence of the scaling laws is introduced by a factor T^{-n}, where n is a fitting parameter that depends upon the specific molecule involved ($n \approx 0.7 - 0.8$, for N_2). This factor takes the decrease in number density of the perturber with increasing temperature, as a result of the ideal gas law, into account. When there are fewer perturber molecules, collisions are less frequent, the efficiency of the rotational energy transfer being reduced. Another, more "indirect" temperature dependence is that based on the thermal population distribution of the perturber, see Figure 3.4. This dependence is responsible for a "shoulder" peaking at the maximum populated state of the perturber. It can be seen, for example, in N_2-N_2 line-broadening coefficients.

3.2.2 Vibration-rotation interaction

In Papers VI and VII, the effects of vibration-rotation interaction on the intensity of the RCARS spectral lines was investigated for two of the diatomic molecules most commonly employed: N_2 and O_2. The study concerned in particular the thermometry of the technique, the sensitivity of which was determined by comparing in terms of the spread in predicated temperatures of different theoretical libraries. The comparison made could deal either with different expressions found in the literature or with the numerical values of a parameter.

The vibration-rotation interaction was described in Section 2.1 as representing the breakdown of the rigid rotor approximation (RRA), emphasizing the need of anharmonic force fields being taken into account in calculations of internal vibrational and rotational energies. This is well known

21

and is referred to as being a centrifugal distortion that increases the internuclear distance and results in rapid rotation of the molecules. It affects the position of a spectral line in terms of frequency and changes the polarizability of a specific transition and thus the corresponding line intensity. This connection was one pioneered by Herman and Wallis (HW) decades ago for dealing with electric dipole transitions in diatomics [44]. It was discussed further within Raman phenomena by James and Klemperer (JK) [45], Asawaroengchai and Rosenblatt (AR) [46], Drake [47, 48], Tipping and Ogilvie (TO) [49], and Buldakov *et al*. [50]. More recently a revision of it for CARS spectroscopy has been launched, Marrocco [51-57] having detailed the effects of the intra-molecular interactions relevant to vibrational and femtosecond CARS. The HW factor for S-branch Raman transitions was introduced by JK, who employed a perturbative approach in dealing with the centrifugal potential in the radial Schrödinger equation. The polarizability expansion was truncated at the second term, the HW factor being calculated as

$$F_{JK}^{S} = 1 + 2\kappa^2 (J^2 + 3J + 3)/\eta \qquad (3.12)$$

where $\kappa = 2B_e/\omega_e$ (B_e and ω_e are the rotational constant and the vibrational frequency, respectively) and $\eta = \beta_0/(r_e\beta_1)$ is a parameter which is related to the ratio of the first to the second term in the anisotropic polarizability expansion about the equilibrium nuclear distance r_e (β_0 and β_1 are the first and second term of the expansion, respectively). The polarizability anisotropy β_0 is the difference between the matrix element parallel and perpendicular to the molecular axis at the equilibrium distance. The term β_1 is the polarizability anisotropy change (the derivative of it) with respect to internuclear distance at the equilibrium position. Theoretical speculations concerning possible η values, based on the experimental data available at the time led to $\eta_{N2}=0.4$ and $\eta_{O2}=0.42$. Later, AR found that η was considerably smaller for oxygen and that $\eta_{O2}=0.23$. Martinsson *et al*. [6] used a different value for nitrogen, one of $\eta_{N2}=0.44965$ [48, 58]. Later, calculations published by TO emphasized the importance of not neglecting the terms in κ^4 in evaluating the HW factor for the S-branch, a more appropriate form for it being assumed to be

$$F_{TO}^{S} = [1 + \kappa^2 (J^2 + 3J + 3)/\eta]^2. \qquad (3.13)$$

In this expression, specific values for the anisotropic polarizability expansion need to be assigned. In Papers VI and VII, the values for nitrogen ($\eta_{N2}=0.3157$) and for oxygen ($\eta_{O2}=0.3386$) reported in the work of Maroulis [59] and of Buldakov *et al.* [50], respectively, were implemented. Buldakov *et al.* calculated the numerical values of the HW contributions for the Raman transitions of nitrogen and of oxygen, obtaining values that coincided with those

reported by TO. For this reason, and also because of the fact that TO's formulation for the Raman transitions of the S-branch is one which is most advanced, it is assumed that Eqn. (3.13) provides the best description of the effects of the vibration-rotation interaction on the Raman intensities of the S-branch. The squared Herman-Wallis factors for N_2 and O_2 are displayed in Figure 3.5 due to the strength of the CARS signal being proportional to the squared modulus of the third-order susceptibility. In this plot the differences in HW factors, reflect the variation in the intensity of the RCARS spectral lines as a result for them being implemented.
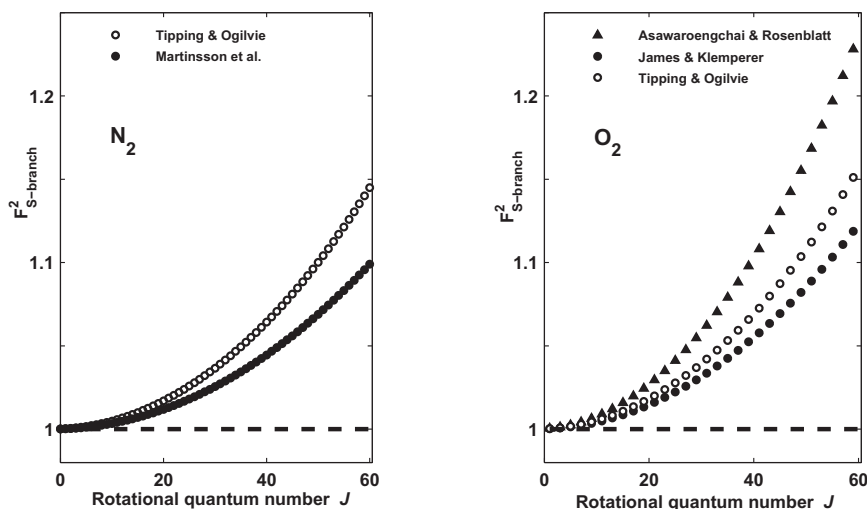
Figure 3.5. *Squared Herman-Wallis factors for N_2 and O_2, displayed as a function of the rotational quantum number.*

3.2.3 N_2O

In Paper VIII the potential of rotational CARS as a diagnostic tool for studying N_2O, particularly as regards thermometry, was investigated. The spectral signature of rotational N_2O CARS spectra was investigated experimentally and was compared with theoretically predicted ones at various temperatures.

To begin with, a rotational CARS spectrum recorded in a mixture of 33 % N_2O and 67 % N_2 at room temperature is shown in Figure 3.6. In this binary mixture, as can be seen, the peak signal strength of each of the molecules is about equally strong. In measuring the pure gases at room temperature, the peak signal strength for N_2O was found to be ~5 times stronger than that for N_2. A strong overlap between the N_2O and N_2 lines can be seen at wavenumbers 27.8 cm^{-1}, 36.2 cm^{-1}, 59.8 cm^{-1}, and 67.8 cm^{-1}, which corresponds to J's of 15(2), 20(3), 34(6), and 39(7), respectively, for $N_2O(N_2)$. Nevertheless, one can note

23

that the spectra of the different species are readily separable enough. This facilitates extraction of the different relative concentrations. That there are greater number of rotational lines for N_2O (~48) than for N_2 (~20) can be noted, together with the very dense spectral line structure of the N_2O, which is located in the spectral vicinity of the probe laser (at wavenumber zero). This feature along with the higher degree of non-resonant susceptibility for N_2O than for N_2 ($\chi_{NR}(N_2O)=1.9 \cdot \chi_{NR}(N_2)$ [60]) which is found, indicate that inter-branch effects stemming from the coherent Stokes Raman scattering (CSRS) side need to be modeled. For N_2, this effect is usually only significant under conditions of elevated pressure [24].
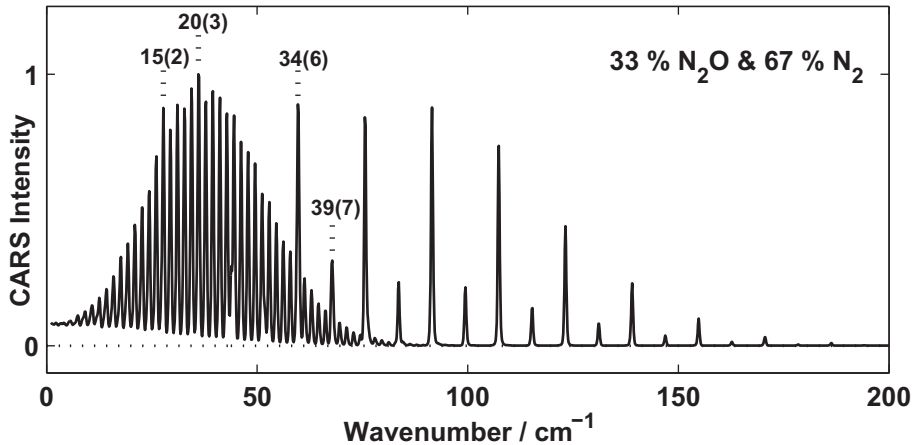
Figure 3.6. *A rotational CARS spectrum recorded at room temperature in a binary mixture of 1/3 N_2O and 2/3 N_2. At these proportions, both species have about the same peak signal strength. A few S-branch transitions have been signed for both the molecules, according to $N_2O(N_2)$.*

Implementation of the N_2O was done utilizing a generic structure from a previous theoretical rotational CARS code for CO_2 [10]. In a polyatomic molecule, the molecular energy structure is much more complex than it is in a diatomic molecule. N_2O is an asymmetric linear triatomic molecule [61] having three fundamental vibrational modes - v_1, v_2 and v_3 (see Figure 3.7) - these corresponding to the N-O stretch, the bending mode, and the N-N stretch, respectively. For the bending mode, an additional *l*-quantum number is assigned an angular bending momentum around the internuclear axis, the complete vibrational state being represented as $v_1v_2lv_3$. The rotational energies of a given vibrational state were calculated using Eqn. (2.6), the effective N_2O vibration-rotation constants employed being those based on the work of Toth [62]. The shape of the rotational lines in the spectrum depends partly on the many sub-lines originating from transitions induced within the different vibrational states.

Contributions of this type were weighted according to the fractions of the vibrational partition function they represent. To provide an idea of how many states altogether contribute to rotational CARS susceptibility here, one can note that the number of vibrational and rotational states involved comprise about 95% of the partition functions involved, which are displayed in Figure 3.7 as a function of temperature.
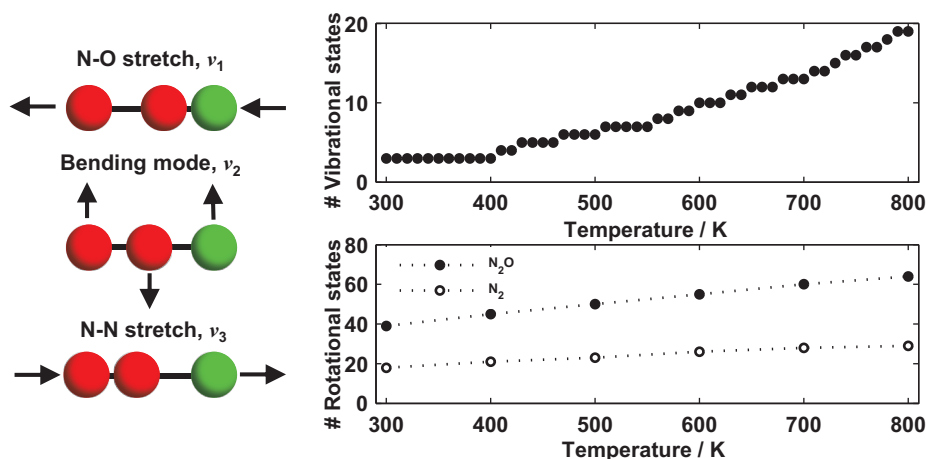

Figure 3.7. *Three fundamental vibrational modes of N_2O, these corresponding to the N-O stretch, the bending mode, and the N-N stretch, respectively (left). The number of N_2O vibrational (right upper panel) and of N_2O/N_2 rotational (right lower panel) states required in order for them to comprise about 95 % of the respective partition function as a whole is shown as a function of temperature.*

In the upper panel, one can note that at least 20 vibrational states are needed to cover some 95% of the vibrational partition function at the temperature limit (800 K) employed in the study. In the lower panel it can be seen that within the temperature range involved, about twice as many rotational states are populated for N_2O than for N_2. Here, the Boltzmann factors are generated by molecular constants at the ground level vibrational state (N_2O, B=0.419 cm^{-1} and D=1.76E-6 cm^{-1} [62] and N_2, B=1.998 cm^{-1} and D=5.76E-6 cm^{-1} [58]).

In completing the expressions for the CARS signal strength for N_2O through the use of Eqn. (3.7), most of the other molecular parameters could be obtained from the reference literature. The value found for the anisotropic polarizability of N_2O [63] was approximated as applying to each of the different vibrational states, the same assumption being made for the self-broadened N_2O-N_2O Raman linewidths [60, 64-66]. The linewidths were those selected by Hall and Shufflebeam [66], based on values reported by Lacombe *et al.* [64], but presented here together with an expression of the additional temperature

25

dependence found for each of the rotational levels as well. The Q-branch coefficients were processed according to the sum-rule, Eqn. (3.10), so as to be applicable to the S-branch. The internuclear distances, $r_{(N-N)}$ and $r_{(N-O)}$, were based on the work of Plíva [67]. Analogous to the approach taken to the rotational CO_2 CARS code, the rule stating that only $J \geq l$ is allowed for bending modes [68] was neglected here for simplicity's sake. At the same time, the correction for the Placzek-Teller coefficient [69] with respect to the quantum number l has been accounted for. In the description given of the rotational CO_2 CARS code as implemented by Vestin *et al*., the S-branch HW factor for CO_2 was omitted for lack of appropriate reference literature. Although published data concerning linear triatomics, such as for N_2O, were found [70-72], the HW factors applying there were obtained for Q-, P-, and R-branches, but are not specified for S-branch rotational Raman scattering. In lack of appropriate values, a HW-factor for N_2 was implemented (see Paper VI). This resulted in excellent thermometric accuracy, as shown in section 4.3.

The thermometric accuracy obtained relies specifically on two parameters, the N_2O-N_2O Raman linewidths and the S-branch HW factor. As pointed out, there are a greater number of sources available for the N_2O-N_2O Raman linewidths (not all of them listed here, but see HITRAN [66] compilation and references therein), yet the relevance of these references to the present work is questionable. Most of the coefficients found in the specialized literature were obtained for a lower and more limited temperature range than here, one applying to N_2O studies at below 300 K conducted in the atmosphere. Also, there was no literature to be found concerning an S-branch HW factor for N_2O. Instead of then using a unitary value (a rigid rotor approximation), data for N_2 were implemented. The choice made was supported by the reduction in the apparent systematic overestimation obtained in measured N_2O CARS temperatures if this parameter is omitted. The difference between N_2O CARS thermometry based on a theoretical library with and one without use of this factor was as large as 20 K or 2.5 % relative to the reference applying to the temperature range that was studied. Thus, in the absence of relevant literature, it is only claimed that the combination of the Raman linewidth model and the HW data employed resulted in the rather close agreement between thermocouple and N_2O CARS temperatures.

3.3   EXPERIMENTAL DEVELOPMENT

In this section, the fundamentals of the experimental tools will be introduced and thereafter various improvements that seem possible will be discussed, concerning both the apparatus and new experimental approaches that could be undertaken.

Lund experimental setup

Figure 3.8 and Figure 3.9 show sketches of the standard dual-broadband rotational CARS setup that was used in the experiments. Single-mode radiation at 532 nm with a pulse duration of about 6 ns, at a repetition rate of 10 Hz, is generated by a frequency-doubled injection-seeded Nd:YAG laser (Quantel, model YG 981E-SLM-2W). A fraction (8%) of the light produced is split off to be used as the probe beam, the remainder serving as a pump source for the dye laser (Quantel, model TDL 90). The broadband dye laser provides the pump and Stokes beams, the general spectral emission profile being centered at 630 nm and being about 280 cm^{-1} FWHM (full width at half maximum) wide, prepared by use of DCM in a solvent containing ethanol. Note that, the dye mixture needs to be carefully selected so as to avoid obtaining a smeared vibrational CARS signal [13]. Typical pulse energies for the beams used in the experiments are in the range of 10-20 mJ/pulse. The beams were aligned in accordance with a planar BOXCARS phase matching scheme, implemented with use of both of a 50% beam splitter so as to separate the dye laser beams into equal parts (pump and Stokes) and of a dichroic mirror reflecting green and transmitting red so as to superimpose the probe upon the Stokes beam.
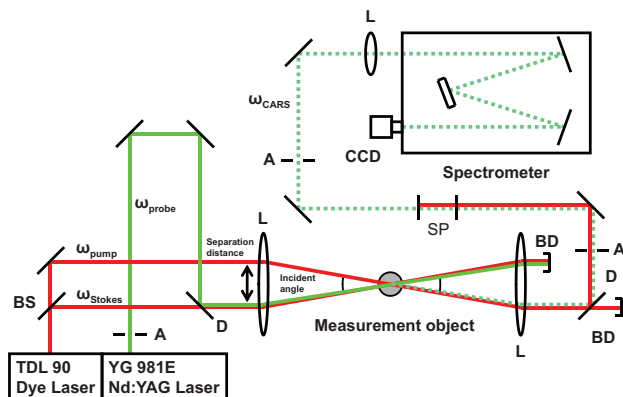

Figure 3.8. *A schematic dual-broadband rotational CARS experimental setup (BS = beam splitter, D = dichroic mirror, L = lens, BD = beam dump, A = aperture, SP = short-pass filter).*

In order to temporally overlap the beams, a delay line for the green beam was introduced to account for the extra travelling distance of the red beam inside the dye laser. The three beams, in being brought to a common point of intersection, are arranged so as to have a separation distance of about 14 mm on a spherical lens with a focal length of 300 or 500 mm. The focal length selected depends upon the measurement situation involved. If optical windows are present, the *f* = 300 mm lens is best selected so as to avoid etching. A motive for having a lens with a short focal length is the reduction in probe volume this provides, which improves the spatial resolution of the measurements accordingly. The spatial resolution can be further improved by use of a steeper crossing angle of the

incident beams, it is being adjusted by increasing separation distance of the beams on the focusing lens. The size of the ellipsoidal shaped probe volume is estimated at 0.1 x 1-3 mm, its size depending upon the alignment.
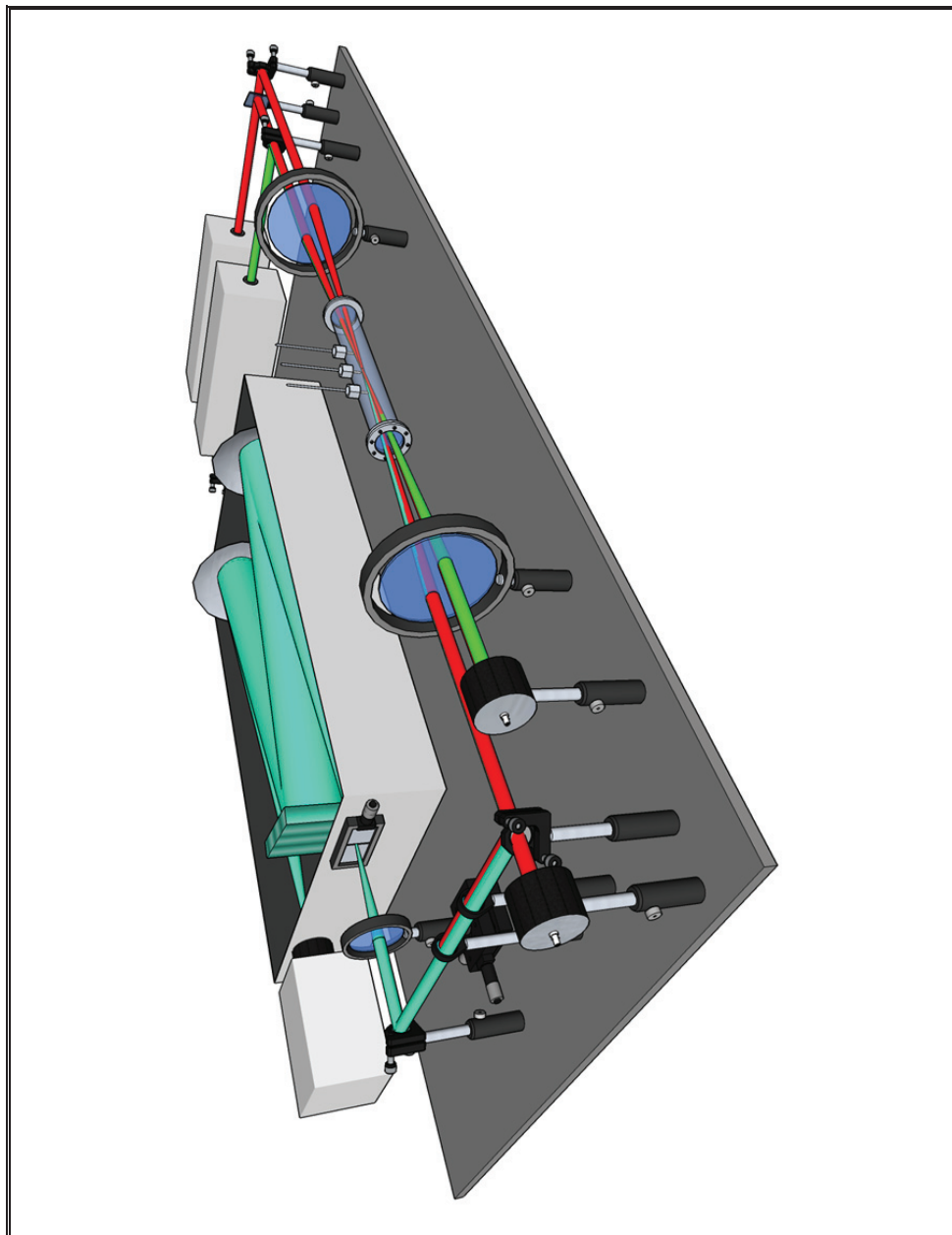

Figure 3.9. *A 3D sketch of the rotational CARS experimental setup used in this work.*

It is measured by sliding a thin glass plate in perpendicular to the surface that encloses the probe volume, while monitoring the four-wave mixing signal. The value this yields is extracted from the signal drop that occurs at a factor e^2 from the peak value of the Gaussian-shaped intensity profile. The generated CARS signal beam is re-collimated by use of another spherical lens (usually with the same focal length), and it then propagates nearly superimposed upon the red pump beam along the detection path. The remaining, overlapping probe and Stokes beams are terminated at a beam dump. Potential interfering light from the pump and from the probe beams is suppressed, the CARS beam being directed through a series of dichroic mirrors, apertures and short-pass filters. An $f = 150$ mm spherical lens focuses the CARS beam on the entrance slit of the 1-m spectrograph, of the Czerny-Turner type, equipped with a holographic grating (Newport Corporation, 2400 grooves/mm). Since the grating has a maximum efficiency for horizontally polarized light, a half-wave plate is placed in front of the entrance slit of the spectrograph and is rotated so as to maximize the recorded signal. Data is collected with a back-illuminated unintensified CCD camera (Andor Technology, Newton DU940N--BV, 2048 x 512 pixels) operated with full vertical binning. The spectrometer provides a dispersion of ~ 0.13 cm^{-1}/pixel and an effective instrument function of ~ 0.4 cm^{-1}.

Measurement cell

Although CARS is relatively mature and today sets a golden standard for point-wise gas-phase thermometry, the accuracy achieved needs to be confirmed and be improved in so far as possible through validation in a controlled environment. In the present work, calibration measurements in different mixtures at varying temperatures play a central role. In various of the projects reported on in thesis, a stainless steel cylindrical cell (length 240 mm, diameter 28 mm) was made used of. A sketch of it is shown in Figure 3.10.
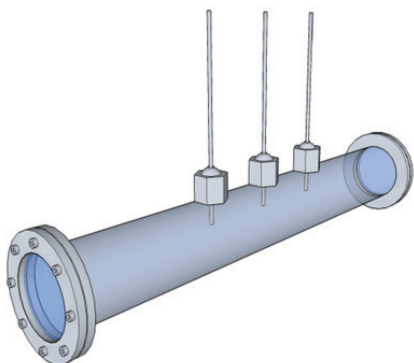

Figure 3.10. *A sketch of the optical cell (length 240 mm, diameter 30 mm), three thermocouples for online monitoring of the temperature being mounted on it. Neither the inlet and the outlet valves or the heating tape which is wrapped around the cell for heating the gas mixtures are shown in the sketch.*

The cell was equipped with anti-reflection - coated quartz windows at both ends and two valves for filling the cell and emptying it. A standard heating tape (Hemi Heating AB, Sweden) with a maximum load of 150 W/m was wrapped around the cell for heating it up to 700K. Three inconel sheathed thermocouples of type K (Pentronic AB, Sweden) were mounted along a line close to the centre of the central axis at an internal distance of 30 mm, their being used for online calibration of the temperature. Baffels were installed to reduce inhomogeneities from potential temperature gradients. The quartz cell windows was shielded by a layer of graphite composite material, access to the incident and outgoing beams only being provided so as to reduce the radiation and the conduction heat losses from the thermocouple, the windows acting as heat sinks.

The binary mixtures for validation measurements of N_2O (Paper VIII) and for the investigation of N_2 spectral line-broadening of H_2 and CH_4 (Papers II, III, and V), were produced using a flowmeter controller (Definer 220, Bios). Each of the species was regulated as a part of a total flow of 2 l/min, the estimated uncertainty of the concentrations being around 1 % according to the specifications of the manufacturer.

An experiment was performed in the optical cell to compare the temporal response of CARS thermometry with the thermocouple measurements obtained. The study was designed in part to illustrate a possible reason for selecting CARS rather than thermocouples for measurements to be carried out in reactive flows. The results, displayed in Figure 3.11, involve a comparison of the two techniques in terms of the temperatures obtained, the following procedural sequence being employed.
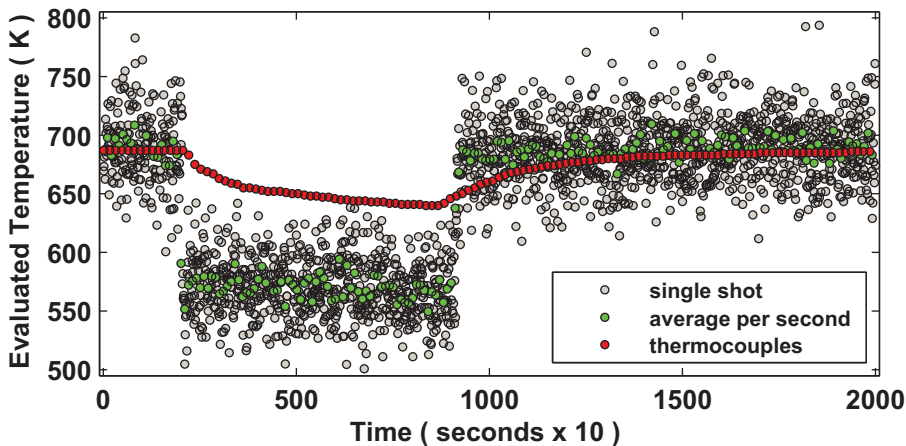

Figure 3.11. *Temperatures registered by CARS measurements and by thermocouples displayed versus time. The experiment was designed to be able to demonstrate the benefits of using this optical technique in measuring reactive flows.*

The cell was first heated to about 700 K and data was collected continuously for 200 seconds. At a point 20 seconds after the start, the inlet and outlet valves were opened to allow nitrogen gas at room temperature to flow through the cell at about 2 l/min. At a point 90 seconds from start, both of the valves were closed, data continuing to be collected then for another 110 seconds. Note that the sampling frequency for CARS is at 10 Hz, which resulted in there being 2000 data points while instead about 130 evenly spread values for the thermocouples being sampled, during this time interval.

The CARS temperatures were measured both on the basis of single-shots and of averaged spectra obtained through the processing of single-shots collected during a 1-second period (10 spectra). In Figure 3.11 it can be seen that the spread (standard deviation) of the CARS temperatures obtained is reduced considerably in moving from single-shot analysis to the statistics that the averaged spectra provide. The overall trend the two approaches reveal is basically the same however, its appearing as a step-function type of dependence on the gas temperature that the procedural sequence adopted provides. The lowest CARS temperature obtained does not reach down to the level of the inlet gas temperature, since the probe volume is located at the centre of the cell. While travelling the distance from the inlet valve to the centre of the cell, the molecules become heated through collisions with the cylinder wall. The behavior shown is quite different in the case of the thermocouples, for which the response time is very slow. While the gas is flowing, the thermocouple does not entirely acclimatize and taking more than 110 seconds after the valves have been closed for this instrument to reach its final temperature limit. Although the lowest temperature limit is not reached entirely, the process occurring appears to be different from that in the case of CARS measurement, this probably being an effect of the heat conduction from the thermocouple junction along the sheathed wire to the lead. Note that the rather considerably thickness (1.5 mm) of the thermocouple is what limits the response time of the instrument, there being other, much thinner alternatives. Nevertheless, the results of the investigation do emphasize the advantages of using the CARS technique to resolve on a time scale events that are much faster than the response time of the thermocouples.

Data acquisition and post-processing

There are two options in acquiring data, that of collecting single-shot spectra and that of accumulating single-shots on the CCD camera so as to obtain averaged spectra. The best option depends upon the measurement situation and on the type of statistics appropriate for the data material at hand. The former method is virtually a necessity for the conditions encountered in turbulent non-stationary combustion devices, as discussed in Paper X, whereas under the more stationary conditions of laminar diffusion flames and of the flat, homogenous

flames produced on a McKenna burner, as discussed in Papers III, A and B, the latter method appears best. If both temperature conditions and the species mixture vary during the period of acquisition, this normally restricts the options. Although it is desired that the physical information be collected from a single-shot spectrum, one should bear the experimental uncertainty concerning the profile of the spectrum that random fluctuations in intensity of each of the individual spectral lines can bring about. It can thus be advantageous to accumulate data since this result in the random fluctuations in intensity being averaged out. Retaining individual saving renders the possibility of simply eliminating unsuccessfully recorded spectra that contain clear artifacts from the material. The averaging of spectra for improving spectral features can be carried out by use of software. The precision and accuracy of the technique was discussed in Paper VIII.

In standard post-processing, the CARS signal spectra collected need to be compensated for by the finite width of the broadband dye laser emission profile. This finite width affects the probability of generating CARS photons at certain frequencies, this skewing the shape of the distribution of the spectrum. The procedure used for cancelling this effect is to divide the resonant CARS spectrum by a reference profile recorded in argon. Since argon has no Raman resonances, this profile reflects the convolution of each the three incident beams and is thus suitable for spectral normalization. The compensation also cancels other features the CARS signal might exhibit, such as the spectral sensitivity of the detection system and various spectral transmission characteristics of the optical components along the detection path. The background, recorded by blocking the red dye laser beam which is not directed at the spectrometer, is subtracted from each of the spectra.

Evaluation procedure

The thermometry is based on contour spectral fitting, a recorded spectrum being compared with a set of theoretical spectra calculated at varying temperature under the experimental conditions at hand. It involves minimizing the sum-of-squares (SSQ) of the residuals of the experimental spectrum and the spectra in the theoretical library, and is carried out by use of a Levenberg-Marquardt nonlinear least-square interpolating algorithm [73]. The temperature to be employed is decided upon by determining the spectrum in the theoretical library that is most similar in shape to the experimental spectrum. This requires careful consideration of the measurement conditions, which usually involves a considerable number of experimental parameters, such as pressure, species concentrations, and Raman linewidth model, for example. In this context one refers to the Raman linewidth model as an experimental parameter, the species-specific coefficients being implied by the mole fractionally weighted proportions of the collisional partners. In thermometry, the mentioned above

parameters are usually modeled explicitly. In the case of relative concentration measurements, the spectral fit is processed along with additional dimensions, theoretical libraries being calculated not only with temperature serving as the progressive variable but also with varying degrees of resonant species contributions. Other experimental parameters, such as instrument function, non-resonant susceptibility, linear dispersion, and calibration channel wavelength are treated instead as fitting parameters, since they are intrinsically determined by minimizing the SSQ in the parametric space spanned by these parameters. To be correct, the global solution obtained needs to take account of all of the floating variables, the temperature and the relative species concentration included. Slight adjustments in the fitting parameters hardly effect the outcome in the evaluated temperatures. There have been attempts, however, to use the impact that non-resonant susceptibility has on vibrational CARS spectra in more quantitative terms, such as extracting relative concentrations of water vapor by using this serve as a constraint on the spectral fit obtained [74]. It is not only experimental parameters that need to be dealt with for accurate simulation of experimental spectra to be achieved, since there is also the need of having adequate theoretical parameters. The Herman-Wallis factor is one such parameter, one that appears in the amplitude of the resonant terms of the third-order susceptibility. This factor impacts the linestrengths non-uniformly, thus contributes critical to the temperature accuracy of RCARS and deserves special attention accordingly.

3.3.1   Short-wave-pass filter

For the calibration measurements carried out it was a necessary to reduce the stray light encountered through reflections on the cell glass windows as much as possible (Papers II, III, V, and VIII). A solution to this was that of angle tuning a newly produced short-wave-pass filter (Semrock, Razor edge), see Paper IX and section 4.4. The specified cutoff wavelength of this filter, 561 nm, could be varied according to

$$\lambda = \lambda_0 \left[1 - \left(\frac{\sin \theta}{n_{eff}} \right) \right]^{1/2} \tag{3.14}$$

where λ_0 is the specified wavelength of the filter, θ is the angle of incidence, and n_{eff} is the effective refractive index. At an angle of incidence of ~24 degrees, the cut-off wavelength of this filter is around 532.0 nm. The cutoff wavelength can be positioned precisely for a specific experimental situation through fine adjustments of the incident angle. How this optical component is implemented is shown in Figure 3.12.
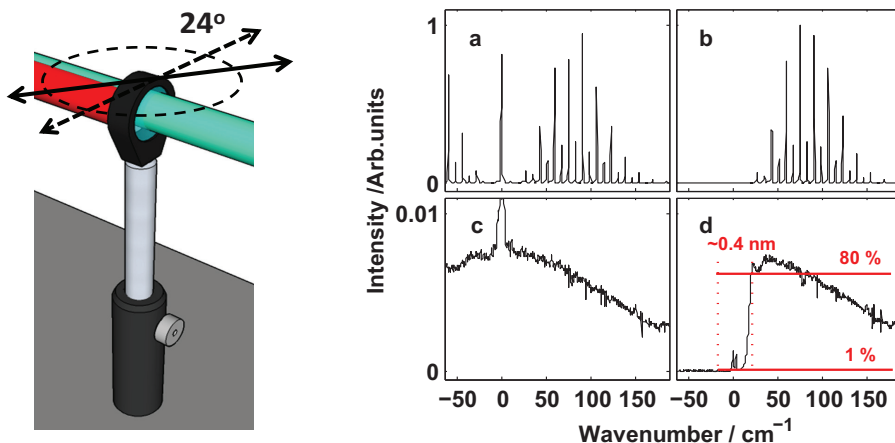
Figure 3.12. *Spectra recorded at room temperature and atmospheric pressure.* **a)** *A rotational CARS spectrum recorded in pure N$_2$ without short-wave-pass filter at positive Raman shifts, together with a stray light peak at 532.0 nm and a rotational CSRS spectrum at negative Raman shifts.* **b)** *Same as in a*) *but with the Razor Edge filter mounted along the detection path.* **c)** *A non-resonant rotational CARS spectrum recorded in methane without use of a short-wave-pass filter.* **d)** *Same as in* c) *but with a razor edge filter in the detection path.*

3.3.2   Mirror for H$_2$ (S$_0$) detection

One of the key topics taken up in Paper III was the simultaneous detection of the H$_2$ S$_0$-spectral line and of the N$_2$ CARS signal, this enabling the relative concentrations of N$_2$ and H$_2$ to be determined. The H$_2$ S$_0$-transition appears spectrally, at a Raman shift of about 354 cm^{-1}, far separated from the N$_2$ CARS spectral envelope, which covers a region of up to about 250 wavenumbers at temperatures of below 800 K. With a limited spectral detection window of about 280 wavenumbers this did not appear feasible, however, as illustrated in panel (a) of Figure 3.13. Normally, the grating can be rotated in order to move the detection window so that both spectral contributions can be detected, as illustrated in panel (b). The problem then is that large parts of the N2 CARS signal fails to be detected, reducing the thermometric accuracy of the technique. The solution to this delicate problem arrived at inserting a mirror to simply reflect the H$_2$ S$_0$-spectral line onto the detection window, as shown in panel (c). If the mirror is carefully aligned, the H$_2$ S$_0$-spectral line can be positioned at the very edge of the detection window without causing any spectral interference with the N$_2$ CARS signal.
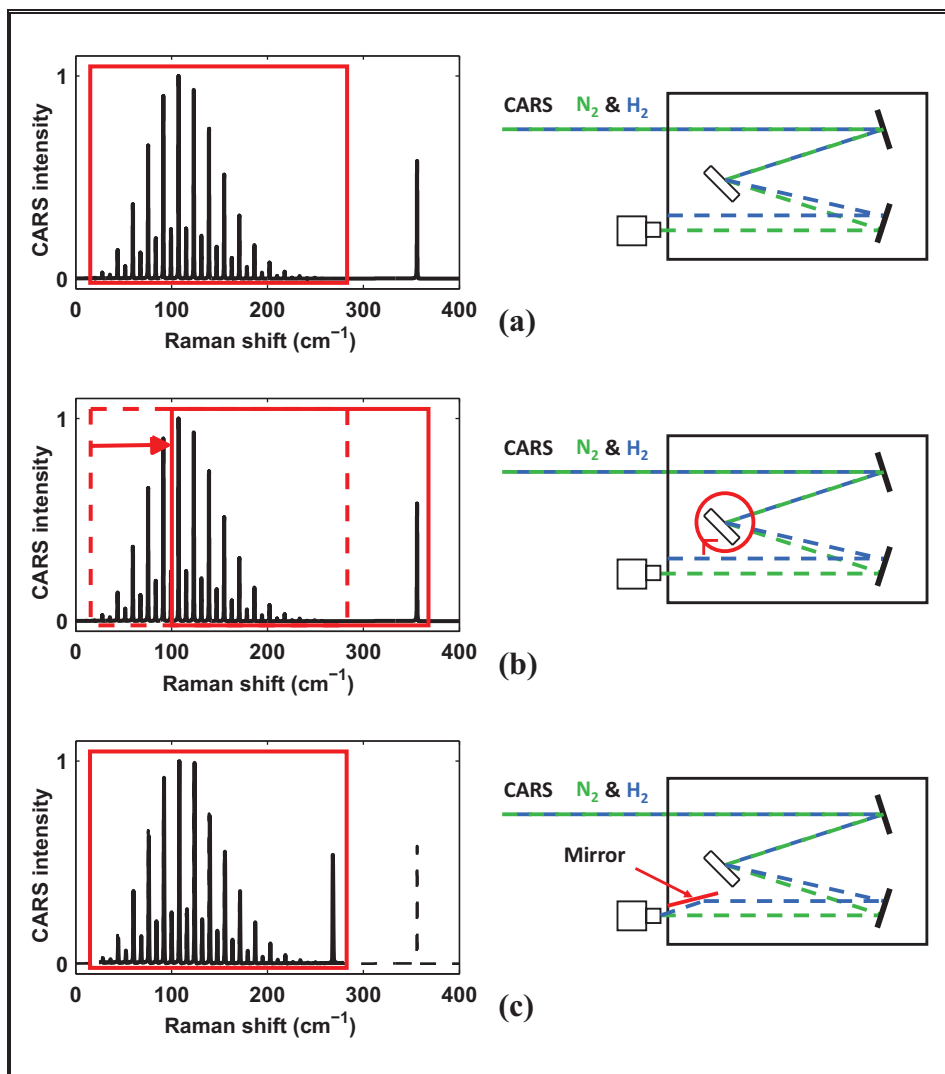
Figure 3.13. (a) *The limited range of the spectral detection window.* **(b)** *The rotated grating used to collect the spectral contributions from both N_2 and H_2.* **(c)** *The inserted mirror for detecting the H_2 S_0 spectral line together with the entire N_2 spectral envelope.*

3.3.3   Detection with improved dynamic range

For measurements carried out in a low-swirl turbulent flame, see Paper X, several diagnostic problems needed to be solved, the most critical of these being the large dynamic range of CARS signal intensities when probing low as well as high temperatures shot-to-shot. This is a well-known issue in the application of CARS to turbulent flames, where the variation in intensity may encompass 2-3 orders of magnitude and needs to be handled by the detection system. A maximum signal-to-noise ratio at flame temperatures generally requires the highest achievable pulse energies, yet this easily leads to the detector becoming saturated for CARS signals generated at low temperatures. Although different solutions to this problem have been realized [75, 76], all of them involve making the experiments carried out more elaborate.

The way this issue was dealt with here was to replace the spherical lens with a cylindrical one in focusing the signal beam on the entrance slit of the spectrometer, this being combined with making use of a "multi-track" acquisition option in the camera. Such a detection scheme distributes the incident light directed at the detector chip more evenly, thus avoiding the saturation of individual pixels, its being possible with use of the "multi-track" mode to register 32 separate 16-bit spectral tracks. It was found to be important to select the settings in such a way that the read-out rate at 10 Hz was maintained, so as to match the repetition rate of the laser flash-lamps. Later, the intensities of the 32 separate tracks were added in software post-processing, as if they were detected by use of full-vertical-binning (FVB). This resulted in an appreciable increase in the dynamic range of the detection system, allowing standard pulse energies of around 20 mJ per pulse to be employed without any neutral density filters in the detection path being needed, allowing the spectra produced through the probing of hot and cold flame pockets in the flame to be detected shot-to-shot.

The principles in use of this setup are shown in the upper panel in Figure 3.14, in which a normal detection scheme having a spherical lens located in front of the entrance slit can be seen, a scheme that can be imagined as replacing use of a cylindrical lens. In the panel below this, two examples of single-shot spectra are displayed that were recorded in the work reported in Paper X. One can note the very large variation in intensity between the hot and the cold spectra, such as one can expect for RCARS measurements obtained in a turbulent flame. A noisy background can be seen in the high-temperature spectrum, one which is due to the increased read-out noise of the multi-track mode, the level of which is related to the square root of the number of tracks.
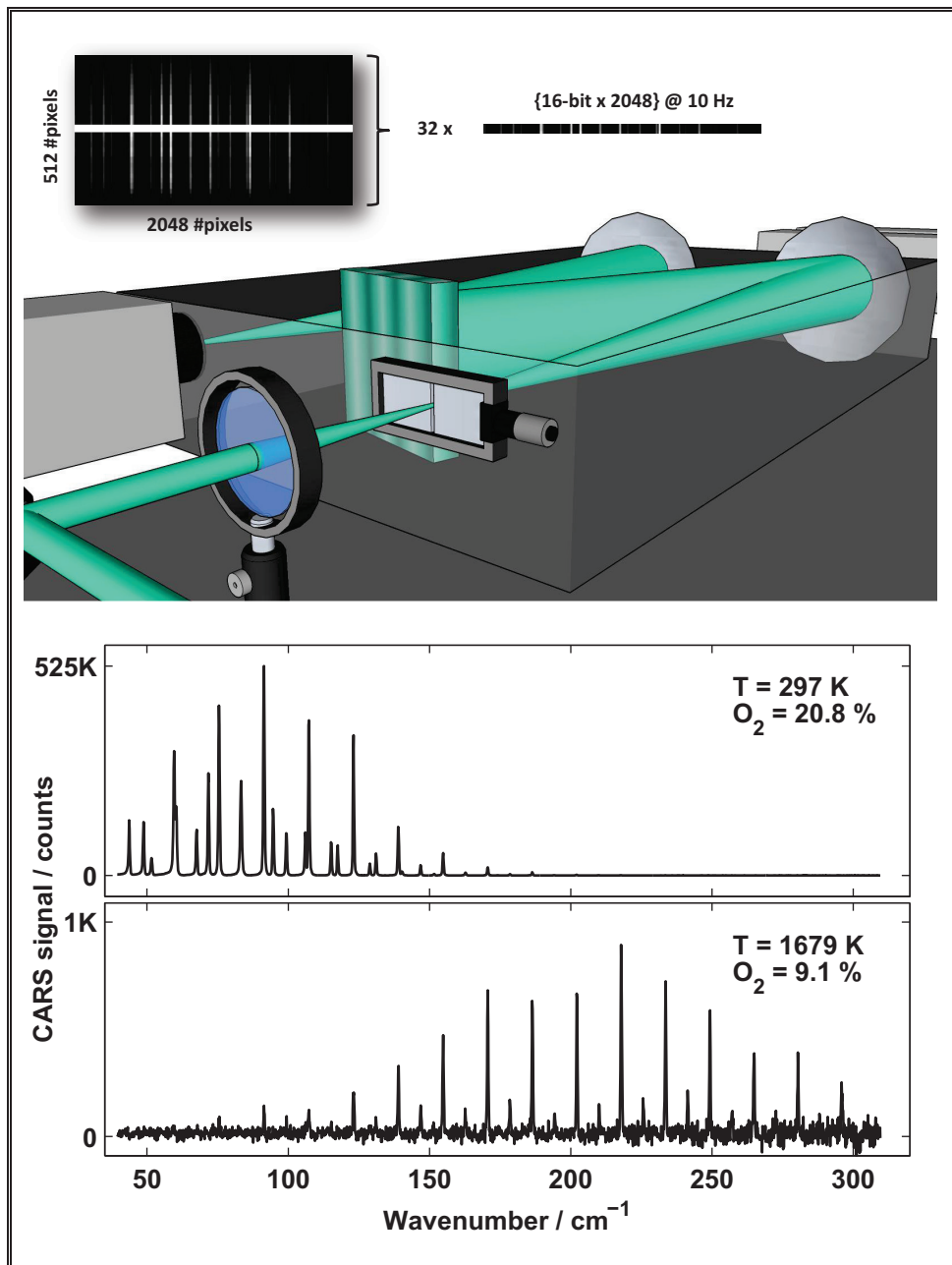
Figure 3.14. (Above) The detection system that was implemented in the work of Paper X, involving the spherical lens in front of the spectrometer being replaced by a cylindrical one and use being made of a multi-track mode for the camera. (Below) Two examples of CARS spectra showing the large difference in signal intensity between the hot and the cold signals.

3.3.4   Time-resolved picosecond RCARS

In Papers IV and V, a recent experimental development was explored aimed at measuring the S-branch N_2 Raman linewidths by use of time-resolved picosecond pure rotational CARS. The technique in question developed during the past few years, has become a candidate for gas-phase thermometry having the same capabilities as a standardized nanosecond setup [77-79]. This approach, having the ability in addition of delaying the probe pulse beyond the temporal envelope of the time-coincident pump and Stokes pulses, has the advantage of being able to circumvent some of the difficulties that tends to be connected with experiments in the nanosecond regime, such as the non-resonant background [77] obtained and the smeared vibrational CARS signals produced [78]. The capabilities just referred to, together with the high peak-power of the picosecond laser pulses produced also permits the rapid determination of accurate Raman linewidths up to elevated temperatures of a level relevant for flame studies. At each temperature, the technique may provide a complete set of *J*-specific line-broadening coefficients. The method is based on monitoring the *J*-dependent CARS signal decay as a function of probe delay, such that the collisional dephasing of each Raman coherence is detected in the time-domain. At atmospheric pressure, RCARS from N_2 is well within the pressure limits of an isolated line approximation [80]. Thus, the Raman Lorentzian linewidth is given by

$$\Gamma_{J"} = \frac{\tau_{CARS,J"}^{-1}}{2\pi c} \tag{3.15}$$

where c is the speed of light (cm/s), $\tau_{CARS,J}$ is the exponential decay time constant for the coherence decay (s), and $\Gamma_{J"}$ is the Raman linewidth (FWHM, cm^{-1}).

Time-domain measurements

The time-domain measurements were performed employing a picosecond RCARS experimental apparatus, one that is outlined in Papers IV and V. The alignment configuration and many of the optical components were similar to those in a nanosecond setup, except for one crucial point, that of a mechanical delay stage placed in the Stokes beam path to reduce to zero the delay between the pump and the Stokes present in the initial setup, in which a beam splitter was used to split the red dye laser beam into pump and Stokes beams of equal-intensity. By way of comparison, a 10 ns pulse extends about 3 m into space whereas a 100 ps pulse extends a distance into space of only about 3 cm. The extra distance travelled (represented by the separation distance in Figure 3.8) not problematic at all in a nanosecond CARS setup, would be truly problematic

in a picosecond CARS alignment such as that used here. The laser system consisted of two 20 Hz regeneratively amplified mode-locked Nd:YAG lasers. The one was used to pump a dye laser, its consisting of an ASE (amplified spontaneous emission) source followed by two amplification stages provided with an ethanol dye solution of DCM, this laser being used to produce the pump and Stokes beams. The second in turn, provided the narrowband probe beam. The pulses were approximately 100 ps in widths. Both lasers were locked to the same RF source, making precise electronic timing of the probe pulse with respect to the pump and the Stokes pulses, extending from -200 ps to + 1 ns in 20 ps time-steps, possible.

The time-domain measurements are performed by use of a procedure shown in Figure 3.15.
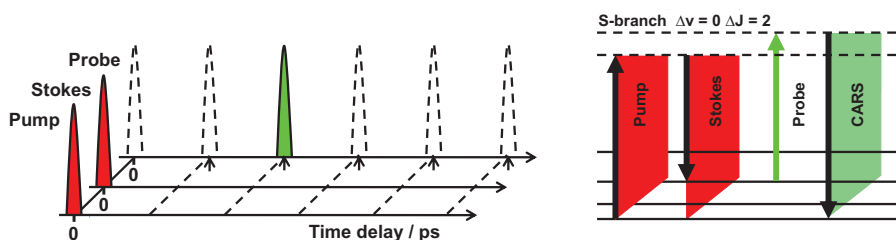
Figure 3.15. *Diagrams of how the three pulses were synchronized. The probe pulse was delayed in time relative to the pump and Stokes pulses. The procedure was to resolve the dephasing rates in the temporal decay of the CARS signal, a decay resulting from collisions in the time-intervals between the pump pulses and the probe pulse.*

The data was extracted by mapping the *J*-dependent dephasing rates of the temporal decay of the CARS signal. The coherence decays were detected in the time-domain by measuring the integrated intensity of the individual spectral lines as a function of probe delay. Spectra were recorded for a series of approximately 30 probe delays. At each probe delay, 20 laser shots were accumulated on the CCD per readout, a series of 40 readouts being individually saved. The *J*-specific exponential decay constant, $\tau_{CARS,J''}$ was determined by an exponential fit to the decay. It was used in calculating the frequency domain Raman linewidth $\Gamma_{J''}$ by use of Eqn. (3.15).

The collisional dephasing, that occurs during the time-interval between the excitation of the Raman coherences and the probe beam scattering of these, is dependent both on the *J*-level and on the collisional partner. In pure nitrogen, the rate of decay decreases with rotational level (see the discussion of this in section 3.2.1). With an increase in the probe delay, the drop in intensity of the spectral lines at the lower Raman shift occurs much faster than they do at higher Raman shifts. This makes the spectrum appear hotter than it would otherwise. The attempt is made in Figure 3.16, to explain this more thoroughly, picosecond RCARS spectra at room temperature with different probe delays being analysed

by use of a standard nanosecond spectral fitting routine (in analogy to what is presented in Ref.[77]). One can see how the evaluated temperature increases markedly as a function of probe delay. For example at a delay of 300 ps (the spectrum in panel (b) of Figure 3.16) the spectrum is estimated as having a temperature of 388 K.
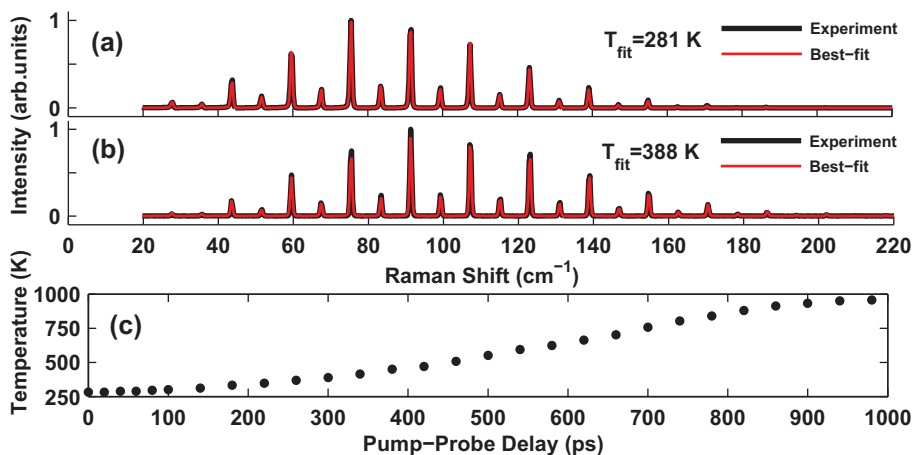

Figure 3.16. *Picosecond N_2 RCARS spectra recorded at room temperature with use of two different time delays between the pump and the probe, (a) zero delay and (b) 300 ps delay. (c) The temperatures are evaluated by use of a standard nanosecond spectral fitting routine performed in the frequency domain.*

In order to avoid non-resonant background and smeared vibrational CARS signals, the probe needs to be delayed beyond temporal overlap with the pump and the Stokes pulses. As has been pointed out, this results in a "heating" of the recorded spectra, although this effect decreases at elevated temperatures since the coherence decays there become less *J*-dependent [77]. Although it might be thought that the spectral heating would produce an undesirable alternation in values of the data, such effect turned out to be quite useful and desirable. When one has no *a priori* knowledge of the temperature, the collision partner, or the species concentration, the Raman linewidths of a given measurement can be determined by means of a probe-delay scan. Potentially, a possibility of this sort would in principle negate altogether the need of a linewidth model in picosecond rotational CARS thermometry (as was explored in Paper C). Also, this technique for acquiring in-situ Raman linewidths can provide useful data to support nanosecond CARS work generally, there being a current lack of literature regarding various collision partners.

DEVELOPMENTS AND APPLICATION

In this chapter the results of the appended papers are summarized in terms of different topics to make a more integrated discussion of the material possible. The chapter also includes additional material and the discussion of a variety of questions that were not brought up in the papers.

4.1 RAMAN LINEWIDTHS – Papers I, II, III, IV, and V

Improvement of rotational CARS thermometry in fuel-rich hydrocarbon flames by inclusion of N_2-H_2 Raman linewidths

Aims

The temperature sensitivity of the CARS line intensities originates mainly from the thermal population of the different ro-vibrational levels contained in a Boltzmann distribution, but also in part from various less certain parameters, such as the Raman linewidths. These linewidths, related to the collisional broadening of the spectral lines, are dependent on the temperature and the rotational quantum number J, as well as on the collisional partners involved. It is well known that obtaining an adequate assessment of the accuracy of rotational CARS measurements, conducted by means of spectral contour fitting is highly dependent upon an adequate Raman linewidth model being employed.

Figure 4.1. *A fuel-rich premixed ethylene/air flame stabilized on a McKenna burner.*

In a previous study, in which N_2 CARS thermometry was performed in the product gas of premixed hydrocarbon flames [81], the collisional broadening of major species colliders such as N_2 [6], H_2O [31], CO_2 [32], and CO [34] was incorporated. The measurements were conducted at a fixed height, the equivalence ratio of the fuel/air mixture being varied, as shown in Figure 4.1. However, in the products of premixed ethylene/air flames operated in the fuel-side region at stoichiometries ranging from 1.0 to 2.5, the gas mixture contains five major species (N_2, H_2O, CO_2, CO and H_2), the mole fraction of H_2 increasing almost linearly from 0% to about 20% according to chemical
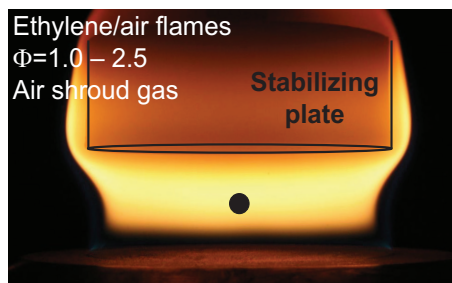
equilibrium calculations. Yet at the time of the study in which it was found to be the case [81] there was a lack in literature on how N_2 is perturbed by H_2, this thus being omitted in the modeling. In view of this, work to clarify this matters was initiated [82, 83], an extended set of N_2-H_2 line-broadening coefficients being published for the first time then in 2008 by Bonamy and co-workers [35].

Results and discussion

As a first attempt, these newly derived N_2-H_2 Raman linewidths were included so as to re-fit the data recorded in the work of Vestin *et al*. [81], the results being compared to those obtained with use of the previous models. When the line-width data from all of the five major species colliders were included, see Figure 4.3, the predicted temperature at a stoichiometry of 2.5 increased by about 4% in comparison with a model taking account only of self-perturbed N_2 spectral lines, see Figure 4.2. About half of this difference was found to be a direct consequence of including the N_2-H_2 line-broadening coefficients. The reason for the discrepancy in thermometry was found to be related to the *J*-dependence of the species-specific linewidths. As can be seen in Figure 4.3, the collisional dynamics when N_2 is perturbed by H_2 is much less dependent on *J* than when N_2 is perturbed by itself. Consequently, in neglecting these coefficients in the model description, the theoretical spectra become skewed relative the experimental spectra which affects the spectral fits and the estimated temperature.

Note that the model as a whole is a linear combination of the specific coefficients of the different colliders weighted in accordance with the mole fractions of the perturbing species. Thus, in a mixture of different proportions of several different species colliders it is difficult to quantify the exact impact on the thermometry that each of the perturbers has, see discussion in Ref.[81]. It would be desirable to find a direct connection between the discrepancies found in Kelvin and the proportions of each the perturbing species. However, the major parts of the previous model and of the one implemented in Paper I are the same, except for the proportions of N_2 self-broadened coefficients and of N_2-H_2 coefficients being partly interchanged. As can be seen in Figure 4.2, the differences in Kelvin between the different models increase about linearly, since they are correlated with the increased production of H_2 above stoichiometry in more fuel-rich mixtures. In conclusion, it can thus be estimated that if the N_2-H_2 Raman linewidths in N_2 RCARS thermometry performed in a flame environment in the presence of H_2 are neglected, the evaluated temperatures become underestimated by roughly 2K for each separate percentage of H_2.

In examining the results presented in Figure 4.2, one can note that the overall temperature dependence viewed as a function of the equivalence ratio appears non-intuitive. Normally, in calculations of the adiabatic flame

temperatures, the highest temperature obtained for premixed hydrocarbon flames are found in fuel-air mixtures of around $\Phi=1.1$.
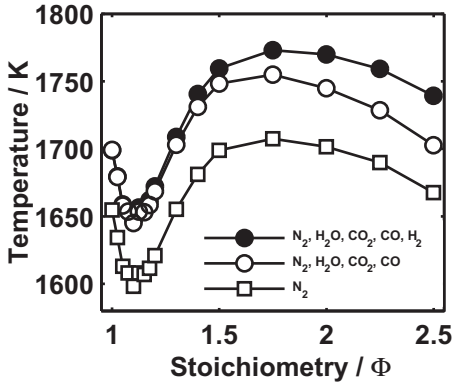

Figure 4.2. *RCARS temperatures evaluated on the basis of N_2 spectra recorded in the product gases of premixed ethylene/air flames. The study was carried out in the fuel-rich region up to a stoichiometry of 2.5. The spectral fits were conducted with use of reference libraries based on three different N2 spectral-line broadening models. The closed circles show the results for the most recent model (Paper I) in which N_2-H_2 Raman linewidths are included. The open circles show the results for the model the implementation of which is described in Ref. [81].*
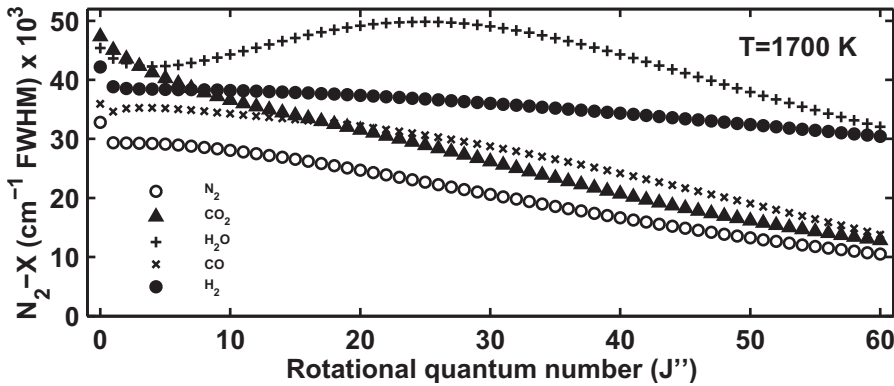
Figure 4.3. *The J-dependence of species-specific N_2 Raman linewidths perturbed by a collider X (N_2-X). The dependence at a temperature of 1700K is shown for five major species (N_2, CO_2, H_2O, CO and H_2) in the products of a fuel-rich hydrocarbon flame.*

The "sudden dip" in the temperature profile obtained can be explained in terms of the heat losses to the water-cooled burner disc being higher, due to the very short stabilization distance, caused by the high burning velocity in mixtures of around $\Phi=1.1$ [84]. For the temperature data presented here, the points having the highest equivalence ratios are overestimated a bit, since the results are higher than obtained at an adiabatic flame temperature. It can be estimated that the technique making use of accumulated spectra recorded in pure nitrogen or in air has uncertainties that are less than 1-2 %, whereas for the flame environment this percentage is higher. The deviation could be explained by uncertainties in the gas composition which is found affecting the proper weighting of the

contributions of the different species-specific Raman line widths involved. Since there are not only these but also other sources of uncertainty, further work concerning the accuracy of these measurements needs to be carried out. For example, in replace the Herman-Wallis factors of Martinsson et al. [6] by those of Tipping and Ogilvie [49], the evaluated temperature would be lowered by about 10 K (see Paper VI).

Rotational CARS N_2 thermometry: Validation experiments for the influence of nitrogen spectral line broadening by hydrogen

Aims

As a natural consequence and intrigued by the results in Paper I, the impact on RCARS thermometry from the influence of N_2 spectral line-broadening by H_2 needed to be confirmed.

Results and discussion

To perform validation measurements in binary mixtures of N_2 and H_2 under temperature-controlled conditions, a calibration-optical cell with a heating capacity and the capability of on-line monitoring of the temperature was constructed. The measurements were performed at three different temperatures, those of about 300K, 500K, and 700K, the H_2 content being varied within the range of 0-90%. The evaluation of spectra was conducted with use of two different theoretical libraries, the one composed of N_2 self-broadened coefficients only and the other using a Raman linewidth model implemented as a weighted linear combination of the species-specific contributions (N_2-N_2 and N_2-H_2), in accordance with their respective mole fractions. The results of this investigation are presented in Figure 4.4, where the CARS-evaluated temperatures are displayed in relation
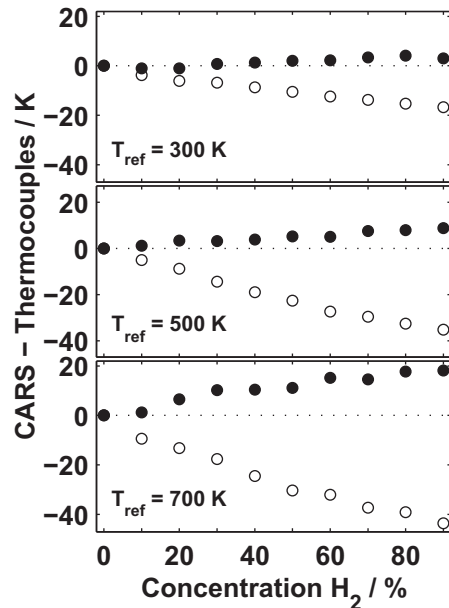

Figure 4.4. *CARS temperatures evaluated on the basis of N_2-N_2 Raman linewidths only (open circles), and weighted N_2-N_2/N_2-H_2 Raman linewidths (closed circles) displayed relative to the reference temperature as a function of hydrogen concentration.*

44

to the thermocouple temperature that serves as reference. The major temperature underestimations obtained in employing a Raman linewidth model with only N_2 self-broadened coefficients can be noted, the thermometry being much more successful with use of linearly combined N_2-N_2 and N_2-H_2 Raman linewidths.

The impact on the thermometry evident here can be explained by the combined consideration of Figure 4.5 and Figure 4.6, taking note of the Raman linewidths of the N_2-N_2/N_2-H_2 colliding systems and the effects these have on the N_2 RCARS spectral envelope.
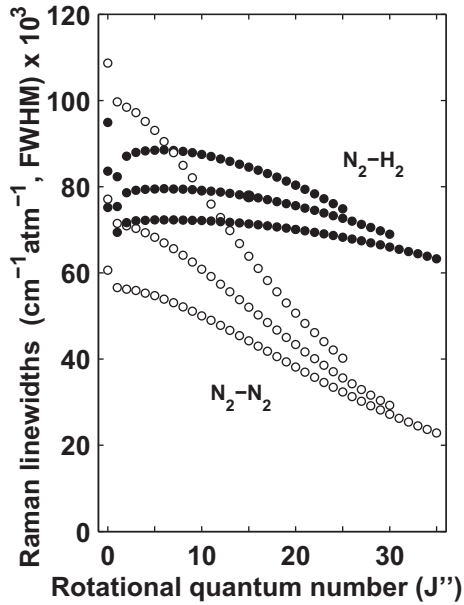
Figure 4.5. *The J-dependence of N_2 line-broadening coefficients perturbed by N_2 and by H_2 displayed for temperatures of 300K, 500K, and 700K (from above to below).*
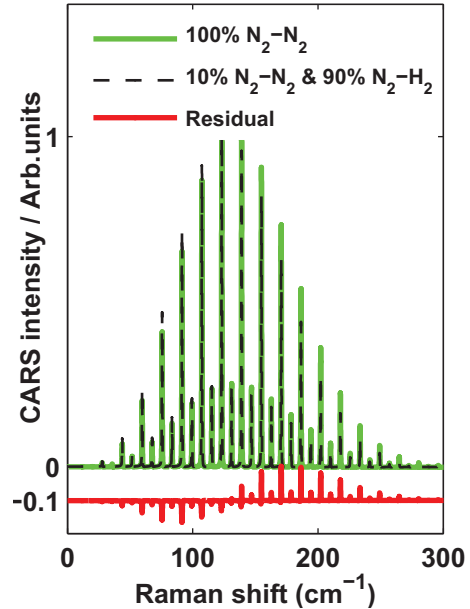
Figure 4.6. *Theoretical RCARS spectra at 700K calculated so as to simulate a mixture with 100% N_2, and 10% N_2 and 90% H_2. The residual obtained in subtracting the latter from the former indicates clearly a shift in position between these spectral envelopes.*

Since the *J*-dependence of the N_2-H_2 line-broadening coefficients is much less pronounced than that of N_2-N_2, the collisions shift the position of the N_2 CARS spectral envelope. This can result, if the N_2-H_2 Raman linewidths are neglected in modeling of the RCARS spectra recorded in binary mixtures with N_2 and H_2, the reference library will interpreting the temperature of the experimental spectra as being relatively lower.

The second analysis was for determining whether the direct processing of the S-branch linewidths from the Q-branch (RPA) alters the accuracy of RCARS estimated temperatures. Spectral fits were performed by use of both RPA and S-branch coefficients derived from pure rotational calculations, its being shown that the deviation in Kelvin between them were negligible, their being less than 2 K at 300 K. The differences between the sets are based on the anisotropic contributions that are omitted in the RPA processing, although this affects mainly the lowest rotational quantum numbers. At temperatures of 300K and higher, the SSQ of the contour fitting depends more on the spectral lines that originate from the higher-order rotational quantum numbers involved.

Rotational CARS thermometry in diffusion flames: On the influence of nitrogen spectral line-broadening by CH_4 and H_2

Aims

Following the results obtained that were reported in Paper II, the aim was to apply the knowledge gained to the fuel-side of a H_2 diffusion flame, where the heating of the fuel prior to ignition was studied. A solution to the need of weighting the N_2 line-broadening proportions of each specific collider was found, by simultaneous detection of the H_2 S_0-transition allowing the relative concentrations of N_2 and H_2 to be determined.

In addition, the effect on N_2 RCARS thermometry being perturbed by CH_4 could be of interest to investigate, since the environment here is one that resembles that of a CH_4 diffusion flame. Since, as been pointed out, there have been very few detailed studies of the N_2-CH_4 colliding system, and the data presented [85] concerns only a few coefficients.

Results and discussion

The flame studied here was produced on a Wolfhard-Parker slot type burner, constructed as an exact replica of the one used at NIST [86], see Figure 4.8. The measurements were performed by scanning the flame horizontally at 1 mm height above burner (HAB), the laser beams propagating along the slots to achieve high spatial resolution in the direction where strong temperature gradients exist. To evaluate the relative N_2/H_2 concentrations, the experiments were designed to detect the N_2 CARS envelope simultaneously with the first transition of H_2, see section 3.3.2. It should be emphasized that evaluation of the concentrations involved was not carried out through use of a standard procedure, by means of a contour-fitting routine progressed along a two-dimensional grid with concentration and temperature.
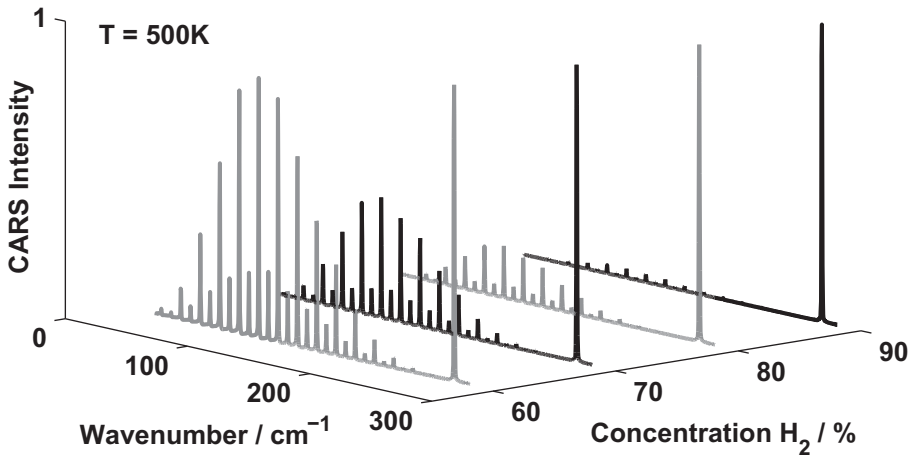
Figure 4.7. *Recorded RCARS spectra in binary mixtures of N_2 and H_2 at a temperature of 500K. The H_2 S_0- transition, which normally appears at a Raman shift of 354 cm^{-1}, is specially designed here to be detected at the far edge of the detection window.*

Figure 4.8. *A H_2-diffusion flame attached on a Wolfhard-Parker burner [86]. The dimension of the inner slot are 40 mm x 8 mm and of the two outer slots 40 mm x 16 mm (length x width), respectively.*
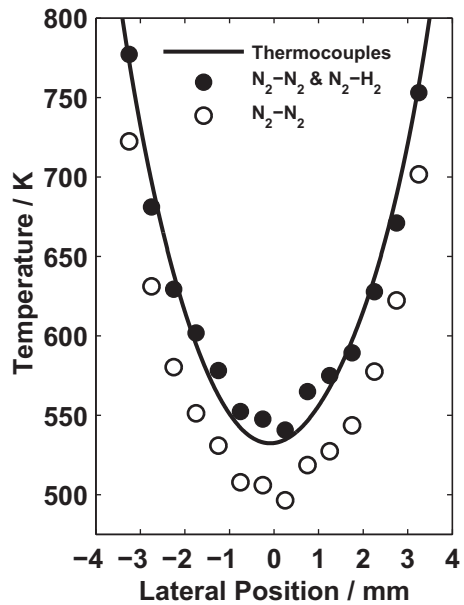
Figure 4.9. *CARS-estimated temperatures obtained using two sets of line-broadening coefficients (N_2-N_2 and N_2-N_2/N_2-H_2) compared with results of thermocouples, as measured at 1 mm HAB.*

Instead, an experimental database was created from calibrated cell measurements in binary mixtures of N_2 and H_2 within the temperature range of 300-700K, using the same detection scheme as applied to the flame. The measurements were conducted in order to describe how the concentration ratio of H_2 to N_2 is related to the intensity ratio of the H_2 (S_0) spectral peak to the rotational N_2 CARS signal measured in the flame. The results are presented in Figure 4.7.

The thermometry was performed by use of a two-step iterative scheme. First a rough estimate of the temperature is achieved by use of pure N_2 self-broadened coefficients to determine from which temperature region of the experimental database the relative concentrations should best be extracted. The intensity of the H_2 (S_0) spectral peak is affected not only by concentration, its also being strongly dependent upon the temperature, since the fractional population of H_2 at the ground level rotational state decreases with temperature, weakening this transition. When information concerning the relative concentrations of N_2 and H_2 had been obtained, the next step was to fit the spectra obtained, using a library implemented by weighted species-specific broadening contributions of the N_2-spectral lines. The results are shown in Figure 4.9, which indicates the CARS-estimated temperatures as compared with the temperatures measured by the thermocouples. The discrepancy in CARS thermometry when employing the two different sets of coefficients (N_2-N_2 and N_2-N_2/N_2-H_2) can be seen. Approximately, the same deviation of around 50K is found for each of the lateral positions (see Figure 4.4 above which helps to explain this). In Figure 4.9, at the lateral position equals zero, the relative concentration of H_2 was found to be about 95%, and at a temperature of about 500K the difference could be expected to be around 50K (see to Figure 4.4). More towards the flame front, at a lateral position about 3 mm, the relative concentrations of N_2 and H_2 are about fifty-fifty, and at a temperature of 700K the difference could likewise be expected to be around 50K (see to Figure 4.4).

The second investigation, in which instead N_2 was probed in calibrated binary mixtures with CH_4, showed there to be only an insignificant change in the evaluated temperatures, although the thermometry was performed with use of only N_2 self-broadened coefficients. The results indicate that no explicit N_2-CH_4 Raman linewidths need to be used in the spectral fitting routine, the N_2-N_2 Raman linewidths providing a reasonably good approximation of the nitrogen spectral lines perturbed by CH_4. This simplifies RCARS thermometry on the fuel-side of methane diffusion flames, since there is an apparent lack of broadening coefficients for this colliding system.

Picosecond pure rotational coherent anti-Stokes Raman spectroscopy for time-domain measurements of S-branch N_2-N_2 Raman linewidths

Direct measurement of S-branch N_2-H_2 Raman linewidths using time-resolved pure rotational coherent anti-Stokes Raman spectroscopy

Aims

The potential of acquiring S-branch N_2 Raman linewidths from time-resolved picosecond RCARS measurements was explored in a wide range of temperatures, 294-1466 K and was applied to two colliding systems. N_2 was studied in collisions with itself since this represents the most important system in combustion applications. In addition, a system in which N_2 is perturbed by a foreign-fuel species collider was investigated. The latter system, N_2-H_2, was related to the series of studies involving implementation (Paper I), validation (Paper II) and application (Paper III) taken up earlier. The species-specific sets of line-broadening coefficients obtained were then tested in individual series of calibration measurements, in which comparisons were made to the results obtained with coefficients of dynamical modeling. The results being used to quantify the sensitivity of nanosecond rotational CARS thermometry to the linewidth model employed. The results were discussed in two separate publications since the material appeared to be too extensive to sensibly be included within a single publication.

Results and discussion

The measurements were performed in accordance with what was discussed in section 3.3.4. At the temperatures investigated, spectra were recorded in a series of probe delays, in N_2/H_2 binary mixtures in which the H_2 content was varied, being set of 0%, 50% and 80%, respectively. As an example, RCARS spectra recorded at 395 K in a mixture of 80% H_2 / 20% N_2 are shown for two probe delays in Figure 4.10. The strong impact of the collisional dephasing on the N_2 spectral envelope can be regarded as a function of probe delay. The intensity of the signal was reduced by a factor of ~3 in changing the delay of the probe from 380 to 460 ps. The dynamic range of the N_2 data (probe delays 0-1ns), obtained at room temperature, spanned six orders of magnitude in signal levels. It is of interest to note that the H_2 S_0-transition had the same drop in signal level over a 5 ns delay of the probe relative to the pump and Stokes beams.

   Coherence decay curves were obtained by integrating the counts of each respective CARS spectral line as function of probe delay. The *J*-specific exponential decay constants were determined by fitting a linear regression to the natural logarithm of the single exponential decay. In order to extract the N_2-H_2 Raman linewidths, a simple linear extrapolation was made from the 0% and

50% H_2 concentrations. One validation of the linear extrapolation was that of agreement being found with the measured N_2-H_2 line-broadening coefficients for the 80% H_2 mixture. Figure 4.11 displays the measured N_2 Raman linewidths obtained at 1466 K in the three different mixtures, the error bars representing the +/- 2 σ uncertainty. For the measurements in pure N_2, the uncertainties of the extracted Raman linewidths are lower due to an increase in the overall signal level. The RCARS signal has a square dependence on the number density and in addition the dephasing of the N_2 coherences gets increased in the presence of H_2. Whereas the 2 σ uncertainty in pure N_2 was typically 2-3% of the Raman linewidth, it was typically 5-6% in the case of 20% and 50% N_2.
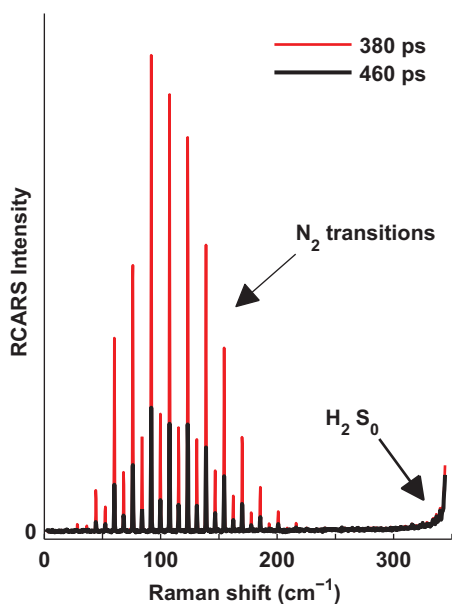
Figure 4.10. *RCARS spectra recorded in a mixture of N_2 and H_2 (20% N_2 / 80% H_2) at 395 K for probe delays of 380 and 460 ps. The Lorentzian wing of the H_2 S_0 transition is noted.*
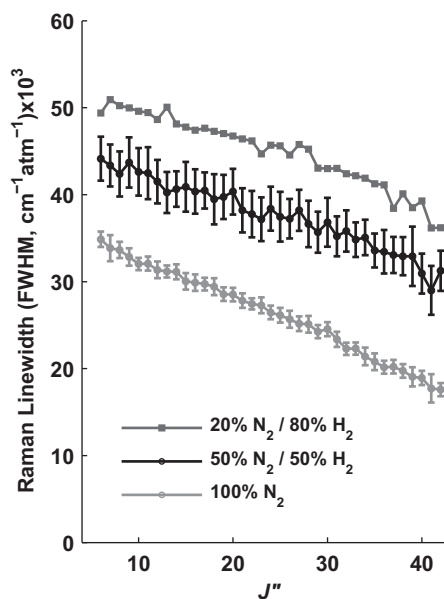
Figure 4.11. *Measured time-domain S-branch Raman linewidths for N_2 mixtures with H_2 at 1466 K. The error bars represent the +/- 2 σ uncertainty found in the measurement.*

The extracted time-domain N_2-H_2 (closed black circles) and N_2-N_2 (open black circles) Raman linewidths are presented in Figure 4.12, together with results of the semiclassical RB (solid line) calculations of the S-branch N_2-H_2 system that was carried out. The measurements were performed at temperatures of 294 K, 395 K, 495 K, 661 K, 868 K, 1116 K, and 1466 K, the calculations being compared at these temperatures. The linewidths generally decrease with

temperature, as can be seen in Figure 4.12, in which the line-broadening coefficients are expressed as cm^{-1}/atm at a full-width-half-maximum (FWHM). A discrepancy can be observed in comparing the absolute levels, but with regard to the *J*-dependency of the coefficients it can be seen that the calculations are in close agreement with results of the experiments.
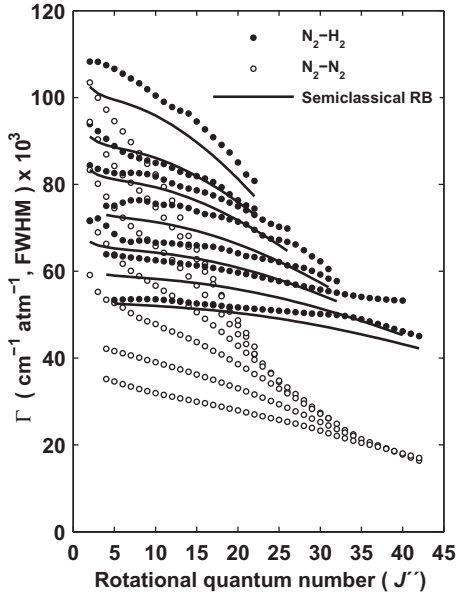

Figure 4.12. *Measured time-domain S-branch linewidths for N$_2$-H$_2$ (closed black circles) and for N$_2$-N$_2$ (open black circles) at temperatures of 294 K, 395 K, 495 K, 661 K, 868 K, 1116 K, and 1466 K, compared with results of semiclassical RB calculations of the N$_2$-H$_2$ (solid lines) system at the same temperatures.*
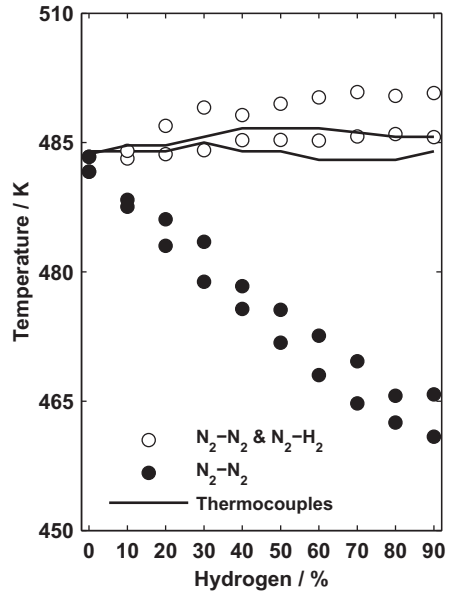
Figure 4.13. *Evaluated RCARS temperatures using two different Raman linewidth models involving measured time-domain coefficients of either pure self-broadened N$_2$ or a concentration weighted linear combination of both N$_2$-N$_2$ and N$_2$-H$_2$ at a reference temperature of 495 K.*

The time-domain coefficients were then employed in spectral fits of nanosecond RCARS spectra recorded in binary mixtures of N$_2$ and H$_2$ in a set of calibrated heated cell experiments. The results are shown in Figure 4.13, in which the estimated CARS temperatures are shown together with on-line monitored thermocouple temperatures, obtained from two recorded experimental series at about 495 K. To contrast the evaluated temperatures obtained using the Raman linewidth model expressed in Eqn. (3.11) in section 3.2.1, a theoretical library of pure self-broadened N$_2$ coefficents was again employed. Similar to the approach taken in Papers II and III, a major underestimation in predicted temperature when effects of N$_2$-H$_2$ collisons on the spectra are neglected could

be demonstrated. It can be seen that the impact this had on the thermometry was about 6% at hydrogen concentrations of 80-90%, which is slightly less than obtained in the previous studies (Papers II and III). By making use of the complete model for combined N_2-N_2 and N_2-H_2 time-domain coefficients, almost perfect agreement between the CARS and the thermocouples could be obtained. The estimated uncertainty in temperature, derived as the difference in percentage terms in comparison with the thermocouples reference temperature, was less than 2%. This is thus the accuracy for RCARS to be expected when it is applied at the fuel-side of a hydrogen/air diffusion flame the investigative conditions resembling those present in the study reported in Paper III. In applying the time-domain coefficents in the 100% N_2 case (Paper IV), the temperature uncertainty was even less, the deviance from the thermocouple reference temperature being less than 1%.

In conclusion, the unique capability of time-resolved pico-second RCARS was demonstrated involving measurement of S-branch N_2 Raman linewidths *in-situ* for an extended range of both temperature and rotational quantum numbers. It was estimated that the range of *J*-coefficients in the data that was presented encompassed more than 95% of the total N_2 thermal population distribution at the measured temperatures that were involved.

4.2   HERMAN-WALLIS FACTOR – Papers VI and VII

On the sensitivity of rotational CARS N_2 thermometry to the Herman-Wallis factor

On the sensitivity of rotational O_2 CARS thermometry to the Herman-Wallis factor

Aims

Vibration-rotation (VR) intra-molecular interaction affects the line intensities of the RCARS spectrum. The magnitude of this correction is not the only consideration involved, since the line strengths are also affected as a function of rotational state, which can be expected to impact the thermometry of the technique. Also, since there is an apparent spread in the values for this factor as reported in the literature, it is highly motivating to investigate to what extent the use of different values of it would impact the thermometric predictions obtained. This was taken as a basis for determining generally the sensitivity to this parameter of rotational CARS thermometry.

Results and discussion

Different values from the literature for both of the diatomic molecules N_2 and O_2, as discussed in section 3.2.2, were compiled. The same basic procedure was used for both the thermometric analyses reported in Papers VI and VII. It involves first simulating the experimental spectra on the basis of theoretical libraries built with a reference HW factor, Tipping and Ogilvie [49]. A contour spectral fitting routine between the reference spectra and theoretical libraries of new simulated spectra was then employed, the new spectra being calculated with use of alternative HW factors, all of the other fitting parameters remaining fixed. A complementary analysis was also performed, using a theoretical library based on the RR approximation (HW factor = 1). The results are displayed in Figure 4.14.
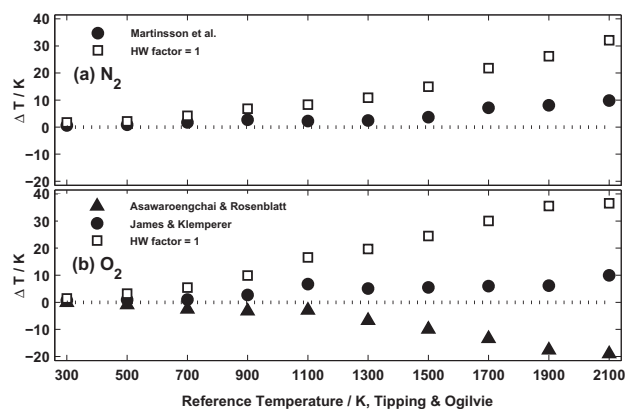

Figure 4.14. *Temperature differences (ΔT) between evaluated temperatures from simulated spectra using a reference HW factor from Tipping and Ogilvie [49] and theoretical libraries calculated with use of alternative HW factors for N_2 (a) and O_2 (b).*

As can be seen, neglecting use of an HW factor in the rotational CARS code leads to an overestimation of the evaluated temperatures, due to the presumed HW factor being the correct representation here. A comparison suggests that the VR correction is highly important for oxygen, since it results in deviations of 1.5-2 % at temperatures of 1300 K – 2100 K and of up to 1.5% in the temperature region below 1300 K, as shown in panel (b). The general trends for nitrogen are similar, but the deviations there are smaller, as can be seen in panel (a). A comparable comparison for N_2 indicates temperature differences of 1-1.5 % at temperatures of 1500 K – 2100 K, and of up to 1% below 1500 K.

A second issue concerns the variation in evaluated temperatures between the different HW factors that were implemented. The solid symbols represent the contrast between temperatures associated with the other values from the literature that were selected and the temperatures reference that was employed. In this respect, the differences are within 1 % and can be considered as typical uncertainties in rotational N_2 and O_2 CARS thermometry concerned with the HW factor.

4.3   IMPLEMENTATION OF N$_2$O – Paper VIII

Validation of a rotational coherent anti-Stokes Raman scattering model for N$_2$O at temperatures from 295 K to 796 K

Aims

There is an inherent desire to expand use of this technique, possibly within new areas as well. N$_2$O, a species having a triatomic linear asymmetric structure and of central interest in atmospheric research was investigated with this aim in mind. This work was a spectroscopic challenge and represented genuine progress in the sense of expanding the list of molecules for RCARS whereas its applicability to combustion is rather limited. CARS can be used to measure concentrations with a lower limit in the order of 0.1-1%, and in normal air-fed combustion situations N$_2$O has concentrations lower than this. In specialized combustion situations in which N$_2$O is used as the oxidant and it is present at high concentrations [87], N$_2$O RCARS thermometry can be employed.
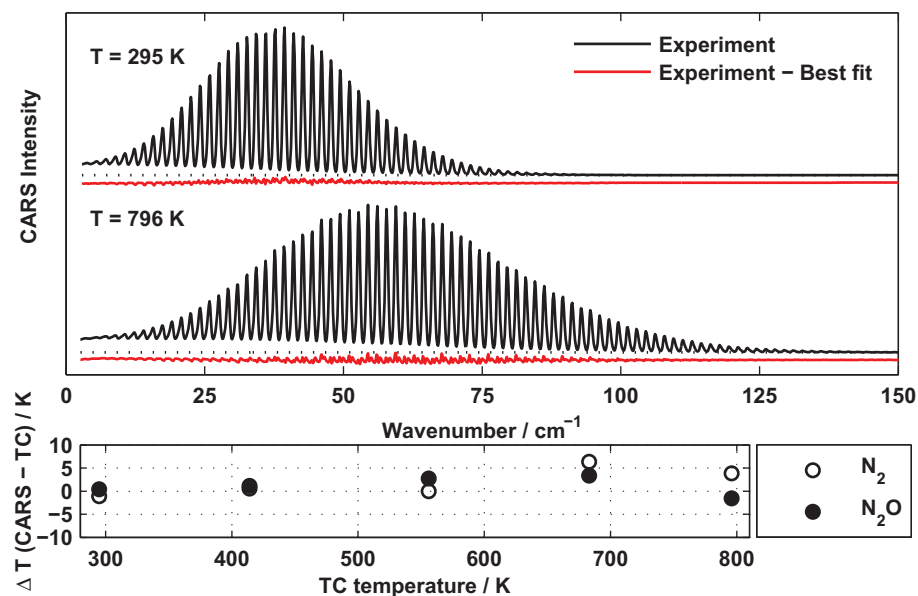
Figure 4.15. *Experimental rotational N$_2$O CARS spectra recorded at 295 K and 796 K, averaged from 1000 laser shots, displayed together with residuals (upper panel). Differences between results of single-shot analysis CARS temperatures and thermocouple temperatures displayed versus reference thermocouple temperatures (lower panel).*

Results and discussion

A theoretical rotational N_2O CARS code was developed (as described in section 3.2.3), temperature analysis being performed by fitting the modeled theoretical spectra to the experimental spectra. Averaged N_2O spectra recorded at temperatures of 295 K and 796 K are shown together with residuals, in the upper panels in Figure 4.15. The excellent agreement in shape between the experimental and the theoretically modelled N_2O spectra is shown by the very small residuals obtained, which are displayed slightly downshifted from the baselines so as not to interfere with the spectra that are displayed. The temperatures evaluated on the basis of the averaged spectra for, 295.3 K and 797.3 K are less than 2 K from the reference thermocouple temperatures. The levels of thermometric accuracy obtained for both N_2O and N_2 are presented in the lower panel in Figure 4.15. A parallel investigation of pure N_2 was performed as a reference to be compared with the results for N_2O. The deviation between the thermocouple temperatures and CARS temperatures was better than 7 K for both types of molecules throughout the temperature range that was studied. This is a difference of 1% or less relative to the thermocouple temperature.

The temperature analysis was based on mean values of evaluated single-shot spectra from both N_2 and N_2O. Such averaging can only be carried out under stationary conditions, whereas for instationary conditions the individual single-shot temperatures are of importance. Since mode noise gives rise to fluctuations in intensity of the individual lines, also with use of the dual-broadband CARS approach [4], the spectral shape is affected and varies from shot to shot. This effect can be illustrated by comparing the smooth envelope of the averaged N_2O spectrum shown in Figure 4.15 with the jagged envelope of the single-shot spectrum shown in Figure 4.16(a). Recording a large number of single-shot spectra at constant temperatures and obtaining the standard deviation of the data set allows the temperature precision of the technique to be obtained. Histograms presented in Figure 4.16(b), based on single-shot data obtained at room temperature, display the spread in predicted temperature for both species. According to these measurements, the standard deviation at room temperature was 5.8 K (2.0 %) for N_2O. This is about half of the value of 12.4 K (4.2 %) obtained for N_2. The results presented in Figure 4.16(c) are consistent over the investigated temperature range as a whole, the temperature precision for N_2O being found to be 2.0 – 2.7%, which can be compared with values in the range of 4.2 – 4.6% for N_2. The high level of precision for N_2O can be attributed to the large number of spectral lines, making the evaluations more robust toward variations in the intensity of the individual lines, where such variations could affect the appearance of the recorded spectral envelope, in terms both of position and of width.
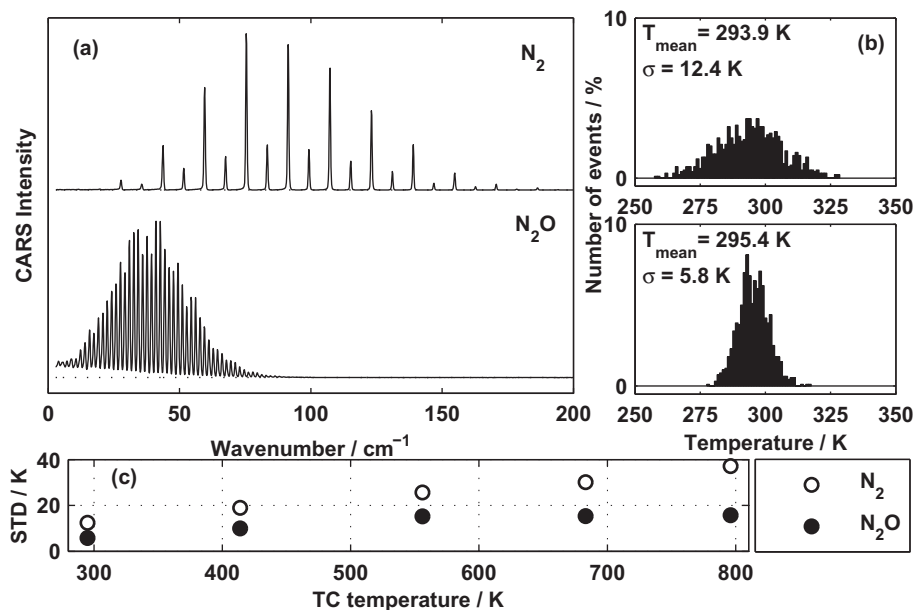
Figure 4.16. *(a) Single-shot spectra of N_2 and N_2O recorded at room temperature, 294 K. The number of spectral lines is higher for N_2O, which is related to the smaller rotational constant for N_2O, 0.42 cm^{-1}, to be compared with 1.998 cm^{-1} for N_2. (b) A temperature probability distribution function for N_2 and N_2O as obtained on the basis of a single-shot temperature analysis. (c) Standard deviations obtained for single-shot temperature analysis displayed for each of the cell temperatures investigated.*

There are numerous papers that have presented temperature precision data from rotational CARS measurements, these having generally shown that the standard deviation of single-shot temperatures increases with temperature (despite the increasing number of spectral lines this involves) [88]. A basic reason for this is that at elevated temperatures the primary parameter affecting the shape of the spectra (the population difference factor in Eqn. (3.9)) becomes less sensitive variations in temperature due to the Boltzmann distribution itself becoming more spread out. In this regard, one can note that in probing the rotational transitions alone slight distortions in the detected spectrum have greater impact on the estimated temperature. Also, there are studies indicating an improved temperature precision with an increase in the number of spectral lines for the evaluation. For example, in a study by Schenk *et al*. [80] the standard deviation of single-shot temperatures was found to decrease with an increase in oxygen concentration in mixtures with N_2. Also, Vestin *et al*. [89] found the standard deviation of single-shot temperatures to be lower for air than for pure nitrogen or oxygen gas.

4.4   STRAY LIGHT SUPPRESSION– Paper IX

Effective Suppression of Stray Light in Rotational Coherent Anti-Stokes Raman Spectroscopy Using an Angle-Tuned Short-Wave-Pass Filter

Aims

In pure rotational CARS, the dispersed spectrum shows up in the spectral vicinity of the probe beam. Because of this spectral proximity, the problem often arises that stray light originating from the probe beam leads to spectral interference in the rotational CARS spectrum. Usually, the probe beam is the second harmonic of a Nd:YAG laser producing light at a wavelength of 532.0 nm.

Results and discussion

A solution to this problem was found involving the angle tuning of a newly produced short-wave-pass filter (Semrock, Razor edge), as demonstrated in Figure 3.12 of section 3.3.1. The effectiveness of this method was analyzed by comparing spectra recorded in methane, with and without this component being in place. The reason for using methane was that it results in no resonant spectral lines, but instead in a strong non-resonant signal that can be used to reveal the transmission characteristics of the filter. At a 24 degree incident angle, the sharpness of the filter could be clearly observed, the transmission having changed from 1 % to 80 % over a spectral distance of 15 cm^{-1}. For the resonant N_2 spectra, use of this filter would only attenuate to an appreciable degree the first three transitions, which are of negligible importance for temperature evaluation since these lines barely contribute to the spectrum which is observed. Note that the filter is so effective that the need of apertures in the detection path is very markedly reduced.

   To conclude, this is a very effective and simple method of suppressing unwanted stray light in rotational CARS experiments. It is a highly useful optical component in measurements within practical devices such as internal combustion engines and gas turbines, where stray light from optical surfaces can be detrimental to successful measurements. Interested readers should also confront other approaches that have been used earlier for reducing stray light. These include a polarization approach [90, 91], spatial filtering in the detection path [92], use of a double spectrometer in which a knife edge can be mounted in the focal plane between the spectrometers [93], as well as a sodium filter [94], an iodine filter [95], a notch-filter [96], a short-edge filter with a cutoff wavelength of 532 nm [97], and a folded BOXCARS approach [98].

4.5   LOW-SWIRL TURBULENT FLAME – Paper X

Pure rotational CARS measurements of temperature and O_2-concentration in a low-swirl turbulent premixed flame

Aims

This work concerns a low-swirl turbulent lean (Φ=0.62) premixed methane/air flame that has been investigated extensively the last few years under identical conditions, see [99] and references therein. Numerous optical techniques have been applied to construct an experimental database to be used for the validation of numerical calculations based on large eddy simulations (LES). Prior to this investigation, only a limited amount of temperature data had been obtained. Temperature information is often requested by modellers for

Figure 4.17. *Photograph of rotational CARS measurements in a low-swirl turbulent premixed flame. Photo: P.-E. Bengtsson.*

improving the understanding of the flame characteristics. Information concerning the O_2-concentration is also important, since this adds information regarding air entrainment from the surroundings and extends knowledge of the flame extinction.

From a diagnostic standpoint, there were many exclusive problems to solve, and this was the first time rotational CARS was applied to a turbulent flame for simultaneous thermometry and relative nitrogen and oxygen concentration measurements. The three main diagnostics problems confronted, all of them well-known within the CARS community, were the following:

- A large dynamic range of CARS signal intensities in probing low and hot temperatures shot-to-shot, this being a problem in need of being handled by the detection system.
- The averaging of signals at different temperatures generated in spatially differing parts of the elongated probe volume (spatial averaging) that can occur.
- Collisional broadening by H_2O, this affecting the temperature obtained somewhat, its being difficult to compensate for this since the concentration is unknown and the rotational CARS signals of H_2O are extremely weak, their only being detectable in specially designed experiments.
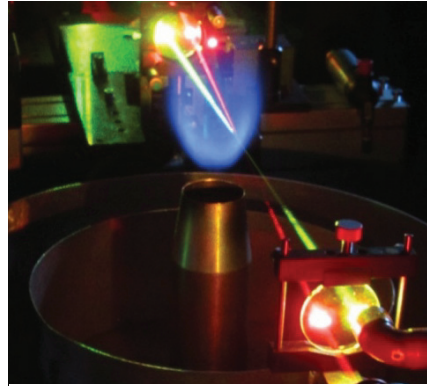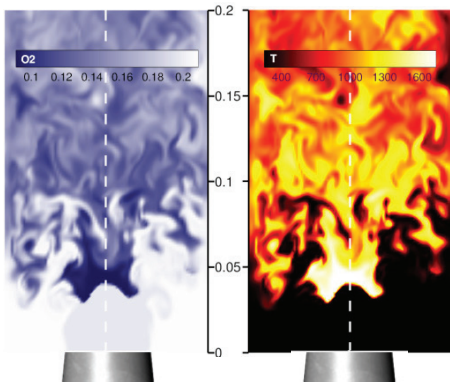
Figure 4.18. *Instantaneous mole fraction of O_2 (left) and temperature (right) in the axisymmetric plane obtained from LES, the vertical axis denoting the height above burner (HAB) in m units.*
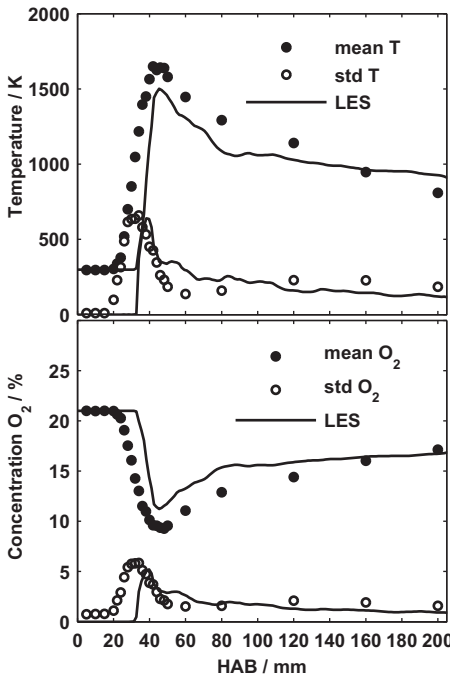

Figure 4.20. *(above) Means and standard deviations of temperatures along the vertical central axis (below) and corresponding data for the relative O_2-concentration.*
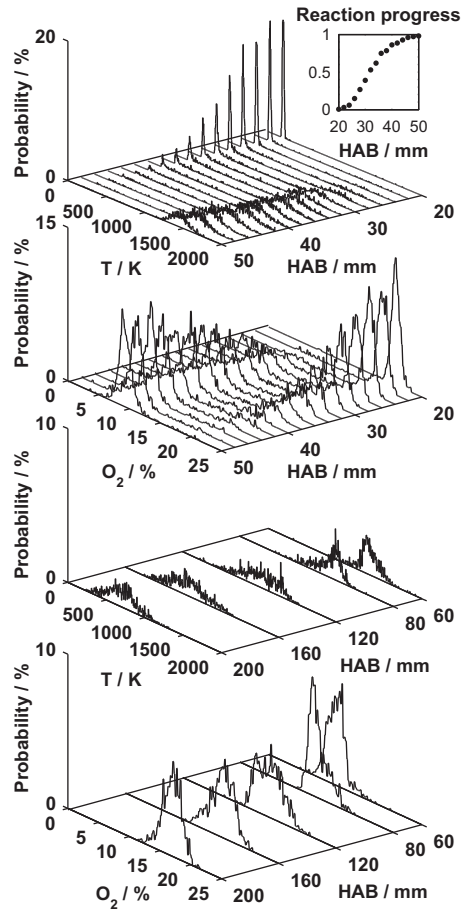

Figure 4.19. *Probability density functions of temperature (T) and relative O_2-concentration at 20-200 mm height above burner (HAB), composed of 1000 evaluated single-shot spectra. Each bin in the temperature histogram is 5 K, and in the oxygen concentration histogram 0.2%. In the insert, the progress of the reaction is shown from 20-50 mm, its being defined as the number of high-temperature spectra (above 1100 K) divided by the total number of spectra. From the data it can be concluded that the flame front position fluctuates strongly in the region of 20 to 50 mm.*

Results and discussion

Figure 4.18 (produced by Henning Carlsson and Xue-Song Bai) is shown first to provide better insight into the conditions under which the measurements were obtained. Instantaneous O_2 mole fraction and temperature maps are shown in the axisymmetric plane simulated by LES. It is at some distance above the burner nozzle that the reaction starts, on that can be sensed as being a W-shape flame front around the central axis, alternating with a V-shape one, in the course of time. Small pockets of unburnt mixtures can be seen to proceed further downstream, where also a dilution occurs through the entrainment of ambient air, brought about by large turbulence eddies, this leading to a cooling of the products. Low-swirl flames are generally referred to as being aerodynamically stabilized, the flame finding a position in the diverging flow field which is present, in which the local flame speed matches the local flow velocity, see Ref. [100].

To understand the stabilization mechanisms adequately, it is important to diagnose where the flame is positioned. This can be derived from Figure 4.19, showing probability density functions (PDF) of both temperature and relative O_2-concentrations as a function of height above burner (HAB). In the region of 20-50 mm a bimodal distribution can be seen, composed of essentially two individual distributions located at a low temperature and a high temperature level, respectively. This indicates there to be a strong fluctuation in the position of the flame. One way of assessing where the flame is located is to consider a progress variable, defined as the number of high-temperature spectra there are (above 1100 K) divided by the total number of spectra. This allows a 50% probability of a reaction occurring at 32 mm HAB to be derived. The results obtained agree well with the results of earlier investigations [100]. At a height of about 50 mm there is a 100% probability of a reaction occurring. In following the temperature PDF further downstream then, a cooling as a result of the entrainment of ambient air is evident.

A comparison of CARS data with results of the numerical LES is presented in Figure 4.20. There are particular difficulties in comparing measurement results with the results a model provides [101], partly because measurements can contain experimental uncertainties, which are not easily de-convolved so as permit a direct comparison of these results with the results of simulations. Also there is a fundamental discrepancy, the exact nature of which depends on the resolved spatial structures inherent to the methods employed. The specific subgrid of the combustion model is not perfectly matched to the extended probe volume of the measurements. The mean values obtained do allow a valid comparison of the two methods to be made in statistical terms, however, since most of the experimental uncertainties involved are averaged out. It is thus argued here that the individual histograms of the bimodal distribution are fairly symmetric, potential spreads due to experimental

60

uncertainties being filtered out. Further downstream, where the distributions of the CARS data become more skew symmetric, the uncertainty increases slightly. This should be taken account of in a direct comparison. The results of the methods involved can be compared in terms of standard deviations so as to provide a reasonable idea of where the flame is situated, in a manner similar to the information a progress variable would provide. Note that this quantity is a bit ambiguous, especially in the region of 20-50 mm, since it is calculated across the entire distribution (bimodal). The spread in statistics due to experimental uncertainties is small, however, in comparison with the difference in centre of mass between the low and the high temperature distributions.

There is a direct correlation between temperature and relative O_2 concentration. This is reflected in a clear majority of the spectra of all heights being either "cold with a high O_2-concentration" or "hot with a low O_2-concentration". Two distinct groups of data can be identified: unreacted (T ~295 K, with an O_2-concentration of 21%) and fully reacted (T~1700K, where $[O_2]$ = 9%), there being only a small fraction of spectra in between the two.

Since the quality of the spectral fits obtained was very much dependent upon the existing framework [26], the species-specific weighting was coded in evaluating the temperature and relative concentrations of N_2 and O_2. In addition, implementing the adequate Herman-Wallis factors for N_2 (Paper VI) and for O_2 (Paper VII), together with knowledge of the fact that N_2-CH_4 Raman linewidths can be replaced by N_2 self-broadening coefficients (Paper III), reinforced the arguments that could be made for the basic accuracy of the results obtained.

Concerning diagnostic matters, three main features were mentioned in the introduction of this section. The first issue was the large range of CARS signal intensities (about 3 orders of magnitude) obtained when intermittently probing low and high temperature gases; this was solved by using a multi-track function of the CCD camera, discussed in section 3.3.3.

The second issue deals with spatial averaging, where signals of different temperatures might well be generated from different parts of the elongated probe volume. This phenomenon has been observed in vibrational CARS thermometry earlier [102], but to the author's knowledge it has not been discussed within the framework of rotational CARS. The interesting observation was made that the two spectral envelopes originating from two distinct groups of temperatures, as discussed above, were detected as being slightly displaced relative to one another. The dispersion was the same but the absolute frequencies of the two spectra were shifted ~1.3 cm^{-1}. Thus, since adjacent lines of S-branch transitions are separated by about four times the rotational constant (= 8 cm^{-1} for N_2), the two signals could be detected with virtually no spectral interference. This provides the possibility of evaluating the two temperatures independently. One could consider this observation in two ways, the one being that a single-shot analysis can proceed normally, without

regarding these specific spectra as being unsuccessfully recorded and need to be discarded, the other being that it provides the possibility of estimating how large part of the spatial region is of high and is of low temperature, respectively based on the knowledge of the CARS intensities. It is believed that the displacement is a result of beam steering, which in this case is beneficial for an interpretation in terms of the CARS data. Since for vibrational CARS the spectral lines are more closely packed, the effect might not be as easily detected there. On the detector chip, however, a displacement of the two spectra could sometimes be observed even vertically (perpendicular to spectral direction), a multi-track reading mode could potentially slice off different portions of the dispersed light, allowing these to be analyzed separately.

The third diagnostic challenge was to consider the impact on N_2 RCARS thermometry of collisions with H_2O. Although the flame was a lean premixed one ($\Phi=0.6$) having about a 12% maximum mole fraction of H_2O in the products, the particular J-dependence of the N_2-H_2O Raman linewidths resulted in perturbation by water vapor being a very critical factor. Another complication was that H_2O provides only very weak RCARS signals and is only detectable in specially designed experiments. Thus, it cannot be used for weighting this contribution to broadening of the N_2 spectral lines. In addition, the spectral fitting routine as it is now coded does not float the linewidth parameter. Instead the Raman linewidth model which is implemented remains fixed to a particular gas mixture composition which is presumed to be present. Accordingly, a deviation in the measured values obtained would systematically impact upon the outcome in the temperature result. It is thus difficult to handle this within the framework of a single-shot analysis, since the composition of the probed mixtures varies from shot-to-shot. It could be of interest, however, to investigate such an option as providing a potential development of the technique. One should be aware, however, of that the spectral fit already depends on several floating variables (as discussed in *Evaluation procedure* in section 3.3). It is thus advisable to reduce the parametric space as much as possible, so as to make the analysis more robust.

The way of treating this problem is similar to the approach explored in the study here of the N_2 and O_2 Herman-Wallis factors (Papers VI and VII). If the type of correction employed is systematic, the results of investigations in this area can be generic for other applied situations. The basic idea is to generate theoretical spectra with use of weighted contributions of N_2-H_2O and N_2-N_2 linewidths, and to evaluate these using a reference library implemented with use of completely pure N_2 self-broadened coefficients. This simulates the situation applying to the measurements that are made. An important thermometric correction can be derived on the basis of wrongly predicted values that have been obtained. For determining the correction at the points in question in the evaluated data, the H_2O mole fraction can be linked intrinsically to the O_2-concentration that has been detected, in accordance with

$$X_{H_2O}\% = 21\% - [O_2]\% \tag{4.1}$$

which in the present study provides a good approximation. Theoretical pure N_2 RCARS spectra were calculated by use of a Raman linewidth model (Γ_{tot}) as follows:

$$\Gamma_{tot} = \left(100 - X_{H_2O} \right) \times \Gamma_{N_2-N_2} + X_{H_2O} \times \Gamma_{N_2-H_2O} \tag{4.2}$$

The concentration of H_2O was varied within the region of 0-14% (in steps of 2%) in the calculations. This corresponds to oxygen values of 21-7%. In addition, the calculations were progressed at varying temperatures from 300 K to 2100 K (in steps of 200 K), since the degree of impact is dependent on the temperature as well.

The results of the evaluations are shown in Figure 4.21. An underestimation of the evaluated temperatures is evident. This indicates the importance of making use of N_2-H_2O Raman linewidths while probing N_2 in the presence of H_2O. As can be seen, the dependence of the results on the H_2O-concentration and the temperature is smooth, use of the rather sparse grid being sufficient for the present investigation. All values in between were extracted by means of bilinear interpolation, resulting in a minor loss in precision, its yielding the temperature correction matrix displayed in Figure 4.22. This matrix covers the span extending from 300 K to 1900 K, of 0-14% in terms of H_2O concentration. It includes all of the physical conditions involved in the measurements. Figure 4.23 deals with the corrections in the case of 32 mm HAB, the sensitivity in connection with the O_2-concentrations and the temperature being shown. In Figure 4.24 the corrections of single-shot data are shown at different positions in the flame. At 10 mm there is no correction, since the position there is below the reaction zone of the flame. At 50 mm, a clear majority of the single-shots are recorded in a reacted mixture at about 1700 K, there being a substantial correction there of some 40 K. Further downstream, at 120 mm, the cluster becomes more elongated, due to the variations in temperature and in the O_2-concentrations of the mixtures there.
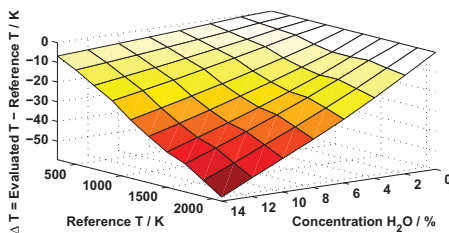

Figure 4.21. *Simulated underestimation of N_2 RCARS evaluated temperatures when N_2-H_2O Raman linewidths are omitted, displayed as a function of H_2O-concentration and temperature.*
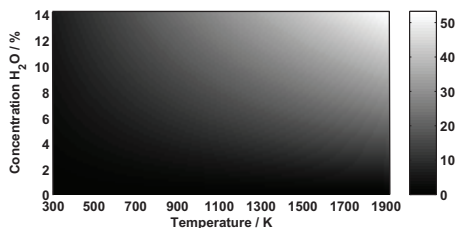
Figure 4.22. *Temperature correction values at evaluated H_2O-concentration and temperature in the regions of 0-14% and 300-1700 K, respectively.*
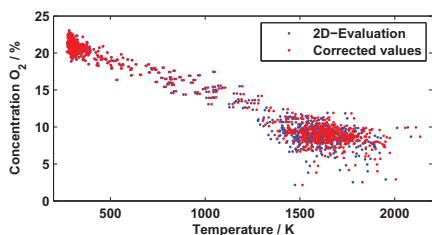

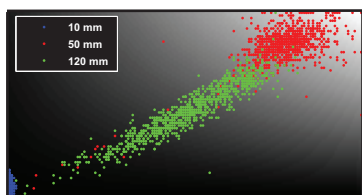**Figure 4.23.** *Evaluated temperatures at 32 mm HAB, displayed before and after correction.*

Figure 4.24. *Corrections of single-shot data at different positions (HAB) in the flame. The scales are the same as in Figure 4.22.*

4.6   MCKENNA BURNER FLAME– Papers A and B

Aims

Temperature is an important indicator in the study of combustion processes as those involved in the preheating of the fuel/oxidizer, exothermic reactions in the flame, and cooling of the reaction products. For validating combustion models predicting processes of this sort the need of accurate thermometry is central. In providing accurate temperature assessments, diagnostic optical research tools have been essential. In developing such optical research tools for combustion applications it is important to assess the accuracy through comparisons with various other methods. A vivid step in progress here is to perform validation experiments with established measurement objects under repeatable conditions. The standardized McKenna-type burner is one such object, its providing flat homogeneous premixed flames under different fuel-air mixture conditions, the temperature varying with the height above burner surface (HAB). The one-dimensional properties of this burner and its capabilities for the study of product gases in connection with use of different fuels under a wide range of mixtures

with air, makes it particular suitable for idealistic experimental laboratory investigations. A photograph of the burner, in which its dimensions are indicated, together with a sketch showing the principles that apply to a premixed burner are presented in Figure 4.25.
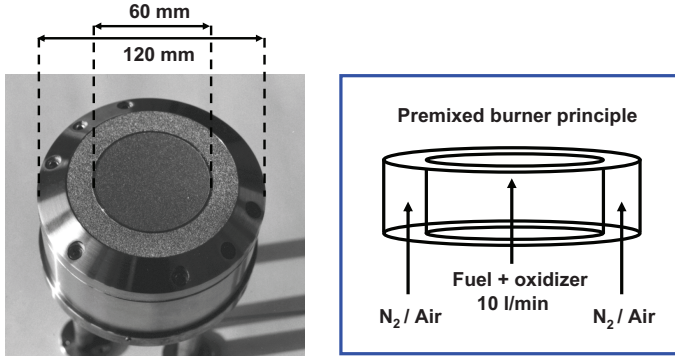

Figure 4.25.
Dimensions of the McKenna burner and a sketch of the premixed burner principle.

The flames a burner of this type provides tends to suffer from heat loss from several sources, such as the water-cooled burner disc and the flame stabilizer, for example. This makes the temperature outcome under the operating conditions present a bit unpredictable and not readily comparable with the adiabatic flame temperature. Accurate thermometry in flames of this sort is thus essential and needs to be addressed in the case of fuel-air mixtures of all types.

An important issue in connection with this concern the importance of experimentalists working in a given field agreeing both on the construction of this burner and on the operating conditions to be employed, so as to be able to compare each other's results and draw adequate conclusions from this. Discussions are in progress concerning both the stability and the uniformity of the flames burners of this type provide [103]. In the use of such burners for soot diagnostics, a common test case is

Figure 4.26. *Composition of the product gas as a function of equivalence ratio (ethylene/air)*

one carried out at an equivalence ratio (Φ) of 2.1 (ethylene/air), the composition of which is illustrated in Figure 4.26. The aim of reaching such an agreement within with the research community is to be able to act appropriately in the further development of such a test case. Characterizing a flame of this sort by use of a temperature map and investigating what impact on the temperatures involved different shielding co-flows of air and nitrogen have is thus highly
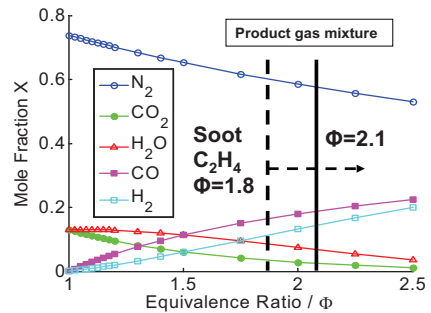
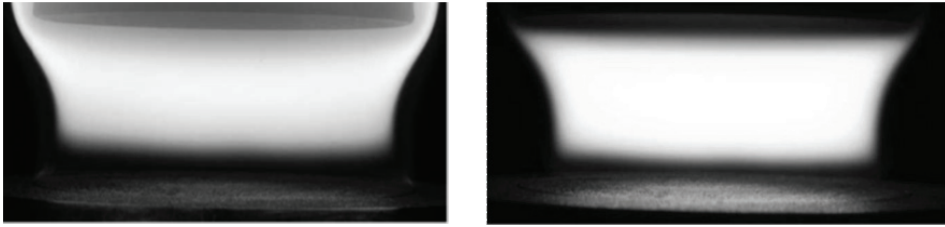important. The two types of premixed flames considered here can be seen in Figure 4.27.

Figure 4.27. *Two standard types of rich flat premixed ethylene-air flames (Φ=2.1) provided by a McKenna burner having different shielding co-flows of air (left) and nitrogen (right).*

Results and discussion

The evaluated CARS temperatures in ethylene-air flames (Φ=2.1) that were provided on a standard bronze porous-plug McKenna burner with two different shielding co-flows of air and nitrogen are displayed in Figure 4.28 as a function of height above burner and in Figure 4.29 radially at a height of 10 mm.
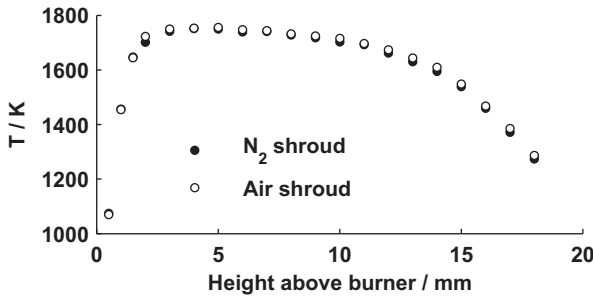

Figure 4.28.
CARS temperatures shown as a function of height above burner, evaluated for ethylene-air flames having shielding co-flows of air (○) and nitrogen (•).
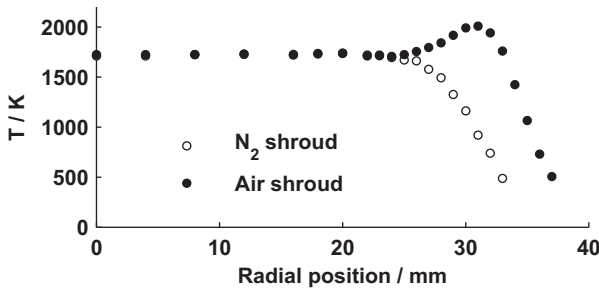

Figure 4.29.
Radial CARS temperatures at a height of 10 mm, evaluated for ethylene-air flames having shielding co-flows of air (○) and nitrogen (•).

One can note in Figure 4.28 how temperature evolves as the history of a combustion process proceeds. From the inflexion point that marks the start of the reaction zone on, the temperature increases due to all of the exothermic

chemical reactions that reach a maximum value about 100 K lower than the adiabatic flame temperature of 1852 K, for a C_2H_4/air-mixture of $\Phi=2.1$. At increasing heights in the flame, from the maximum value of the curves located in the product zone, the temperature decreases successively, since the products are being cooled, due mainly to losses through radiation. At heights of 14 mm and upwards, the temperature of the product gases diminishes still more, due to the cooling process of heat being conducted to the stabilizing plate located at 21 mm HAB. When a shielding co-flow of air rather than nitrogen is employed the temperatures assessed in the centre of the burner are ~ 10 K higher. The very flat homogenous temperature profile of this type of burner can be seen in Figure 4.29. At the edge of the flame, where there is a shielding co-flow of air, a strong temperature increase can be observed, due to the outer diffusion flame found there, which provides heat. The gas temperature along the central axis of the burner is about 10 K higher when air serves as the shroud gas. It can be speculated that infrared radiation from the outer flame becomes absorbed at the centre of the flame, under these conditions, primarily through the soot particles there acting as black bodies. This heat is then conducted partly to the molecules that impinge upon the surface of the soot particles.

CONCLUSIONS AND OUTLOOK

The aim of the thesis has been to find ways of improving the capabilities of rotational CARS in connection with combustion diagnostics. The work has been concerned with different ways of achieving accurate thermometry within a large range of temperatures and under a variety of different operational conditions. It has included studies of essentially three main topics: collisional Raman line-broadening (Papers I-V), the effects of vibration-rotational interaction on line-intensities (Papers VI and VII), and its potential in the application of rotational CARS thermometry to N_2O (Paper VIII). Efforts have been made to improve the experimental setup through the effective suppression of stray light (Paper IX) and through progress in detection achieved through improvements in the dynamic range (Paper X). The rotational CARS technique was also employed in flame diagnostics: in a laminar H_2 diffusion flame (Paper III), in a laminar premixed ethylene/air-flame (Papers A and B), and in a low-swirl premixed turbulent flame burning methane (Paper X).

Studies aimed at simulating the impact of collisions with foreign species on the N_2 spectra were carried out. It was shown in particular that in an environment dominated by collisions with H_2 the temperatures assessed become strongly underestimated if this species specific perturbation of the N_2 spectral lines was neglected. This uncertainty could be substantially reduced through the implementation of N_2-H_2 Raman linewidths (Papers I-III). A step in this direction was to employ time-resolved picosecond rotational CARS for obtaining direct measurements of the N_2-N_2 and N_2-H_2 line-broadening coefficients (Papers IV and V). The time-domain coefficients obtained were employed in the evaluation of nanosecond N_2 CARS spectra, recorded in binary mixtures with H_2 under temperature-calibrated conditions. The close agreement obtained with the reference temperature, measured by means of thermocouples, validates the accuracy of the line-broadening coefficients acquired in the time-domain involved. The effect of the spectral line-broadening of N_2 by CH_4 was also investigated (Paper III). There it was found that in a lower temperature region (below 500 K) no special attention needs to be directed at these collisions, since their impact upon the thermometry is negligible. There was found to be a similarity in J-dependence between N_2-CH_4 coefficients and self-perturbed N_2-N_2 coefficients. This simplifies the application of N_2 RCARS thermometry to CH_4 diffusion flames. Also, an important temperature correction was derived for taking account of collisional Raman line-broadening by H_2O (Paper X). Such compensation is normally difficult to achieve, since the concentration is unknown and the rotational CARS signals of H_2O are

69

extremely weak. In the present study, however, the mole fraction of H_2O could be linked intrinsically to the O_2-concentration that was detected, and be used to correct the assessed temperatures of the single-shot spectra. Thus, the importance of employing an adequate Raman linewidth model in the temperature assessment of rotational CARS spectra could be clearly shown. It could be of interest to explore the use of the procedures here within vibrational CARS. It is not known, for example, how vibrational N_2 CARS thermometry would be affected in an environment in which N_2 is perturbed by H_2. Future work should go on to consider colliding systems regarding which there is currently a lack of literature, which is the case for most N_2-fuel collision partners. Finally, I would call attention to the very fruitful cross between the picosecond and the nanosecond CARS techniques that was explored in the projects carried out. Picosecond CARS has the potential of being able to overcome many of the diagnostic problems present in the nanosecond regime. Developing a time-domain code for picosecond CARS is currently under progress at Sandia. It can also be used to aid the nanosecond CARS community by providing accurate Raman linewidth values. However much there may be that is yet to be carried out. Nanosecond CARS is already a mature technique. It was of very great help here for validating important potentialities of picosecond CARS.

Another possible improvement was shown in investigating thermometric sensitivity of pure rotational N_2 and O_2 CARS caused by the Herman-Wallis factor (Papers VI and VII). Although this parameter is not as critical as it is in connection with Raman linewidths, it was found that the spectral line strengths could be modified appreciably more here than in cases in which vibration-rotation interaction was neglected. It was found that neglecting use of the Herman-Wallis factors in rotational N_2 and O_2 CARS thermometry leads to a slight but systematic overestimation of the temperatures. A fruitful continuation of this project could be to explore the general sensitivity of measurements of the relative concentrations of N_2 and O_2 to different expressions of the HW factor.

A model for rotational N_2O CARS spectra was also developed and was tested for thermometric accuracy in a lower temperature region (below 800 K). Excellent agreement between the experimental and the modeled spectra and a high level of thermometric accuracy were obtained. The relative standard deviation was reduced by a factor of two in comparison with N_2. This can be attributed to the increased number of spectral lines for N_2O. Rotational N_2O CARS thermometry shows very considerable potential, due to the large Raman cross-section and the large number of populated rotational states at any temperature it involves (Paper VIII).

The rotational CARS technique was also used for a number of applications, serving as an important input to various optical techniques as well being used in the validation of numerical simulations. Use of this technique can contribute to discussions concerning the homogeneity of standardized flat

flames produced on a McKenna burner through making it possible to map the temperatures there as a function of height, and in the radial direction at a fixed height (Papers A and B). For these measurements the burner was operated with two different shielding co-flows of either air or nitrogen. Information in such cases regarding the temperature can help appreciably in the choice of suitable operating conditions for standard McKenna burner flames. Finally, one can note that temperature and relative O_2 concentrations were measured in a low-swirl turbulent premixed flame (Paper X). This lean flame burning methane had previously been investigated using a variety of laser diagnostic techniques. In the present work, single-shot CARS measurements provided probability density functions for temperature and relative O_2/N_2 concentration. In comparing the results with LES model results, close agreement was found. The technique was successful in the entire range of temperatures (300 K to 1700 K) and of relative O_2 concentrations involved. Various potential problems in connection with the technique were solved, such as the limited spatial resolution in one dimension, and the large dynamic range of CARS signal intensities (2-3 orders of magnitude) in probing both cold and hot temperatures shot-to-shot.

ACKNOWLEDGEMENTS

I am deeply grateful to my supervisor Professor *Per-Erik Bengtsson*, who has served as a valuable asset more than I am capable of expressing, always present, and a master in producing solid scientific ideas like a source of a never-ending kind. He has been absolutely essential to the progress of the thesis and participated very actively in the lab in helping to realize it. The guidance and support he has provided, his integrity and character have made a deep impression upon me. It has been a great pleasure and thank you Per-Erik for all moments we shared.

Thanks also to my closest colleague *Emil Nordström*, with whom I have spent many hours in the lab. I will always be impressed by his persistence in sharpening arguments and his leaving no stones unturned. The unit that the three of us together have represented has taught me the great value of communication and I will miss you both tremendously when I leave.

I thank *Fredrik Vestin* who introduced me during my master thesis project to the type of laboratory work I have carried out. I was destined to shoulder the responsibility in the CARS lab and endeavored in so doing to echo his skill.

I would like to express my appreciation to Professor *Marcus Aldén*, my co-supervisor, for his knocks on the door to instill in me a strong portion of working spirit. His deep involvement as Head of the Division has created a congenial working atmosphere and it has been a true pleasure and privilege to take part in the work of this Division during these years.

I was fortunate to work in close collaboration with various researchers with whom I had rewarding contacts and shared enlightening discussions with. Thanks to *Pierre Joubert*, *Miguel Dhyne* and Professor *Jeanine Bonamy* for your help in enabling me to gain insight into line-broadening mechanisms through the understanding of them that you had. I am grateful to *Michele Marrocco* for the conversations we have had in discussing CARS and your strong support in the hectic period of my writing the thesis. Per-Erik, Emil and I are truly delighted for have been invited to collaborate with *Chris Kliewer*, *Brian Patterson* and *Tom Settersten* at Sandia National Labs in Livermore, and would like to express our gratitude in being able to partake of their expertise within picosecond CARS. If I were to collect hard copies of the many inspiring conversations in Physics I have had via email with *Chris Kliewer*, it would fill a bookshelf itself. I thank *Henning Carlsson* and *Xue-Song Bai* for our fruitful discussions in sharing with me your views and perspectives as modelers of turbulent combustion. Thanks to the soot diagnostic group at the Division,

REFERENCES

1. G. Herzberg, *Molecular spectra and molecular structure. I. Spectra of diatomic molecules.* 1989, Florida: Robert E. Krieger Publishing Company.

2. C.N. Banwell and E.M. McCash, *Fundamentals of Molecular Spectroscopy 4th ed.* 1994, London: The McGraw-Hill Companies.

3. P.R. Regnier and J.P.E. Taran, *On the possibility of measuring gas concentrations by stimulated anti-Stokes scattering.* Applied Physics Letters, 1973. **23**(5): p. 240-242.

4. A.C. Eckbreth, *Laser diagnostics for combustion temperature and species.* Vol. 3. 1996, Amsterdam: Gordon and Breach.

5. S. Roy, J.R. Gord, and A.K. Patnaik, *Recent advances in coherent anti-Stokes Raman scattering spectroscopy: Fundamental developments and applications in reacting flows.* Progress in Energy and Combustion Science, 2010. **36**(2): p. 280-306.

6. L. Martinsson, P.-E. Bengtsson, M. Alden, S. Kroll, and J. Bonamy, *A Test of Different Rotational Raman Linewidth Models - Accuracy of Rotational Coherent Anti-Stokes-Raman Scattering Thermometry in Nitrogen from 295 K to 1850 K.* Journal of Chemical Physics, 1993. **99**(4): p. 2466-2477.

7. L. Martinsson, P.-E. Bengtsson, and M. Alden, *Oxygen concentration and temperature measurements in N_2-O_2 mixtures using rotational coherent anti-Stokes Raman spectroscopy.* Applied Physics B-Lasers and Optics, 1996. **62**(1): p. 29-37.

8. M. Afzelius, C. Brackmann, F. Vestin, and P.-E. Bengtsson, *Pure rotational coherent anti-Stokes Raman spectroscopy in mixtures of CO and N_2.* Applied Optics, 2004. **43**(36): p. 6664-6672.

9. M. Schenk, T. Seeger, and A. Leipertz, *Time-resolved CO_2 thermometry for pressures as great as 5 MPa by use of pure rotational coherent anti-Stokes Raman scattering.* Applied Optics, 2005. **44**(31): p. 6526-6536.

10.   F. Vestin, K. Nilsson, and P.-E. Bengtsson, *Validation of a rotational coherent anti-Stokes Raman spectroscopy model for carbon dioxide using high-resolution detection in the temperature range 294-1143 K.* Applied Optics, 2008. **47**(11): p. 1893-1901.

11.   J. Bood, P.-E. Bengtsson, and M. Alden, *Temperature and concentration measurements in acetylene-nitrogen mixtures in the range 300-600 K using dual-broadband rotational CARS.* Applied Physics B-Lasers and Optics, 2000. **70**(4): p. 607-620.

12.   J. Buldyreva, J. Bonamy, M.C. Weikl, F. Beyrau, T. Seeger, A. Leipertz, F. Vestin, M. Afzelius, J. Bood, and P.-E. Bengtsson, *Linewidth modelling of C_2H_2-N_2 mixtures tested by rotational CARS measurements.* Journal of Raman Spectroscopy, 2006. **37**(6): p. 647-654.

13.   M. Alden, P.-E. Bengtsson, and H. Edner, *Rotational Cars Generation through a Multiple 4-Color Interaction.* Applied Optics, 1986. **25**(23): p. 4493-4500.

14.   A.C. Eckbreth and T.J. Anderson, *Simultaneous rotational coherent anti-Stokes Raman spectroscopy and coherent Stokes Raman spectroscopy with arbitrary pump-Stokes spectral separation.* Opt. Lett., 1986. **11**(8): p. 496-498.

15.   R.W. Boyd, *Nonlinear optics.* 1992, San Diego: Academic Press.

16.   R.J. Hall, *Cars Spectra of Combustion Gases.* Combustion and Flame, 1979. **35**(1): p. 47-60.

17.   D.A. Greenhalgh and R.J. Hall, *A Closed Form Solution for the Cars Intensity Convolution.* Optics Communications, 1986. **57**(2): p. 125-128.

18.   D. Nilsson, *Theoretical and experimental investigations of rotational CARS as a technique for temperature probing.* 1987, Lund University: Lund.

19.   L. Martinsson, *Theoretical development of rotational CARS for combustion diagnostics.* 1994, Lund University: Lund.

20.   J. Bood, *Development of dual-broadband rotational CARS for combustion diagnostics*. 2000, Lund University: Lund.

21. C. Brackmann, *Development and application of rotational coherent anti-Stokes Raman spectroscopy and laser-induced fluorescence for combustion diagnostics.* 2004, Lund University: Lund.

22. M. Afzelius, *Rotational coherent anti-Stokes Raman spectroscopy : experimental and theoretical developments in gas-phase thermometry.* 2004, Lund University: Lund.

23. F. Vestin, *Development of dual-broadband rotational CARS for applied flame diagnostics.* 2008, Lund University: Lund.

24. M. Afzelius and P.-E. Bengtsson, *Dual-broadband rotational CARS modelling of nitrogen at pressures up to 9 MPa. I. Inter-branch interference effect.* Applied Physics B-Lasers and Optics, 2002. **75**(6-7): p. 763-769.

25. M. Afzelius, P.-E. Bengtsson, J. Bood, J. Bonamy, F. Chaussard, H. Berger, and T. Dreier, *Dual-broadband rotational CARS modelling of nitrogen at pressures up to 9 MPa. II. Rotational Raman line widths.* Applied Physics B-Lasers and Optics, 2002. **75**(6-7): p. 771-778.

26. F. Vestin, M. Afzelius, and P.-E. Bengtsson, *Improved species concentration measurements using a species-specific weighting procedure on rotational CARS spectra.* Journal of Raman Spectroscopy, 2005. **36**(2): p. 95-101.

27. D.A. Greenhalgh, *Quantitative CARS spectroscopy.* In Advances in Non-Linear Spectroscopy, ed. R.H.J. Clark and R.E. Hester. 1988, New York: John Wiley & Sons Ltd.

28. J.M. Hartmann, C. Boulet, and D. Robert, *Collisional effects on molecular spectra.* 2008, Oxford: Elsevier.

29. R.J. Hall, J.F. Verdieck, and A.C. Eckbreth, *Pressure-induced narrowing of the cars spectrum of N_2.* Optics Communications, 1980. **35**(1): p. 69-75.

30. R.C.H. Tam and A.D. May, *Motional narrowing of the rotational Raman band of compressed CO, N_2, and CO_2.* Canadian Journal of Physics, 1983. **61**(11): p. 1558-1566.

31. J. Bonamy, D. Robert, J.M. Hartmann, M.L. Gonze, R. Saintloup, and H. Berger, *Line Broadening, Line Shifting, and Line Coupling Effects on N_2-*

H$_2$O Stimulated Raman-Spectra. Journal of Chemical Physics, 1989. **91**(10): p. 5916-5925.

32. M.L. Gonze, R. Saintloup, J. Santos, B. Lavorel, R. Chaux, G. Millot, H. Berger, L. Bonamy, J. Bonamy, and D. Robert, *Collisional Line Broadening and Line Shifting in N$_2$-CO$_2$ Mixture Studied by Inverse Raman-Spectroscopy.* Chemical Physics, 1990. **148**(2-3): p. 417-428.

33. G. Millot, R. Saint-Loup, J. Santos, R. Chaux, H. Berger, and J. Bonamy, *Collisional effects in the stimulated Raman Q branch of O$_2$ and O$_2$-N$_2$.* The Journal of Chemical Physics, 1992. **96**(2): p. 961-971.

34. M. Afzelius, P.-E. Bengtsson, and J. Bonamy, *Semiclassical calculations of collision line broadening in Raman spectra of N$_2$ and CO mixtures.* Journal of Chemical Physics, 2004. **120**(18): p. 8616-8623.

35. P. Joubert, J. Bonamy, L. Gomez, and D. Bermejo, *N$_2$-H$_2$ isotropic Raman Q-branch linewidths: an Energy-Corrected Sudden scaling law.* Journal of Raman Spectroscopy, 2008. **39**(6): p. 707-710.

36. A.E. DePristo, S.D. Augustin, R. Ramaswamy, and H. Rabitz, *Quantum number and energy scaling for nonreactive collisions.* The Journal of Chemical Physics, 1979. **71**(2): p. 850-865.

37. F. Thibault, S.V. Ivanov, O.G. Buzykin, L. Gomez, M. Dhyne, P. Joubert, and M. Lepere, *Comparison of classical, semiclassical and quantum methods in hydrogen broadening of acetylene lines.* Journal of Quantitative Spectroscopy and Radiative Transfer, 2011. **112**(9): p. 1429-1437.

38. D. Robert and J. Bonamy, *Short range force effects in semiclassical molecular line broadening calculations.* J. Phys. France, 1979. **40**(10): p. 923-943.

39. F. Thibault, B. Corretja, A. Viel, D. Bermejo, R.Z. Martinez, and B. Bussery-Honvault, *Linewidths of C$_2$H$_2$ perturbed by H$_2$: experiments and calculations from an ab initio potential.* Physical Chemistry Chemical Physics, 2008. **10**(35): p. 5419-5428.

40. L. Gomez, S.V. Ivanov, O.G. Buzykin, and F. Thibault, *Comparison of quantum, semiclassical and classical methods in hydrogen broadening of nitrogen lines.* Journal of Quantitative Spectroscopy and Radiative Transfer, 2011. **112**(12): p. 1942-1949.

41. J.I. Steinfeld, P. Ruttenberg, G. Millot, G. Fanjoux, and B. Lavorel, *Scaling laws for inelastic collision processes in diatomic molecules.* The Journal of Physical Chemistry, 1991. **95**(24): p. 9638-9647.

42. L.A. Rahn and R.E. Palmer, *Studies of nitrogen self-broadening at high temperature with inverse Raman spectroscopy.* J. Opt. Soc. Am. B, 1986. **3**(9): p. 1164-1169.

43. M.L. Koszykowski, L.A. Rahn, R.E. Palmer, and M.E. Coltrin, *Theoretical and experimental studies of high-resolution inverse Raman spectra of molecular nitrogen at 1-10 atm.* The Journal of Physical Chemistry, 1987. **91**(1): p. 41-46.

44. R. Herman and R.F. Wallis, *Influence of Vibration-Rotation Interaction on Line Intensities in Vibration-Rotation Bands of Diatomic Molecules.* Journal of Chemical Physics, 1955. **23**(4): p. 637-646.

45. T.C. James and W. Klemperer, *Line Intensities in the Raman Effect of Sigma-1 Diatomic Molecules.* Journal of Chemical Physics, 1959. **31**(1): p. 130-134.

46. C. Asawaroengchai and G.M. Rosenblatt, *Rotational Raman Intensities and the Measured Change with Inter-Nuclear Distance of the Polarizability Anisotropy of H_2, D_2, N_2, O_2, and CO.* Journal of Chemical Physics, 1980. **72**(4): p. 2664-2669.

47. M.C. Drake, C. Asawaroengchai, and G.M. Rosenblatt, *Temperature from Rotational and Vibrational Raman-Scattering - Effects of Vibrational-Rotational Interactions and Other Corrections.* Abstracts of Papers of the American Chemical Society, 1979(Sep): p. 39-39.

48. M.C. Drake, *Rotational Raman Intensity Correction Factors Due to Vibrational Anharmonicity - Their Effect on Temperature-Measurements.* Optics Letters, 1982. **7**(9): p. 440-441.

49. R.H. Tipping and J.F. Ogilvie, *Herman-Wallis Factors for Raman Transitions of 1-Sigma-State Diatomic-Molecules.* Journal of Raman Spectroscopy, 1984. **15**(1): p. 38-40.

50. M.A. Buldakov, V.N. Cherepanov, B.V. Korolev, and I.I. Matrosov, *Role of intramolecular interactions in Raman spectra of N_2 and O_2 molecules.* Journal of Molecular Spectroscopy, 2003. **217**(1): p. 1-8.

51. M. Marrocco, *Reliability of Herman-Wallis factors for Raman spectroscopy of Q-branch molecular transitions.* Chemical Physics Letters, 2007. **442**(4-6): p. 224-227.

52. M. Marrocco, *Herman-Wallis factor to improve thermometric accuracy of vibrational coherent anti-Stokes Raman spectra of H_2.* Proceedings of the Combustion Institute, 2009. **32**: p. 863-870.

53. M. Marrocco, *Comparative analysis of Herman-Wallis factors for uses in coherent anti-Stokes Raman spectra of light molecules.* Journal of Raman Spectroscopy, 2009. **40**(7): p. 741-747.

54. M. Marrocco, *CARS thermometry revisited in light of the intramolecular perturbation.* Journal of Raman Spectroscopy, 2010. **41**(8): p. 870-874.

55. M. Marrocco, *Herman-Wallis correction in vibrational CARS of oxygen.* Journal of Raman Spectroscopy, 2011. **42**(10): p. 1836-1842.

56. M. Marrocco, G. Magnotti, and A.D. Cutler, *Herman–Wallis corrections in dual-pump CARS intensities for combustion temperature and species.* Journal of Raman Spectroscopy, 2012. DOI: 10.1002/jrs.3131.

57. M. Marrocco, *Vibration–rotation interaction in time-resolved coherent anti-Stokes Raman scattering for gas-phase thermometry.* Journal of Raman Spectroscopy, 2012. DOI: 10.1002/jrs.3135.

58. K.P. Huber and G. Herzberg, *Molecular Spectra and Molecular Structure - IV. Constants of Diatomic Molecules.* 1979, New York: Van Nostrand Reinhold.

59. G. Maroulis, *Accurate electric multipole moment, static polarizability and hyperpolarizability derivatives for N_2.* Journal of Chemical Physics, 2003. **118**(6): p. 2673-2687.

60. R.J. Hall and J.H. Stufflebeam, *Quantitative Cars Spectroscopy of CO_2 and N_2O.* Applied Optics, 1984. **23**(23): p. 4319-4327.

61. E.K. Plyler and E.F. Barker, *The infrared spectrum and the molecular configuration of N_2O.* Physical Review, 1931. **38**(10): p. 1827-1836.

62. R.A. Toth, *Line-Frequency Measurements and Analysis of N_2O between 900 and 4700 cm^{-1}.* Applied Optics, 1991. **30**(36): p. 5289-5315.

63.   M.P. Bogaard, A.D. Buckingham, R.K. Pierens, and A.H. White, *Rayleigh-Scattering Depolarization Ratio and Molecular Polarizability Anisotropy for Gases.* Journal of the Chemical Society-Faraday Transactions I, 1978. **74**: p. 3008-3015.

64.   N. Lacome, A. Levy, and C. Boulet, *Air-Broadened Linewidths of Nitrous-Oxide - an Improved Calculation.* Journal of Molecular Spectroscopy, 1983. **97**(1): p. 139-153.

65.   N. Lacome, A. Levy, and G. Guelachvili, *Fourier-Transform Measurement of Self-Broadening, N_2-Broadening, and O_2-Broadening of N_2O Lines - Temperature-Dependence of Linewidths.* Applied Optics, 1984. **23**(3): p. 425-435.

66.   L.S. Rothman, *The Hitran Molecular Database - Enhancements for Remote-Sensing.* Atmospheric Propagation and Remote Sensing Ii, 1993. **1968**: p. 687-694.

67.   J. Pliva, *Infrared Spectra of Isotopic Nitrous Oxides.* Journal of Molecular Spectroscopy, 1964. **12**(4): p. 360-&.

68.   G. Herzberg, *Molecular spectra and molecular structure. II. Infrared and Raman spectra of polyatomic molecules.* 1945, New York: Van Nostrand Cop.

69.   D.A. Long, *Classical Theory of Rayleigh and Raman Scattering*, in *The Raman Effect.* 2002, John Wiley & Sons, Ltd. p. 31-48.

70.   R.A. Toth, *Line Strengths of N_2O in the 1120-1440-cm^{-1} Region.* Applied Optics, 1984. **23**(11): p. 1825-1834.

71.   J.K.G. Watson, *Quadratic Herman-Wallis Factors in the Fundamental Bands of Linear-Molecules.* Journal of Molecular Spectroscopy, 1987. **125**(2): p. 428-441.

72.   J.K.G. Watson, *Quadratic Herman-Wallis Contributions Associated with Vibration-Rotation Resonances.* Journal of Molecular Spectroscopy, 1988. **132**(2): p. 483-491.

73.   D.W. Marquardt, *An Algorithm for Least-Squares Estimation of Nonlinear Parameters.* Journal of the Society for Industrial and Applied Mathematics, 1963. **11**(2): p. 431-441.

74.   S. O'Byrne, P.M. Danehy, S.A. Tedder, and A.D. Cutler, *Dual-Pump Coherent Anti-Stokes Raman Scattering Measurements in a Supersonic Combustor.* AIAA Journal, 2007. **45**(4).

75.   L.P. Goss, D.D. Trump, B.G. Macdonald, and G.L. Switzer, *10-Hz Coherent Anti-Stokes Raman-Spectroscopy Apparatus for Turbulent Combustion Studies.* Review of Scientific Instruments, 1983. **54**(5): p. 563-571.

76.   W. Meier, I. Plath, and W. Stricker, *The Application of Single-Pulse Cars for Temperature-Measurements in a Turbulent Stagnation Flame.* Applied Physics B-Photophysics and Laser Chemistry, 1991. **53**(5-6): p. 339-346.

77.   T. Seeger, J. Kiefer, A. Leipertz, B.D. Patterson, C.J. Kliewer, and T.B. Settersten, *Picosecond time-resolved pure-rotational coherent anti-Stokes Raman spectroscopy for N_2 thermometry.* Optics Letters, 2009. **34**(23): p. 3755-3757.

78.   T. Seeger, J. Kiefer, Y. Gao, B.D. Patterson, C.J. Kliewer, and T.B. Settersten, *Suppression of Raman-resonant interferences in rotational coherent anti-Stokes Raman spectroscopy using time-delayed picosecond probe pulses.* Optics Letters, 2010. **35**(12): p. 2040-2042.

79.   C.J. Kliewer, Y. Gao, T. Seeger, J. Kiefer, B.D. Patterson, and T.B. Settersten, *Picosecond time-resolved pure-rotational coherent anti-Stokes Raman spectroscopy in sooting flames.* Proceedings of the Combustion Institute, 2011. **33**: p. 831-838.

80.   M. Schenk, T. Seeger, and A. Leipertz, *Simultaneous Temperature and Relative O_2-N_2 Concentration Measurements by Single-Shot Pure Rotational Coherent Anti-Stokes Raman Scattering for Pressures as Great as 5 MPa.* Appl. Opt., 2000. **39**(36): p. 6918-6925.

81.   F. Vestin, M. Afzelius, C. Brackmann, and P.-E. Bengtsson, *Dual-broadband rotational CARS thermometry in the product gas of hydrocarbon flames.* Proceedings of the Combustion Institute, 2005. **30**: p. 1673-1680.

82.   L. Gomez, D. Bermejo, P. Joubert, and J. Bonamy, *Theoretical and experimental analysis of N_2-H_2 stimulated Raman spectra.* Molecular Physics, 2006. **104**(12): p. 1869-1878.

82

83.   L. Gomez, R.Z. Martinez, D. Bermejo, F. Thibault, P. Joubert, B. Bussery-Honvault, and J. Bonamy, *Q-branch linewidths of N_2 perturbed by H_2: Experiments and quantum calculations from an ab initio potential.* Journal of Chemical Physics, 2007. **126**(20).

84.   S. Prucker, W. Meier, and W. Stricker, *A Flat Flame Burner as Calibration Source for Combustion Research - Temperatures and Species Concentrations of Premixed H_2/Air Flames.* Review of Scientific Instruments, 1994. **65**(9): p. 2908-2911.

85.   H.G.M. Edwards, D.A. Long, and S.W. Webb, *Line Widths in the Pure Rotational Raman-Spectra of Nitrogen, Oxygen and Hydrogen Broadened by Foreign Gases.* Journal of Raman Spectroscopy, 1988. **19**(7): p. 457-461.

86.   K.C. Smyth, J.H. Miller, R.C. Dorfman, W.G. Mallard, and R.J. Santoro, *Soot Inception in a Methane Air Diffusion Flame as Characterized by Detailed Species Profiles.* Combustion and Flame, 1985. **62**(2): p. 157-181.

87.   K. Aron, L.E. Harris, and J. Fendell, *N_2 and CO Vibrational Cars and H_2 Rotational Cars Spectroscopy of CH_4/N_2O Flames.* Applied Optics, 1983. **22**(22): p. 3604-3611.

88.   T. Seeger and A. Leipertz, *Experimental comparison of single-shot broadband vibrational and dual-broadband pure rotational coherent anti-Stokes Raman scattering in hot air.* Applied Optics, 1996. **35**(15): p. 2665-2671.

89.   F. Vestin, M. Afzelius, and P.-E. Bengtsson, *Improved temperature precision in rotational coherent anti-Stokes Raman spectroscopy with a modeless dye laser.* Applied Optics, 2006. **45**(4): p. 744-747.

90.   I.R. Beattie, T.R. Gilson, and D.A. Greenhalgh, *Low-Frequency Coherent Anti-Stokes Raman-Spectroscopy of Air.* Nature, 1978. **276**(5686): p. 378-379.

91.   F. Vestin, M. Afzelius, and P.-E. Bengtsson, *Development of rotational CARS for combustion diagnostics using a polarization approach.* Proceedings of the Combustion Institute, 2007. **31**(1): p. 833-840.

92.   F. Vestin, D. Sedarsky, R. Collin, M. Alden, M. Linne, and P.-E. Bengtsson, *Rotational coherent anti-Stokes Raman spectroscopy (CARS)*

applied to thermometry in high-pressure hydrocarbon flames. Combustion and Flame, 2008. **154**(1-2): p. 143-152.

93.   F. Beyrau, A. Bräuer, T. Seeger, and A. Leipertz, *Determination of the Gas-Phase Temperature in the Vaporizing Spray of a GDI-Injector Using Pure Rotational CARS.* SAE Technical Paper 2004-01-1350, 2004.

94.   J. Bood, P.-E. Bengtsson, and M. Alden, *Stray light rejection in rotational coherent anti-Stokes Raman spectroscopy by use of a sodium-seeded flame.* Applied Optics, 1998. **37**(36): p. 8392-8396.

95.   K.W. Brown, N.H. Rich, and J.W. Nibler, *High-Resolution Rotational Cars Spectrum of Oxygen.* Journal of Molecular Spectroscopy, 1992. **151**(2): p. 482-492.

96.   C. Brackmann, J. Bood, M. Afzelius, and P.-E. Bengtsson, *Thermometry in internal combustion engines via dual-broadband rotational coherent anti-Stokes Raman spectroscopy.* Measurement Science & Technology, 2004. **15**(3): p. R13-R25.

97.   M.C. Weikl, *Thesis ESYTEC Energie- und Systemtechnik Gmbh Erlangen.* 2009, Nurnberg.

98.   J.A. Shirley, R.J. Hall, and A.C. Eckbreth, *Folded Boxcars for Rotational Raman Studies.* Optics Letters, 1980. **5**(9): p. 380-382.

99.   K.J. Nogenmyr, P. Petersson, X.S. Bai, C. Fureby, R. Collin, A. Lantz, M. Linne, and M. Alden, *Structure and stabilization mechanism of a stratified premixed low swirl flame.* Proceedings of the Combustion Institute, 2011. **33**: p. 1567-1574.

100.   P. Petersson, J. Olofsson, C. Brackman, H. Seyfried, J. Zetterberg, M. Richter, M. Alden, M.A. Linne, R.K. Cheng, A. Nauert, D. Geyer, and A. Dreizler, *Simultaneous PIV/PH-PLIF, Rayleigh thermometry/OH-PLIF and stereo PIV measurements in a low-swirl-flame.* Applied Optics, 2007. **46**(19): p. 3928-3936.

101.   R.S. Barlow, *Laser diagnostics and their interplay with computations to understand turbulent combustion.* Proceedings of the Combustion Institute, 2007. **31**: p. 49-75.

102. S.P. Kearney, K. Frederickson, and T.W. Grasser, *Dual-pump coherent anti-Stokes Raman scattering thermometry in a sooting turbulent pool fire.* Proceedings of the Combustion Institute, 2009. **32**: p. 871-878.

103. F. Migliorini, S. de Iuliis, F. Cignoli, and G. Zizak, *How "flat" is the rich premixed flame produced by your McKenna burner?* Combustion and Flame, 2008. **153**(3): p. 384-393.